SEL 74-042

Fast Hisslers: A Form of Magnetospheric Radio Emissions

by

Jan C. Siren

Prepared under
National Science Foundation Section on Atmospheric Sciences
Grant GA-32590X
National Science Foundation Office of Polar Programs
Grant GV-28840X
Air Force Office of Scientific Research
Grant F44620-72-C-0058

Technical Report No. 3464-1

AUGUST 1974

RADIOSCIENCE LABORATORY

STANFORD ELECTRONICS LABORATORIES

STANFORD UNIVERSITY · STANFORD, CALIFORNIA

SEL 74-042

FAST HISSLERS: A FORM OF MAGNETOSPHERIC RADIO EMISSIONS

by

Jan C. Siren

August 1974

Technical Report No. 3464-1

Prepared under
National Science Foundation Section on Atmospheric Sciences
Grant GA-32590X
National Science Foundation Office of Polar Programs
Grant GV-28840X
Air Force Office of Scientific Research
Grant F44620-72-C-0058

Radioscience Laboratory
Stanford Electronics Laboratories
Stanford University Stanford, California

ABSTRACT

Auroral radio hiss bursts in the frequency range 2-18 kHz have been observed, with rise or turn-on times of 20-50 ms, and fall or turn-off times of 20-80 ms. These time scales are too brief to reconcile with the Cerenkov radiation emission mechanism often proposed as the transducer that converts precipitating auroral electron kinetic energy into very-low-frequency radio wave energy. The auroral hiss bursts, called here "fast hisslers," are observed to be "dispersed," that is, their arrival time at the receiving site is not simultaneous at all frequencies, but depends on frequency in a way that is consistent with propagation in the whistler mode of electromagnetic wave propagation. Since whistler mode wave propagation at these frequencies occurs only in the earth's magnetosphere, it is inferred that these fast hisslers are of magnetospheric origin. On the assumption that all the observed dispersion results from whistler mode dispersion at high latitudes, altitudes of origin of 1800 km to 30,000 km are calculated for these emissions.

Fine details of some of the amplitude spectra of fast hisslers have been examined. The hisslers are noise-like: their spectra are like those that would be produced by an ensemble of independently radiating oscillators.

Potential double layers have been investigated as a highly localized region of acceleration of the auroral electrons that are believed to be the source of energy of the fast hisslers. It is concluded that the present state of double layer theory and observation is not sufficiently refined to permit an unambiguous association of double layers with fast

hisslers, nor with auroral hiss in general.

Evidence is strong that a plasma instability exists which rapidly converts electron kinetic energies into whistler-mode wave energy traveling in the same direction relative to the rest frame of the thermal magnetospheric plasma.

ACKNOWLEDGMENTS

The author wishes to thank Professor Robert A. Helliwell for his guidance and helpful discussions during the course of the research. As a scientist he is so in tune with the phenomena he studies that it becomes difficult at times to tell where the phenomena themselves leave off, and his understanding of them begins. Professor Arthur L. Schawlow is to be thanked for the guidance derived from his concise but penetrating scrutiny of this work. Dr. Donald L. Carpenter's encyclopedic knowledge of the magnetosphere has been tapped many times by the author, who gratefully acknowledges the unfailing generosity shown in the time spent sharing this knowledge. The author is in the debt of Mr. John Katsufrakis for training in field research practice. Mr. Jerry Yarbrough is to be thanked for his efforts in pushing to their limits techniques of data analysis, when required by this work.

The National Research Council of Canada supplied the all-sky camera photographs.

This research was supported in part by the National Science Foundation Section on Atmospheric Sciences under grant GA-32590X, in part by the Office of Polar Programs of the National Science Foundation under grant GV-28840X, and in part by the Office of Scientific Research of the U.S. Air Force under grant F44620-72-C-0058.

TABLE OF CONTENTS

LIST OF FIGURES

LIST OF FIGURES (cont.)

LIST OF TABLES

I. INTRODUCTION

The fundamental insight of science is that
the world is infinitely deeply structured.

Auroral hiss is a high-latitude incoherent magnetospheric radio-wave emission. Fine structure in auroral hiss takes several forms, one of which, the "fast hisslers," is investigated here at depth. The outline of this study is as follows: in the present chapter background information is presented concerning the history of experimental and theoretical studies of auroral hiss. In Chapter 2 the observing site and experimental equipment complement used for the present study will be described. Appendix A will describe an experiment performed by the author and co-workers at the field site. This experiment, although not directly related to the subject of this thesis, has served to establish confidence in the equipment used for receiving the hissler data, particularly the longwire antenna, and (in its purpose) established that whistler-mode waves are right-hand elliptically polarized, which had of course been predicted theoretically but had not been previously verified experimentally. Chapter 3 will review the initial fast hissler observation [Siren, 1972] with an elaboration of the method used to calculate the altitudes of origin. Appendix B contains a listing of the program used for these calculations and a brief explanation of its use. Chapter 4 will describe the systematic search for fast hisslers conducted in Byrd longwire continuous VLF broadband recordings made during substorm "breakup" (or "expansion") phases in the interval 16 June - 17 July 1967. Chapter 5 will describe a "nose" hissler (hissler with a nose frequency or non-extremal frequency of earliest arrival) event at Byrd Station at a time other than a substorm breakup phase. The relationship of nose hisslers

to nose whistlers, which are much more widely known among the scientific community and can be used as a basis for the development of understanding of the new phenomenon, will be examined there. Chapter 6 discusses an alternative model of fast hissler sources, in which individual sources are assumed to move along an auroral-zone magnetic field line with the velocities of 5-50 keV electrons.

The amplitude spectrum in frequency-time space of fast hisslers is examined in detail in Chapter 7. The 14 August 1967 fast hisslers (the subject of Chapter 3) are found to possess an amplitude spectrum indistinguishable from that of pure noise having a Rayleigh distribution, even when examined with a resolution finer than that of any analysis procedure that has previously been applied, in the author's knowledge, to auroral hiss. Possible extensions of this technique of analysis will be discussed. Chapter 8 discusses the applicability of the "potential double layer" theory of Block [1972] and Carlqvist [1972] to the acceleration-and deceleration-of precipitating auroral electrons in distances small compared with the calculated altitudes of origin of the fast hisslers in the fixed source model. It will be shown that theory and experiment concerned with double layers are still in too undeveloped a stage to permit an unambiguous association of double layers with fast hisslers or with auroral hiss in general. Finally, Chapter 9 expresses the author's final conclusions and suggestions for further work.

Original contributions by the author are asserted to be: 1) the observation and description of a class of VLF radio emission phenomena--the "fast hisslers"--not previously reported in the literature; 2) the performance of an experiment which for the first time measured the sense of polarization of whistler-mode waves in space; 3) a simplified method

for calculating group delays of ducted whistler-mode signals in inhomogeneous media; 4) the determination of the occurrence of fast hisslers in the breakup phases of substorms, and the characteristics of some breakup phase fast hisslers; 5) the prediction of characteristics of dispersed noise impulses whose sources are postulated to be moving with constant velocity along auroral-zone magnetic field lines; 6) the development of a method of comparing, on a region of the frequency-time plane whose time-bandwidth product is small, the amplitude characteristics of the Fourier-analyzed signal within that region with those of pure noise; 7) investigation in part of the possibility that all transforms have, at least potentially, a fast version; and 8) investigation of the Block-Carlqvist theory of "potential double layers" with a view to establishing what test of the theory must be made in order to confirm double layers as the acceleration site for auroral electrons and the origin of auroral hiss.

A colorful nomenclature has grown up around very-low-frequency radio phenomena, a nomenclature that reflects the transition in analysis techniques from the aurally-dominated era ("whistlers," "tweeks," "chorus," and "hiss") to the visually-dominated era ("nose whistlers," "hooks," "risers," "striations," and "walking traces"). Hiss appears even more amorphous to the eye than it sounds to the ear. The word "hissler" is a bit of nomenclature coined to apply to a hiss phenomenon discovered since the transition in analysis technique. The word is actually a throwback, describing as it does the sound, rather than the visual appearance, of the phenomenon. It is hiss, but with a fairly well-defined center frequency that changes in time, usually decreasing like low latitude whistlers or the lower frequency branch of nose whistlers. Hiss in general is however

a high magnetic latitude natural emission, occurring more often the closer the observing station or satellite is to an auroral zone, north or south. Hiss often occurs simultaneously with visual or subvisual aurora observed from the VLF receiver site, when viewing conditions and ionospheric transmissivity permit it. A published report by Burton and Boardman [1933] has been cited [Jørgensen, 1968] as the first mention of an association between visual aurora and VLF hiss. Because, in the author's opinion, their observation is open to an alternative interpretation, the relevant section of Burton and Boardman's paper is quoted here:

> During one night of the New Hampshire work an auroral arc appeared extending from northwest to northeast. Near the northwest end of the arc frequent flashes occurred but these were too obscure for any details to be made out. A similar but much weaker flashing was observed to the southwest. At times the flashes appeared to extend along the horizon from northwest to southwest. By visual observation while listening to the atmospherics, it was found that nearly every flash coincided with a static crash possessing the prominent frying sound. These crashes, were in most cases followed by swishes, usually of the descending variety, although occasionally a short ascending whistle occurred simultaneously with the start of the descending swish.
>
> According to information supplied by the United States Weather Bureau, no lightning storms occurring during this period lay in the direction where flashes were observed to be concentrated and no storms were reported as near as one hundred miles to our observation point. The Weather Bureau supplies the information that, under favorable reflecting condition, lightning flashes might be seen forty miles, but could not be seen one hundred miles. It therefore appears reasonable to suppose that the flashes were of auroral origin.

"Swishes" is the word Burton and Boardman applied elsewhere to what we now call "whistlers." To the author's knowledge this is the only published report suggesting that aurora emits VLF radio energy (if that is what the "static crashes" were) sufficiently intense to have excited whistlers. The only other sources known to produce whistlers are lightning flashes

and nuclear explosions [Allcock et al., 1963; Helliwell and Carpenter, 1963; Dinger and Garner, 1963; Helliwell, 1965]. Further, the author has personally observed (in Pittsburgh, Pennsylvania) overhead cloud-to-cloud lightning discharges at an estimated altitude of 13 km, the estimate based upon a repeated lightning-thunder delay of 40 seconds and an assumed sound velocity of 331 m/sec. The horizon distance from an altitude of 13 km is 405 km (250 miles). Only clouds in the line of sight or hills near the viewing site could prevent lightning at this altitude from being observed directly as far as the 405 km horizon distance. Recently, astronauts in earth orbit have seen lightning flashes in thunderstorms on the nightside of the earth. The Weather Bureau's quoted hundred mile limit to the visibility of lightning seems, in light of the above observations, too conservative. An alternate interpretation of Burton and Boardman's observation is that there occurred a thunderstorm more distant than one hundred miles, whose lightning flashes they saw; that these lightning flashes produced atmospherics ("static crashes") and excited two-hop whistlers, which were heard to follow the atmospherics. It is not the author's intention to discredit Burton and Boardman as observers. Other observations they made have stood the test of time. In this case, however, the purely verbal (non-mathematical) description they give does not permit an unambiguous interpretation of their observation.

Interest in a possible connection between VLF phenomena and aurora grew. Storey [1953a,b], Bell [1964], Helliwell [1965], Kimura [1967], Jørgensen [1968], and Lim and Laaspere [1972] have chronicled this growth in interest, in more detail than will be provided here.

Ellis [1957] calculated that precipitating auroral electrons could satisfy the Cerenkov condition (particle velocity exceeds wave velocity)

and emit radio noise in the frequency range of "hundreds of kilocycles per second to low audio frequencies." He predicted that radio noise of Cerenkov origin would be expected to show a strong correlation in time with auroral activity. Then existing radio antennas and receivers would suffice to detect the higher frequencies of this radio noise but they would not be sensitive enough to pick up the emissions below 25 kHz. Nevertheless Duncan and Ellis [1959] did observe simultaneous occurrence of sub-visual aurorae and radio noise bursts at 4.6 kHz from Camden, near Sydney, Australia (42°S geomagnetic).

The first reported simultaneous observation of visual aurorae and VLF hiss at an auroral-zone station was that of Martin et al., [1960]. Their procedure was to regularly tabulate the presence or absence of visual aurora during the International Geophysical Year 2 minutes per hour VLF recording schedule. Their observing site was Byrd Station, Antarctica (80°S, 120°W; 71°S geomagnetic). In 213 of these intervals hiss and aurorae occurred together; in 334 intervals both were absent, and in 49 intervals either hiss or aurora, but not both, occurred. The correlation was found to have been very unlikely to have happened by chance. Martin et al. attributed 31 intervals of hiss without aurora to obscuration of the latter by clouds or bright moonlight, and 18 intervals of auroral without hiss to increased D-region absorption along the ray paths from the hiss source to the receiver.

"Auroral" hiss, as so termed by Martin, et al., was also observed by VLF receivers on the polar orbiting satellites INJUN 3 [Gurnett and O'Brien, 1964] and OGO 2 [Jørgensen, 1968]. Intensities of the wave fields were sufficiently high--up to 10^{-12} $Wm^{2}Hz^{-1}$--that the question of interest was no longer whether very-low-frequency Cerenkov radiation from

auroral electrons would be observable, but whether the predicted intensities of Cerenkov radiation could suffice to account for the observed radio noise. Most notable among the recent attempts to account for auroral hiss by the Cerenkov radiation are those of Jørgensen [1968], Lim and Laaspere [1972], Taylor [1973], and English and Hughes [1973].

Jørgensen [1968] compared the observed auroral hiss spectra from Byrd Station and from the OGO 2 satellite VLF receiver in high latitude passes, with the theoretically calculated hiss spectrum in the lower ionosphere produced by Cerenkov radiation in a flux tube extending up to an altitude of 26,000 km. In his calculations, he found that the single-electron spectrum is strongly altitude dependent, and that the single-electron spectrum is sharply peaked at the lower hybrid resonance frequency f_{LHR}, given by the expression

$$\frac{1}{M_{eff}} \cdot \frac{1}{f_{LHR}^2} = \frac{1}{f_0^2} + \frac{1}{f_H^2} \tag{1.1}$$

where f_0 is the electron plasma frequency, f_H is the electron gyrofrequency, and M_{eff} is the effective mean ion mass to electron mass ratio, given by

$$\frac{1}{M_{eff}} = \sum_i \frac{\alpha_i}{M_i} \tag{1.2}$$

where α_i is the fractional abundance of the i^{th} ionic species, and M_i is the mass to charge ratio of the i^{th} ionic species, divided by the electron mass. He assumed that all radiation generated within a flux tube is ducted to the ionosphere where a broad hiss spectrum peaking at 10 kHz, and falling off approximately as $1/f$ above the peak, and as f below the peak, would be observed. Peak intensity predicted at 10 kHz is

10^{-14} $Wm^{-2}Hz^{-1}$. The predicted spectral shape was found to be in agreement with that observed, both by ground and satellite VLF receivers, but fell short in intensity by a factor of 100. Jørgensen's calculated spectrum was produced by electrons with energies above 1 keV only. In his opinion, the gap would be significantly narrowed by the inclusion of electrons with energies below 1 keV in the calculation of the hiss spectrum.

In a commentary on the paper of Jørgensen [1968], Rao et al. [1973] showed that much larger whistler duct enhancement factors than the "few percent or in some cases even less than 1%" assumed by him, would be required for the ducting of auroral hiss along field-aligned tubes of enhanced ionization down to the ionospheric level where the refracting medium becomes isotropic, permitting the wave energy to spread out and reach the ground. Enhancement factors of from 20% to 400% are required at 10 kHz. Even enhancements of this magnitude do not suffice to trap in ducts, waves of the largest wave-normal-angles (within a fraction of a degree of the resonance cone), at which the bulk of the Cerenkov emission calculated by Jørgensen is emitted. They concluded that the calculated Cerenkov radiation would fall short of that observed by a larger factor than Jørgensen had estimated.

The model calculation of Jørgensen was extended by Lim and Laaspere [1972] who made the following refinements to Jørgensen's model: 1) Very soft (100 eV-1 keV) electrons were included in the hiss generation calculations, and at each stage their contribution was calculated separately from the contribution of the electrons of energies greater than 1 keV, so that the separate contribution to the total could be evaluated. 2) The "low energy infinity catastrophe," a consequence of the $E^{-1/2}$ dependence of Cerenkov radiation intensity on particle energy, was avoided by the

requirement that the wave phase velocity exceed the thermal velocity of the thermal electrons by two times or more, equivalent to setting the maximum wave refractive index to 400. Lim and Laaspere found that the contribution to the total intensity from the 100 eV - 1 keV electrons was more than 100 times greater than the contribution from the 1 keV and above electrons; however, the peak power they calculated was only about an order of magnitude in excess of Jørgensen's [1968] peak calculated power, possibly because of the restriction they placed on the maximum refractive index. The peak power was calculated to occur at a frequency of 70 kHz. Since ray tracing methods were not applied in this work, no estimate could be made of the fraction of energy that would be expected to penetrate the ionosphere. Like Jørgensen, they found that the single-electron spectrum was strongly altitude-dependent, with lower frequencies tending to be emitted at higher altitudes.

Further extensions to the theory of Cerenkov radiation calculations at very low frequencies were made by Taylor [1973] and Taylor and Shawhan [1974]. Their contributions, in part, were to employ the most recent satellite data on fluxes of precipitating electrons, to energies as low as 45 eV (at which energies the electrons are most copious); to include the effects of collisions both to further refine the expression for power radiated incoherently by a single particle in the Cerenkov mode and to provide a new lower energy cutoff to avoid the "low energy infinity catastrophe"; to employ ray tracing to investigate the divergence of the generated wave energy away from the field line of generation; and to apply the method of calculation not only to unstructured auroral hiss, as Jørgensen [1968] and Lim and Laaspere [1972] had done, but also to structured forms such as V-shaped VLF hiss, saucers, fast hisslers, upper hybrid resonance noise, extremely

low frequency hiss, and decametric radiation bursts from Jupiter. As had his predecessors, Taylor found that at a given altitude, the single-particle emission spectrum was sharply peaked at a frequency characteristic of that altitude, and that the peak frequency decreased with increasing altitude. He concluded that except for the UHR noise, the calculated intensities were not sufficiently high to account for the observed emissions.

VLF emissions at latitudes greater than 60^{o} (geomagneiic) as detected by the low altitude polar orbiting satellite ARIEL 3 were compared by English and Hughes [1973] with Cerenkov radiation spectra calculated from Jørgensen's [1968] program, modified by the additions of Lim and Laaspere [1972]. They further extended the spectrum of electrons down to 10 eV in their calculations, and were able to reproduce the shape of Jørgensen's [1968] hiss spectrum (peak at 10 kHz) and that of Lim and Laaspere [1972] (peak at 70 kHz) by adjusting the plasma frequency models. The power radiated incoherently at a frequency f by a single, zero-pitch angle electron ($E = \frac{1}{2} mv_{\|}^2$) for which $v_{\|} \ll c$, is given by the approximate expression

$$\left(\frac{dp}{df}\right)_e = \frac{\pi e^2}{v_{\|}} \left(\frac{f_H}{f_0}\right)^2 \left(\frac{f}{\varepsilon_0}\right) . \qquad (1.3)$$

The peak in the spectrum is determined largely by the altitude at which f_H falls below f_0. This is lower in Lim and Laaspere's [1972] plasma frequency model than in Jørgensen's [1968]. ARIEL 3 hiss spectra however often showed enhancements at 3.2 kHz over that at 9.6 kHz, and many of the enhancements were very much more than 3 db. These enhancements could only be obtained from the incoherent Cerenkov calculation by using an artificial plasma frequency model which differed markedly from the theoretically derived models. The ARIEL 3 experiment was not sensitive

to the wave normal nor Poynting vector directions of the VLF waves observed, so that the direction of the source or sources of the hiss detected in this experiment could not be determined. Occurrence of the emissions was maximum at 2300 magnetic local time, suggesting an association with electrons of about 500 eV.

Common to all these calculations of the single-particle incoherent Cerenkov radiation spectrum is that the power peaks sharply at a frequency that is a function of altitude but is independent of particle energy, as long as the motion of the particle satisfies the Cerenkov condition $\mu\cos\theta = c/v$. Here μ is the wave refractive index, θ is the wave normal angle relative to the static magnetic field, c is the velocity of light, and v is the component of the particle velocity parallel to the static magnetic field. The generic term hisslers has been applied to forms of auroral hiss that are banded in frequency and whose center frequency varies in time. The variation in center frequency seems not to be related through the altitude dependence of incoherent Cerenkov radiation to any known high-latitude wave or particle phenomenon. For the purposes of this study, the hisslers have been divided into two categories. The first was initially noted by Morozumi [1965] and Morozumi and Helliwell [1966] and is currently the subject of a statistical study by Ungstrup and Carpenter [personal communication, 1974]. According to Ungstrup and Carpenter, its "fine structure typically presents a quasi-periodic falling-tone characteristic on frequency-time spectrograms, with spacing between individual falling tones of order 2 seconds. At ground stations, the tones or noise elements appear in sequences lasting from minutes to several hours. Satellite data suggest that centers of falling-tone activity may be somewhat localized in space, but may be active for periods

of several hours." A rough propotionality has been found between the inverse of the rate of frequency change $\Delta f/\Delta t$ and the individual element separation. The author has examined some of these hissler records and found what he would describe as a "protocol effect," in that the occurrence of one hissler noise element inhibits, for its duration, the initiation of the successive hissler noise element. If the sources of these hisslers were at the altitudes characteristic of incoherent Cerenkov radiation at the hisslers' center frequency, the sources would rise in altitude 2000 to 5000 km from the beginning to the end of the individual hissler noise elements. It is difficult to propose an inhibitory mechanism that could operate at these distances. The category of hisslers described above will be referred to in this thesis as "long" hisslers.

The second category of hisslers is characterized by brief (20-50 ms) rise times and dispersions that are only a fraction of the dispersions of whistlers propagating along auroral-zone magnetic field-aligned ray paths. This category, designated "fast hisslers," has its archetype in an event previously described by the author [Siren, 1972] and which is investigated in much greater depth in this study. Although a priori there is no conceptual distinction between the two categories of hisslers, the author has not found examples of hisslers with intermediate dispersions (comparable, for instance, to whistler dispersions) though he has found other examples of hisslers in the established categories.

II. THE VLF RECEIVERS AND OTHER GEOPHYSICAL RECORDING APPARATUS AT BYRD STATION, ANTARCTICA

Byrd Station, Antarctica (80°S, 120°W; -72° geomagnetic latitude) was established during the International Geophysical Year (1957-1958) as a center of upper atmosphere observation. In 1967 at this observatory Stanford University operated very-low-frequency receivers and other geophysical measuring apparatus, and produced permanent records from these instruments in a variety of forms. The VLF receivers amplified the signals from loop antennas buried beneath the snow surface. The amplified signals were either recorded directly on magnetic tape at 9.5, 19, or 38 cm/sec, or filtered through various bandpass filters, detected by dual-time-constant detectors, and recorded as analog voltages on continuous paper strip charts. An example of such a Byrd Station "correlation" chart, so designated because of the multiplicity of geophysical quantities recorded on it simultaneously, is shown in Figure 2.1. The bottom four lines of the chart show the integrated signal amplitude in four VLF passbands: 0.5-1, 2-4, 11-13, and 31-38 kHz (technically the last is an "LF" passband). The calibration shown at left is strictly accurate only for steady signals, or signals varying in amplitude with a time constant of several minutes or longer. For signals varying more rapidly in amplitude the recorded signal level is less than the actual signal level, because the "rise time" of the detector, which is about one minute, is very much longer than the "fall time" of the detector, which is a few tens of milliseconds. Lightning atmospheric impulses, with typical rise times of a few milliseconds, are the strongest signals in these frequency ranges but produce comparatively much less deflection on the chart records than the

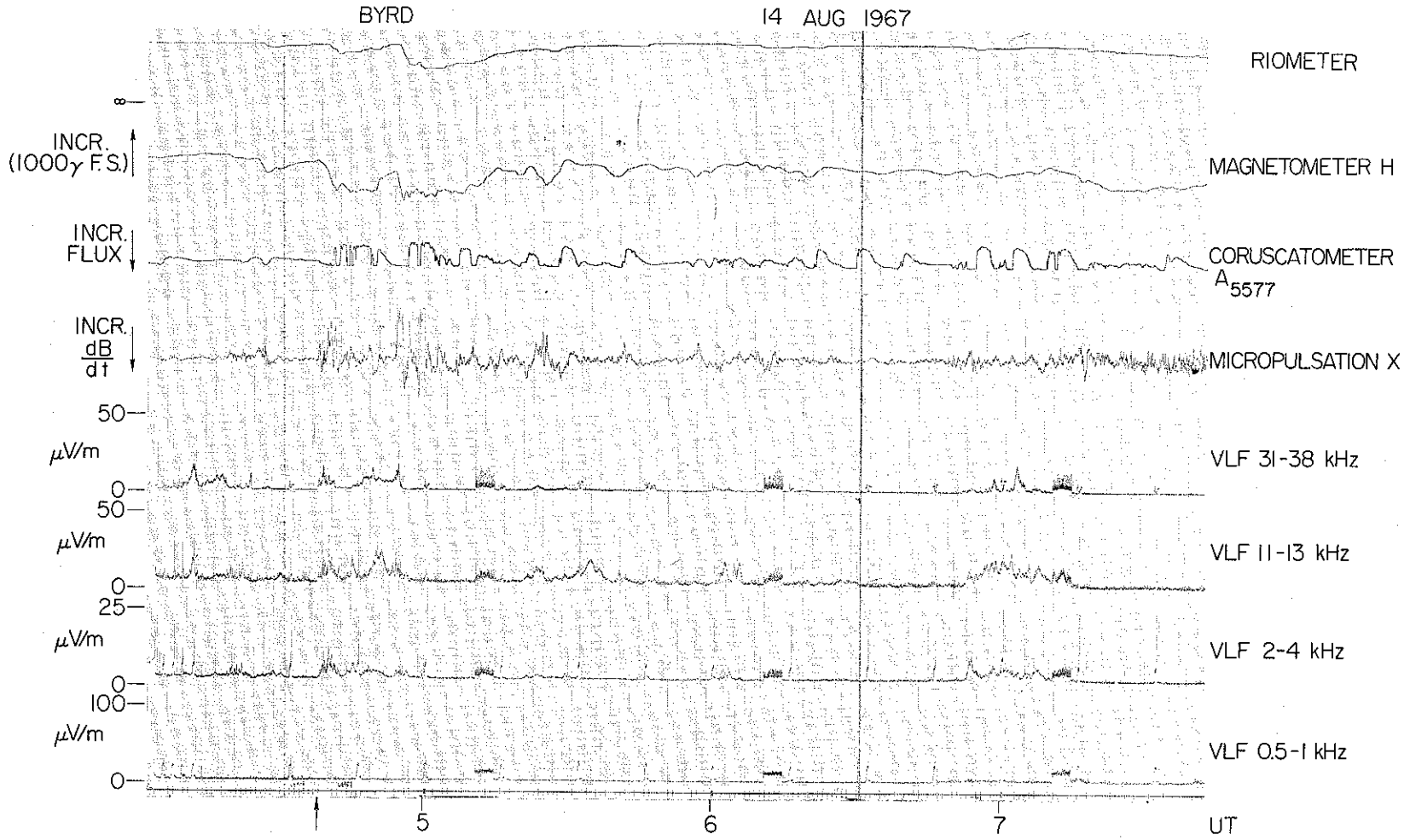

FIGURE 2.1. BYRD STATION "CORRELATION" CHART RECORDING. From bottom to top: VLF signal amplitudes in passbands 0.5-1, 2-4, 11-13, and 31-38 kHz; X-component (geographic north-south) magnetic micropulsations; auroral 5577 Å light coruscations; magnetometer H (horizontal) component; relative ionospheric opacity.

weaker but more slowly varying (and more geophysically interesting) whistler, chorus, and hiss signals.

The fifth line from the bottom of the chart shows the X-component (geographic north-south) magnetic micropulsations, as detected by a multi-turn coil wrapped on a high permeability alloy cylindrical core. (This instrument and the magnetometer to be described below were installed at Byrd Station by Pacific Naval Laboratory of Esquimalt, British Columbia.) The sixth line shows the coruscations or fluctuations in intensity of the green oxygen line at 5577 Å in the auroral spectrum. The detector views a cone of 4.3° half-angle about the zenith and is sensitive to coruscations in the frequency range .01-1 Hz. The seventh line shows the H or horizontal component of the magnetic intensity. Zero is suppressed by over 60,000γ in order that the scale can be expanded to reveal the fine structure of magnetic disturbances. The eighth line shows the Relative Ionospheric Opacity Meter record. This instrument is a sensitive radio receiver tuned to 30 MHz; its antenna beam is aimed toward the zenith, from which it receives radio waves of cosmic origin. The signal is detected and recorded as an analog voltage. Absorption in the ionosphere shows up as a negative "bay" or excursion of the riometer signal below its steady-state value.

Also available at Byrd Station were satellite tracking facilities which enabled the operators to record broadband VLF signals from the NASA satellites OGO's 1, 2, 3, and 4, all of which had on board Stanford University VLF experiments, and the Canadian satellites Alouette 1 and 2, which had on board VLF experiments and topside sounders.

Byrd VLF substation ("longwire" site) was located about 20 km WNW of Byrd Station. It was the center of a long horizontal dipole antenna

complex, which is described further in Appendix A of this report. The continuous broadband VLF data inspected in Chapter 4 were recorded at Byrd VLF substation. The data are characterized by a greater signal-to-noise ratio at frequencies above about 1 kHz than are the VLF broadband data from Byrd Station.

All-sky cameras were operated at Byrd Station during hours of darkness, to photograph the aurora. These cameras took one picture per minute. The all-sky-camera data shown or referred to in this report were supplied by the National Research Council, Ottawa, Canada.

III. OBSERVATION AND ANALYSIS OF DISPERSIVE AURORAL HISS AT BYRD STATION

At the frequencies characteristic of propagation in the whistler mode in the magnetosphere (theoretically, up to 1 MHz; in practice, seldom over 20 kHz) the magnetoionic medium is dispersive. The wave or phase velocity is dependent on frequency. Bursts of auroral hiss so brief as to have distinctly exhibited whistler-mode dispersion were recorded during a substorm on August 14, 1967 at Byrd VLF substation, Antarctica [Siren, 1972]. The observation was made at 0439 UT, two minutes after the substorm breakup phase appeared in Byrd Station records. Whistlers occurred also within the preceding 5 minutes. The fast hisslers, as the hiss bursts are designated, were less than half as dispersed in time as the whistlers. Dynamic spectra of the fast hisslers are given in Figure 3.1. The data have been analyzed by two methods and are presented twice. A fast Fourier transform computer program produced the spectra in Figure 3.1a. A Raytheon Rayspan spectrum analyzer produced the spectra in Figure 3.1b. In the usual way [Helliwell, 1965] the darkening of the display is in proportion to the signal intensity. The digital analysis of the Fourier transform method brings out the noise-like character of the fast hisslers, as indicated by the "salt and pepper" appearance of the spectra in Figure 3.1a. (The Fourier transform method and its application to these data will be discussed further in Chapter 7.) The continuous tone Rayspan analysis shows more clearly their whistler-mode dispersion. That these bursts of VLF signal are not whistlers is deduced primarily from their very small dispersion or tilt, relative to the frequency axis: whistlers with this little dispersion are observed

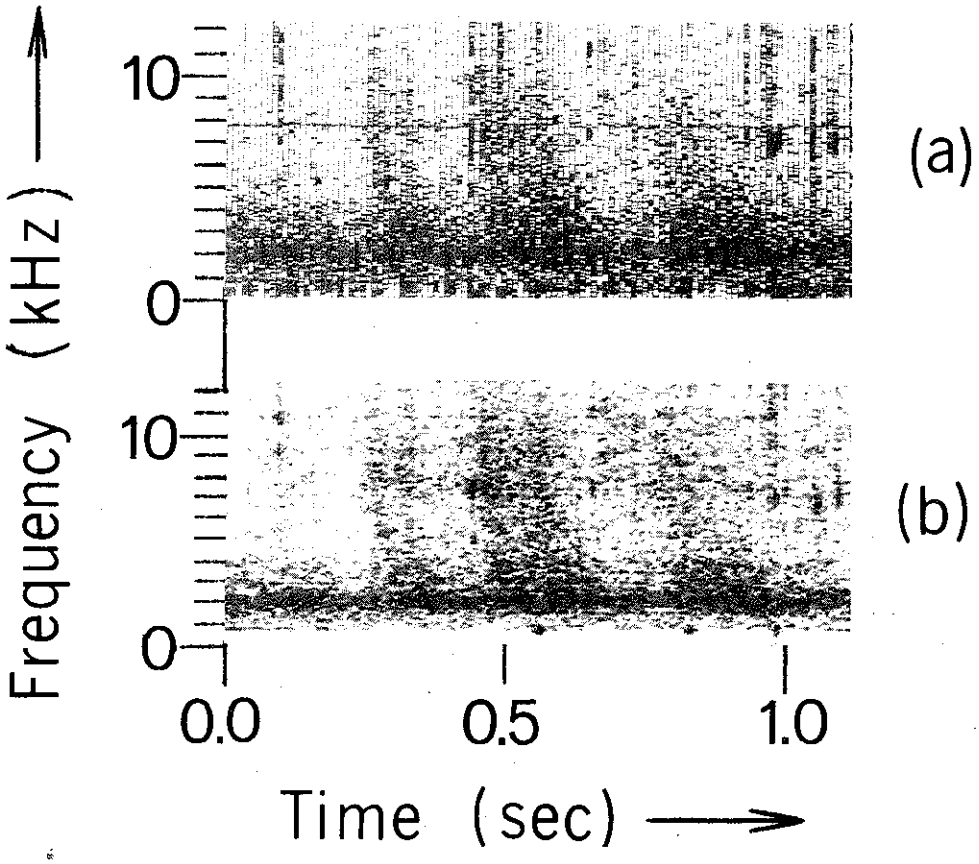

FIGURE 3.1. FAST HISSLER DYNAMIC SPECTRA; 0439 UT 14 August 1967. a) Fast Fourier transform. b) Raytheon Rayspan.

only in rocket-borne or low-altitude satellite-borne VLF receiver data [Helliwell, 1965] or in frequency ranges well below 2 kHz (the "sub-protonospheric" whistlers [Carpenter et al., 1964]). Secondarily, these bursts lack causative atmospherics. Since many whistlers also lack causative atmospherics, especially those observed from Byrd Station, this lack by itself is not conclusive.

The fast hisslers were continuous from about 12 kHz down to 2 kHz, where they terminated in a background of band-limited hiss. Arrival time of each hissler was a monotonic decreasing function of frequency, and there was no evidence of a "nose" or non-extremal frequency of earliest arrival as is often observed in whistlers arriving in Antarctica. In Figure 3.1 time of origin is arbitrary. The first fast hissler, at 0.3 s, was the briefest, least dispersed, and was bifurcated in time. The second fast hissler, at 0.5 s, had a longer duration at all frequencies than the first and was more dispersed. Like the first, it was bifurcated. The third fast hissler, at 0.8 s, had about the same duration at all frequencies as the second, was most dispersed and was not bifurcated. The maximum signal intensity, 1.1×10^{-17} $Wm^{-2}Hz^{-1}$, was measured in the third fast hissler at 3 kHz. The fast hisslers were less intense than the observed maximum auroral hiss intensity at Byrd Station by about a factor of 100, so Cerenkov radiation cannot be excluded as a possible source mechanism on the basis of intensity alone. In the remainder of this chapter, a phenomenological model accounting for the dispersion of the fast hisslers in terms of propagation from fixed "point" sources is developed. The fast hisslers have a broader bandwidth than can be accounted for by Cerenkov radiation, if this interpretation is correct. The source mechanism of the fast hisslers may be similar to that of the 1-9 kHz

"saucer-like" emissions observed by Gurnett and Frank [1972] on the INJUN-5 satellite, and interpreted by them as having originated at altitudes of 5000 -- 10,000 km. It is not possible to determine from the data whether the fast hisslers and the narrowband hiss centered at 2 kHz propagated along the same magnetic field line, although the common lower cutoff frequency suggests that part of the propagation path from source to receiver was shared by the two phenomena.

The whistler mode of electromagnetic wave propagation is anisotropic. In the quasi-longitudinal approximation to the whistler mode refractive index (the use of which is justified below) the refractive index μ is given by

$$\mu^2 = 1 + \frac{f_0^2}{f(f_H \cos \theta - f)} \qquad (3.1)$$

where f_0 is the plasma frequency, f is the wave frequency, f_H is the electron gyrofrequency (or "cyclotron frequency"), and θ is the "wave normal angle"--the angle the wave normal vector makes with $\vec{B}$, the local static magnetic field. The plasma frequency f_0 is given by $f_0 = (Ne^2/4\pi^2 m\epsilon_0)^{1/2}$, where N is the electron number density, e is the electron charge, m is the electron mass, and ϵ_0 is the permittivity of free space. The electron gyrofrequency f_H is given by $f_H = (eB/2\pi m)$, where B is the strength of the static magnetic field.

Downcoming whistler mode waves that penetrate the ionosphere and are received at the ground (which includes all the wave phenomena examined here) must satisfy Snell's law,

$$\mu_1 \sin \varphi_1 = \mu_2 \sin \varphi_2 \qquad (3.2)$$

at the lower boundary of the ionosphere. φ_1 is the angle of incidence

measured between the wave normal in the ionosphere and the normal to the boundary, φ_2 is the angle of refraction measured between the wave normal in free space below the ionosphere and the normal to the boundary, and μ_1 and μ_2 are, respectively, the wave refractive indices in the ionosphere and free space. Since $\mu_2 = 1$ and whistler mode refractive indices in the lower ionosphere at frequencies around 10 kHz are typically greater than 20, only a small angle of incidence φ_1 of the order of 5^o or less can satisfy Snell's law. Wave normals within the ionosphere are within 5^o of vertical so that, at Byrd Station where the dip angle is 74^o, wave normal angles in the ionosphere fall in the range 11^o- 21^o. The validity of the quasi-longitudinal approximation holds where

$$\frac{\sin^2\theta}{\cos\theta} < \frac{2}{3} \cdot \frac{f_0^2}{f f_H} \qquad (3.3)$$

[Helliwell, 1965]. For wave normal angles in the range 11^o- 21^o the lefthand-side of the expression is of the order of 0.1 or less, while for a wave frequency of 10 kHz and typical ionospheric plasma frequency 5 MHz and ionospheric gyrofrequency 500 kHz the righthand-side is greater than 3000. Therefore the use of the quasi-longitudinal approximation is completely justified for present purposes.

The group velocity, also called the wave packet velocity, is the velocity of propagation of the electromagnetic wave energy. It is this velocity that determines the group delay $T(f)$ of a whistler mode signal traveling over a given path, through the expression

$$T(f) = \int_{path} \frac{ds}{v_g(f)} \qquad (3.4)$$

[Helliwell, 1965]. The group velocity $v_g = c/\mu'$ where the group refractive index μ' is given by

$$\mu' = \frac{d}{df}(\mu f) \quad . \tag{3.5}$$

Applying this formula to the expression for the refractive index in the whistler mode we obtain

$$v_g = c/\mu' = 2c \frac{\left[\left(\frac{f}{f_H}\right)^2 + \frac{f_0^2 f}{f_H^3(\cos\theta - \frac{f}{f_H})}\right]^{1/2}}{2\frac{f}{f_H} + \frac{f_0^2}{f_H^2(\cos\theta - \frac{f}{f_H})^2}} \quad . \tag{3.6}$$

When f_0 is appreciably greater than f_H this expression reduces to the simpler expression derived by Helliwell [1965] in his Eq. (3.15):

$$v_g = 2c \frac{f^{1/2}(f_H \cos\theta - f)^{3/2}}{f_0 f_H \cos\theta} \quad . \tag{3.7}$$

However Eq. (3.6) is more general and is preferred for group delay calculations for high latitudes, where f_0 often is actually smaller than f_H.

Time of arrival of the fast hisslers as a function of frequency was measured by use of the OSCAR digitizer, which projects a magnified image of Rayspan-produced spectra, such as those of Figure 3.1b, on a ground glass screen, where a precision cursor registers the position of selected data points with a resolution of 1 part in 10^3. Although the signal-to-noise ratio was not greater than 3-5 db for these hisslers, the intensity maxima as a function of frequency could be located to within a few milliseconds by employing the eye's special sensitivity to edge- or line-type discontinuities. (Figure 3.2 shows the integrated signal strength in three frequency bands--4.0 to 4.8 kHz, 8.0 to 8.8 kHz, and 10.0 to 10.8

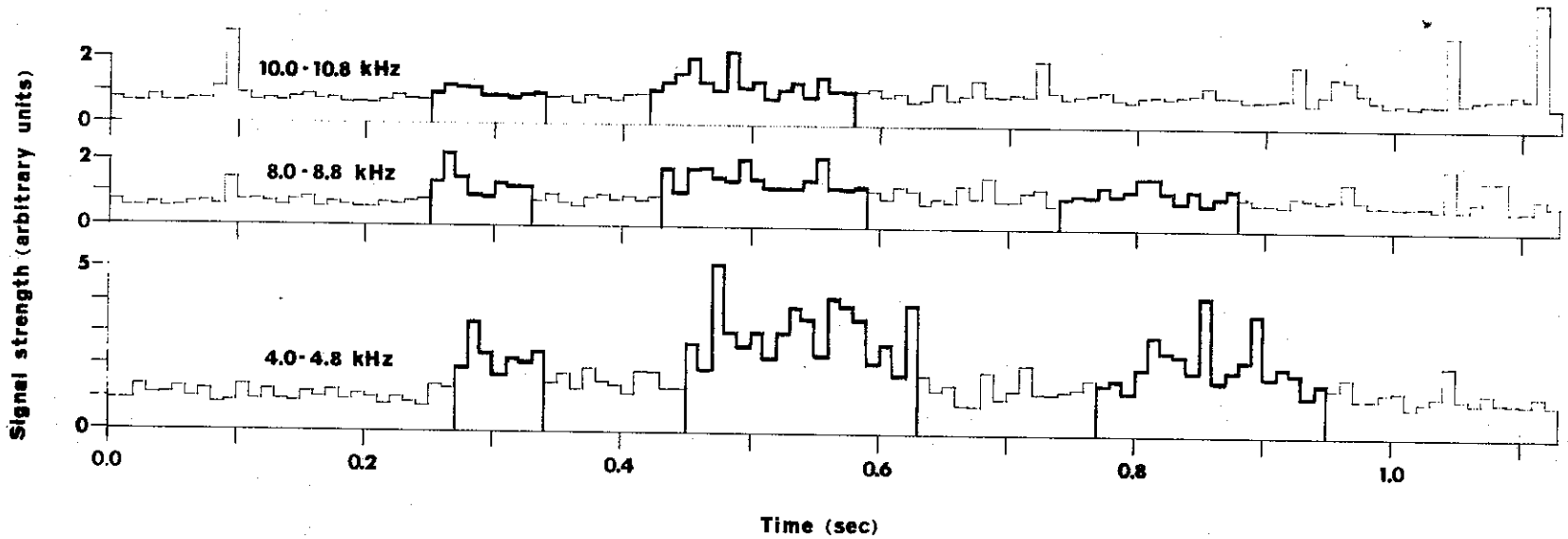

FIGURE 3.2. INTEGRATED FAST HISSLER SIGNAL STRENGTH IN 3 FREQUENCY BANDS: 4.0-4.8 kHz, 8.0-8.8 kHz, and 10.0-10.8 kHz.

kHz--as a function of time. The time scale has the same origin as Figure 3.1. This figure was derived from the fast Fourier transform data. The dark outline indicates the fast hisslers. The light outline indicates the background level of steady hiss on which the fast hisslers are superimposed. The maximum signal-to-noise ratio, about 5 db, occurs at 0.56 sec in the 4.0-4.8 kHz band.)

A computer program was prepared which calculates the group refractive index μ' as a function of frequency and altitude for model ionosphere-magnetospheres, and integrates the group delay from a selected source altitude to the ground, along a magnetic field-aligned propagation path. Inputs to the program are three parameters describing the electron gyrofrequency model, six parameters describing the plasma frequency model and an integer parameter selecting the source altitude. Output is in the form of a plot, in frequency-time coordinates, of group delay as a function of frequency from the selected altitude. The computer used is the Hewlett-Packard 9810 Calculator-Plotter. A listing of the program is given in Appendix B. Group delay is calculated in discrete steps by use of the group velocity as given by Eq. (3.6). Step size increases with altitude, by 100 km per step, starting with a 100 km step at minimum altitude 301 km. Although the group delay resulting from propagation from 301 km down to the ground has been neglected in this program, for the ionosphere-magnetosphere models used that neglect is estimated to introduce an error of not more than 30 msec at 2 kHz, falling smoothly to less than 15 msec at 12 kHz. The ionosphere-magnetosphere model used is based on that of Lim and Laaspere [1972] in their Figure 3, reproduced here as Figure 3.3. The heavy curves are those of Lim and Laaspere; the light solid curves, the plasma frequency and gyrofrequency functions used

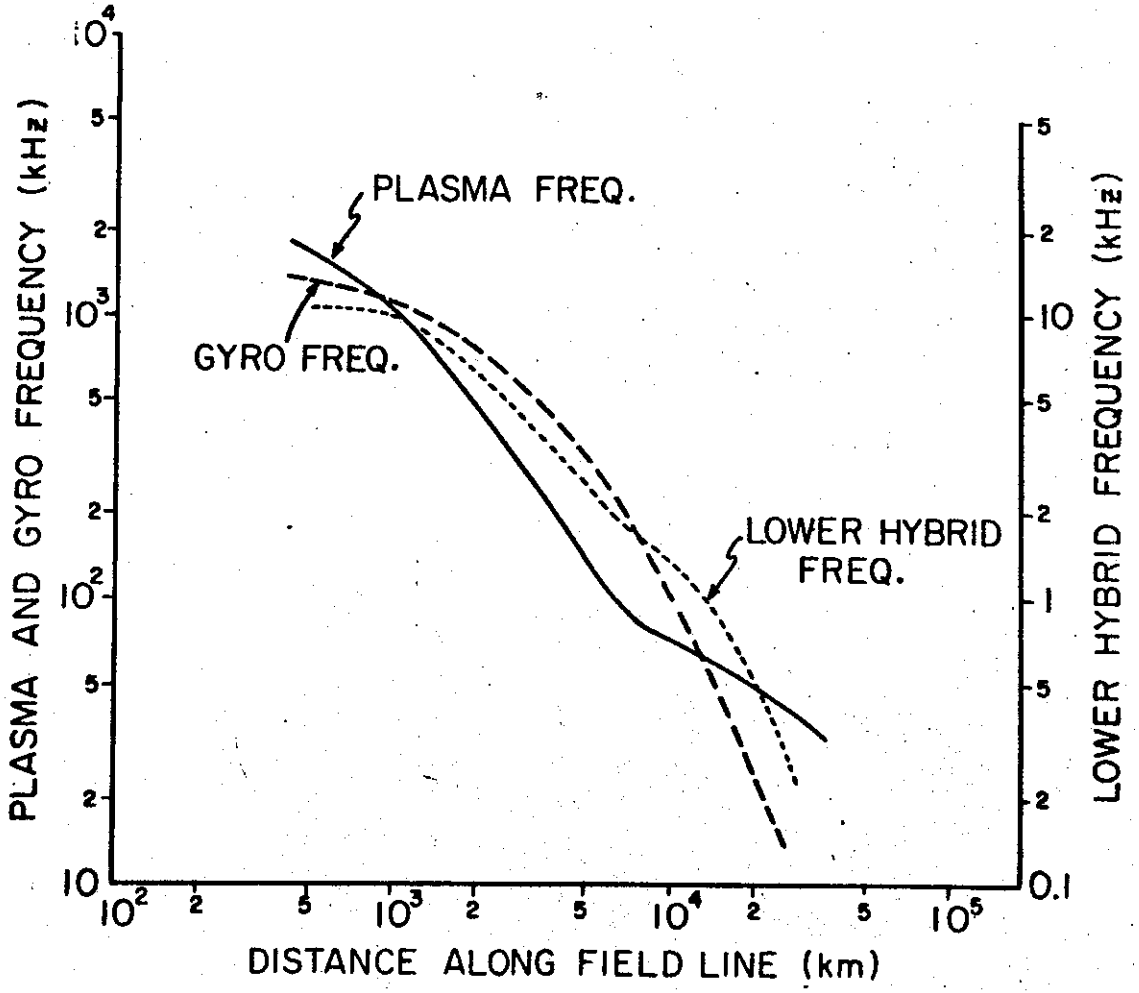

FIGURE 3.3. PLASMAFREQUENCY AND GYROFREQUENCY ALONG AN AURORAL ZONE MAGNETIC FIELD LINE. Heavy curves: Lim-Laaspere model. Light curves: this work.

in this work. The maximum difference between the plasma frequency curves is about 20%; between the gyrofrequency curves, about 5%. In Figure 3.4 are frequency-vs-time curves traced from plots generated by this program. The curves are parametric in altitude of origin, and are referenced to a common time origin. The dashed portions of the curves correspond to frequencies above half the minimum electron gyrofrequency at the altitude of origin. If duct trapping of the hissler wave energy were required at each point along the propagation path from source to receiver, these frequencies would not be observed at the ground, as $f < \frac{1}{2} f_H$ is a condition for duct trapping [Smith et al., 1960]. The general resemblance of these curves to the "trajectories" in frequency-time space of whistler traces is clear. The principal differences are, first, that the time scale is shortened by a factor of 3 to 5 relative to that of whistler traces with the same general shape and second, that the half gyrofrequency upper cutoff (should it exist) falls below the nose frequency, whereas the upper cutoff of nose whistlers is usually 1.33±.08 times the nose frequency [Carpenter, 1968].

The latter difference can be understood qualitatively as follows: In a homogeneous magnetosphere, that is, in a magnetosphere in which the electron plasma frequency and gyrofrequency are constant, the upper cutoff frequency, assumed to be half the gyrofrequency, would be twice the nose frequency. (Strictly, this would be exactly true only in the high-density approximation of Eq. (3.7); anticipating one result of the next chapter, however, it is found that when $f_0 \approx f_H$, a 41% increase in f_0 causes only a 1% increase in the nose frequency f_n, which is therefore unaffected to first order by changes in f_0.) In interhemisphere whistler propagation approximate homogeneity holds for those portions of field-aligned

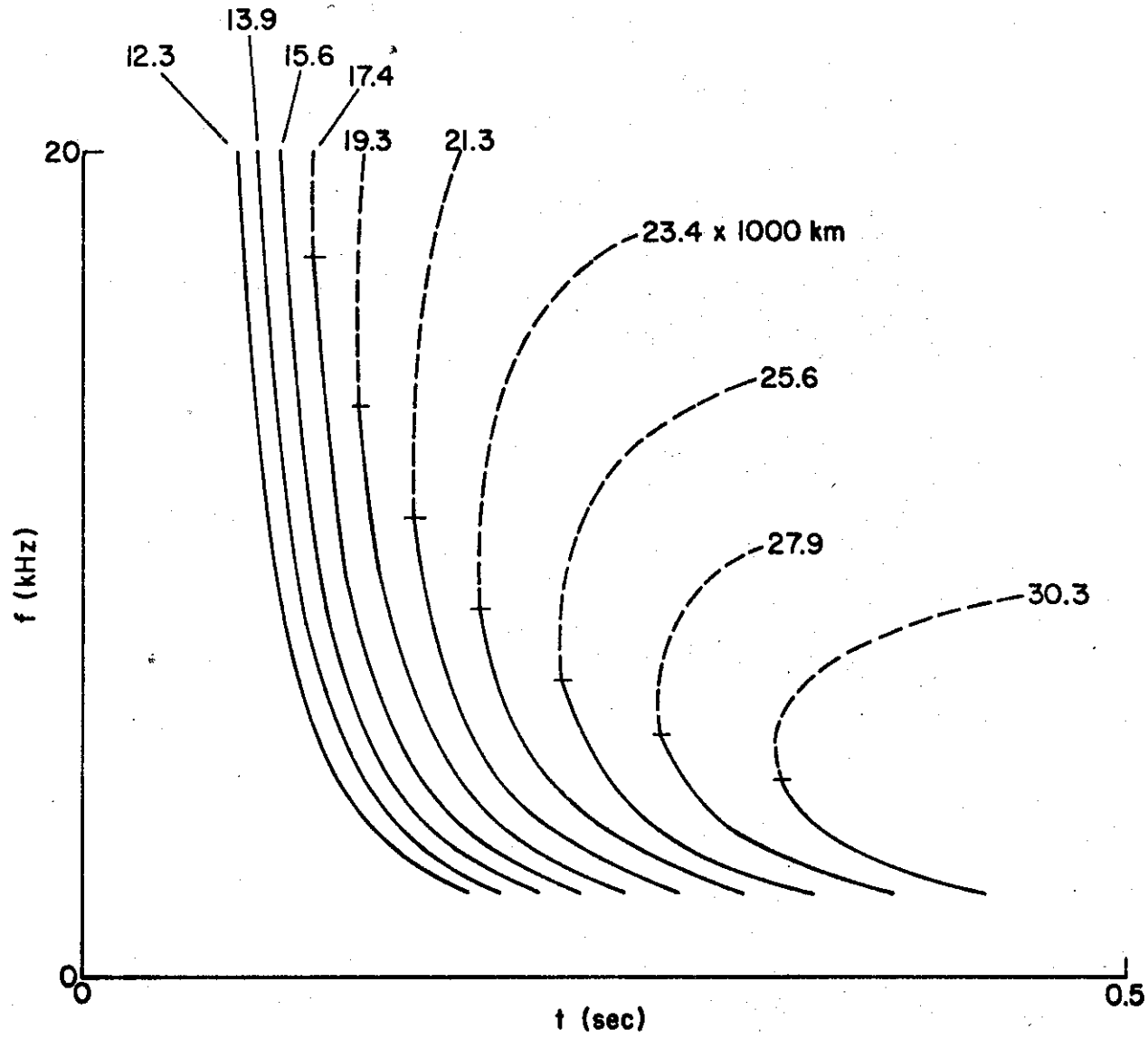

FIGURE 3.4. FAST HISSLER GROUP DELAY VS FREQUENCY CURVES PARAMETRIC IN ALTITUDE OF ORIGIN. Derived from the model in Figure 3.3.

propagation paths within 20^{o} of the geomagnetic equator. In such a quasi-homogeneous portion, the upper cutoff frequency is half the electron gyrofrequency and the group velocity is a maximum at half the upper cutoff frequency. In the higher latitude portions of the propagation path, the electron gyrofrequency increases rapidly away from the geomagnetic equator, and the frequency of maximum group velocity rises proportionally to the electron gyrofrequency. Thus for the path taken as a whole the frequency of maximum average group velocity is higher than the frequency of maximum group velocity in the quasi-homogeneous portion, however, the upper cutoff frequency is established in the quasi-homogeneous portion. Consequently the ratio of upper cutoff frequency to nose frequency of nose whistlers is expected to be less than 2.0 and, in fact, was found by Carpenter to lie in the range $1.33 \pm .08$, as mentioned above. For a hypothetical fast hissler propagation path such as those considered in this study, there is no quasi-homogeneous portion and the half electron gyrofrequency upper cutoff (should it exist) is established at the point of origin. At all points of the propagation path the electron gyrofrequency is higher than at the point of origin, and the increase is relatively rapid, as the electron gyrofrequency increases in proportion to B, which varies approximately as the inverse cube of the radial distance R from the earth's center. For this approximation the ratio of upper cutoff frequency to nose frequency is even smaller than for nose whistlers and is found by calculation to be less than 1.0.

The "hissler plotter" program described above was used to draw curves of frequency vs time delay with the same "aspect ratio" of the frequency and time scales as in high time resolution Rayspan spectra of the fast hissler data. The curves were then photographed on positive

transparency film with a reduction chosen to equalize the frequency (and time) scales of the plotted curves and the data. The photograph was employed as an overlay against which to compare the shapes of the fast hisslers in the Rayspan spectra. The shapes of the fast hisslers, except for their broadening along the time axis, could be fit directly with frequency vs time delay curves of the overlay, with suitably chosen altitude of origin. The results of this fitting are as follows: The altitude of origin of the curve fitting the first fast hissler is 10,000 ± 1000 km; that of the second is 15,000 ± 1300 km; and that of the third is 22,000 ± 3000 km. The errors given here are based upon a subjective judgment of "goodness of fit" which an independent observer might estimate differently. The duration of the individual hisslers at selected fixed frequencies was not the criterion on which the error estimates were based.

Figure 3.5 shows schematically the altitudes of origin calculated above. The circle represents the earth, with Byrd Station a point in the nightside (shaded) high latitude southern hemisphere. The centered-dipole magnetic field line passing through Byrd Station is shown for altitudes below about 30,000 km. The heavy curve segments labeled A, B, and C represent, respectively, the altitudes of origin (including errors) calculated for the frequency-time curves fitting the first, second, and third fast hisslers. Shown also adjacent to the Byrd Station field line are curve segments labeled A', B', C', and A''. The segments labeled A', B', and C' represent respectively the altitudes of origin (with their respective errors indicated by the segment lengths) calculated for the frequency-time curves fitting the first, second, and third fast hisslers when the assumption is made that the electron plasma frequency at each point of the field line propagation path is twice that of Lim and

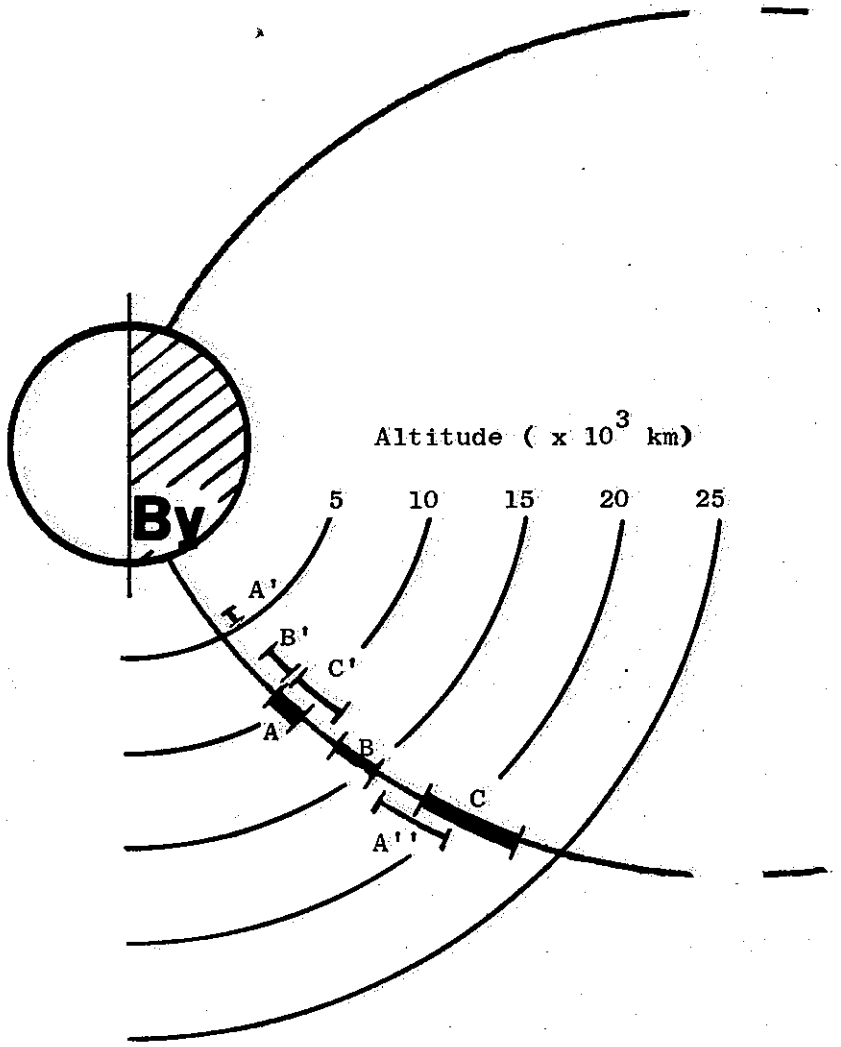

FIGURE 3.5. CALCULATED ALTITUDES OF ORIGIN OF FAST HISSLERS. A, B, C: normal plasma frequency model. A', B', C': double plasma frequency model. A'': one-half plasma frequency model.

Laaspere's [1972] model. A' is at 4200 ± 500 km; B is at 7700 ± 800 km; and C' is at 10,300 ± 1600 km. The segment labeled A'' represents the altitude of origin (with its associated error indicated by the segment length) calculated for the frequency-time curve fitting the first fast hissler when the assumption is made that the electron plasma frequency at each point of the field line propagation path is half that of the model of Lim and Laaspere. A'' is at 18,400 ± 1900 km. It was found that fits to the second and third fast hisslers could not be obtained with this half-density model, because this model predicts that frequency-time curves with altitudes of origin sufficiently high to possess sufficient low-frequency dispersion to fit the low-frequency halves of the fast hisslers would also possess noses below 12 kHz. Noses or non-extremal frequencies of earliest arrival were not observed in these hisslers. Figure 3.6 is a plot of calculated nose frequency vs altitude of origin for the frequency-time curves derived from the Lim and Laaspere ionosphere-magnetosphere model.

The simplest assumption consistent with the experimental data is that the fast hisslers originate as undispersed noise pulses at fixed altitudes on the Byrd Station field line. Several conclusions follow immediately from this assumption. These will be discussed in the remainder of this chapter.

Duration of a fast hissler should be independent of frequency. The August 14, fast hisslers are consistent with this conclusion. It should be pointed out that the "long hisslers" often are not consistent with this conclusion. In one example of long hisslers investigated by Ungstrup and Carpenter [personal communication, 1974] the duration at 6 kHz is more than 5 times longer than that at 8 kHz.

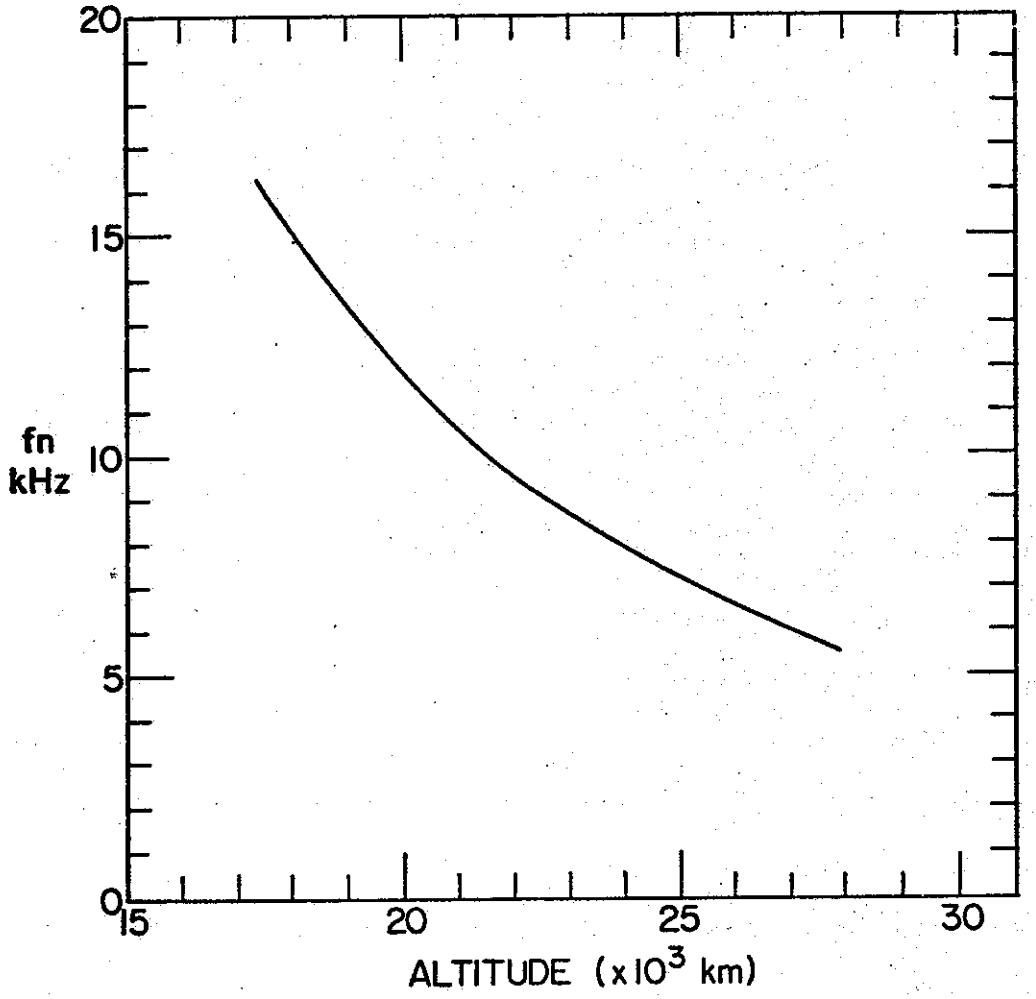

FIGURE 3.6. NOSE FREQUENCY OF FAST HISSLERS VS ALTITUDE OF ORIGIN.

If a fast hissler possesses a nose, at least part of its propagation is nonducted. This conclusion has not yet been tested. The fast hisslers of August 14, did not possess noses. It is not clear what criterion could be applied to "nose hisslers" to test to what extent their propagation is nonducted. Sub-protonospheric whistlers as observed on the ground [Carpenter et al., 1964] were thought to be nonducted from their dispersion characteristics [Smith, 1964] but the verification was not complete until Poynting-vector measurements had been made on a satellite [Gurnett et al., 1971]. Fast hisslers have not yet, to the author's knowledge, been observed in satellite VLF data.

The Poynting-vector ($\vec{E}\times\vec{H}$) of fast hisslers observed above the ionosphere should be directed downward. This has not yet been measured.

Nose frequency should be a monotonic decreasing function of altitude or origin. Figure 3.6 gives the predicted dependence.

Propagation of fast hisslers observed on the ground is at wave normal angles less than 21^{o}. Taylor [1973] has performed ray tracing calculations to determine the dispersion characteristics of fast hisslers. He has found that the range of wave normal angles at 15,000 km altitude for rays which penetrate the ionosphere is an increasing function of frequency. The distribution relative to the direction of $\vec{B}$ becomes increasingly skewed with frequency. At 12 kHz, the maximum frequency of the August 14, fast hisslers, the range of wave normal angles extends from 0^{o} to 12^{o} equatorward of the direction of $\vec{B}$. The skewness of the distribution results from the curvature of the field line between 15,000 km altitude and the ground.

Incoherent Cerenkov radiation from precipitating auroral electrons is too weak to account for the strength of the fast hisslers. Taylor

[1973] calculated the volume of the region of space from which the August 14, hisslers would have been radiated, assuming incoherent Cerenkov radiation from precipitating auroral electrons was the source. He found the volume required is that of a cube 3000 km on a side, if the source region altitude was 15,000 km. He was assuming, however, that the proposed source region had a cross section 750x750 km in the plane perpendicular to the local magnetic field. The source region would therefore have had to extend along the field line many times 3000 km, in order that the source region have sufficient volume. This is distinctly in contradiction with the model assumption made here.

Power spectral densities of fast hisslers in the source regions are $4x10^3$ to $6x10^4$ times more intense than those measured on the ground. Several assumptions have been made here. The sources are assumed to be spherical isotropic radiators with radii equal to the altitude error estimates given previously (1300 km for a source at 15,000 km). The power spectral density is assumed to be measured at the surfaces of the spherical radiators. Ray spreading away from the sources is assumed to be the same in longitude as in latitude (taking into account the cos (latitude) factor). Penetration of the rays through the ionosphere is assumed to be lossless and the geometry of the ray spreading below the ionosphere given by Taylor's [1973] ray tracing results, from which it is predicted that the source/ground intensity ratio is frequency-dependent, and is a decreasing function of frequency. The ratio $4x10^3$ given above is calculated for 12 kHz; the ratio $6x10^4$ is calculated for 3 kHz. Alternatively, if one assumes that fast hissler wave intensity just above the ionosphere is in the same ratio ($\sim 10^2$) to the intensity at the ground as that measured for steady hiss by Jørgensen [1968], then the ratio of source to ground

power spectral densities is 1.3×10^4 and is independent of frequency. The determination that a rocket or satellite-borne instrument was measuring source fields would depend upon the absence of dispersion of the hiss bursts.

IV. FAST HISSLERS IN SUBSTORMS

Broadband VLF data tape-recorded at Byrd Station have been examined to determine the occurrence of fast hisslers in substorms. The data base is a sequence of 19 cm/s tape recordings made during a high duty cycle continuous recording campaign in 1967 covering the interval 0005 UT on June 16, to 2000 UT on July 17. During each hour of this interval, the 300 Hz - 20 kHz signal received with the longwire 32-km horizontal dipole antenna was recorded according to the following schedule: recorder on, minutes 02:06 through 08:47, 18:06 through 30:47, 34:06 through 44:47, and 48:06 through 58:47; recorder off, all other times. Tape changes were made during off intervals when possible. The average duty cycle over the interval was 62%.

The data set examined in this investigation was selected under the requirement that the geophysical conditions prevailing during the recordings selected resemble those prevailing at 0439 UT on August 14, 1967, when the phenomenon had occurred. A substorm or high latitude magnetic disturbance was then in progress. Morozumi [1965] and Morozumi and Helliwell [1966] have described Byrd Station substorm phases in detail. By their nomenclature, an "N-2" or expansion phase had begun at 0437 UT. Brice [1968] has interpreted the N-2 as the passing of the "auroral bulge" over the location of the observing site. During this phase, which lasted 5 min, there occurred a 380γ negative bay in the magnetometer H component; an increase in 558 mμ aurora intensity; the passing overhead of a westward traveling surge of aurora (Figure 4.1); a 1.45 db 30 MHz riometer (Relative Ionospheric Opacity) negative bay; 23 db increase in (north-south) micropulsation intensity; and increases

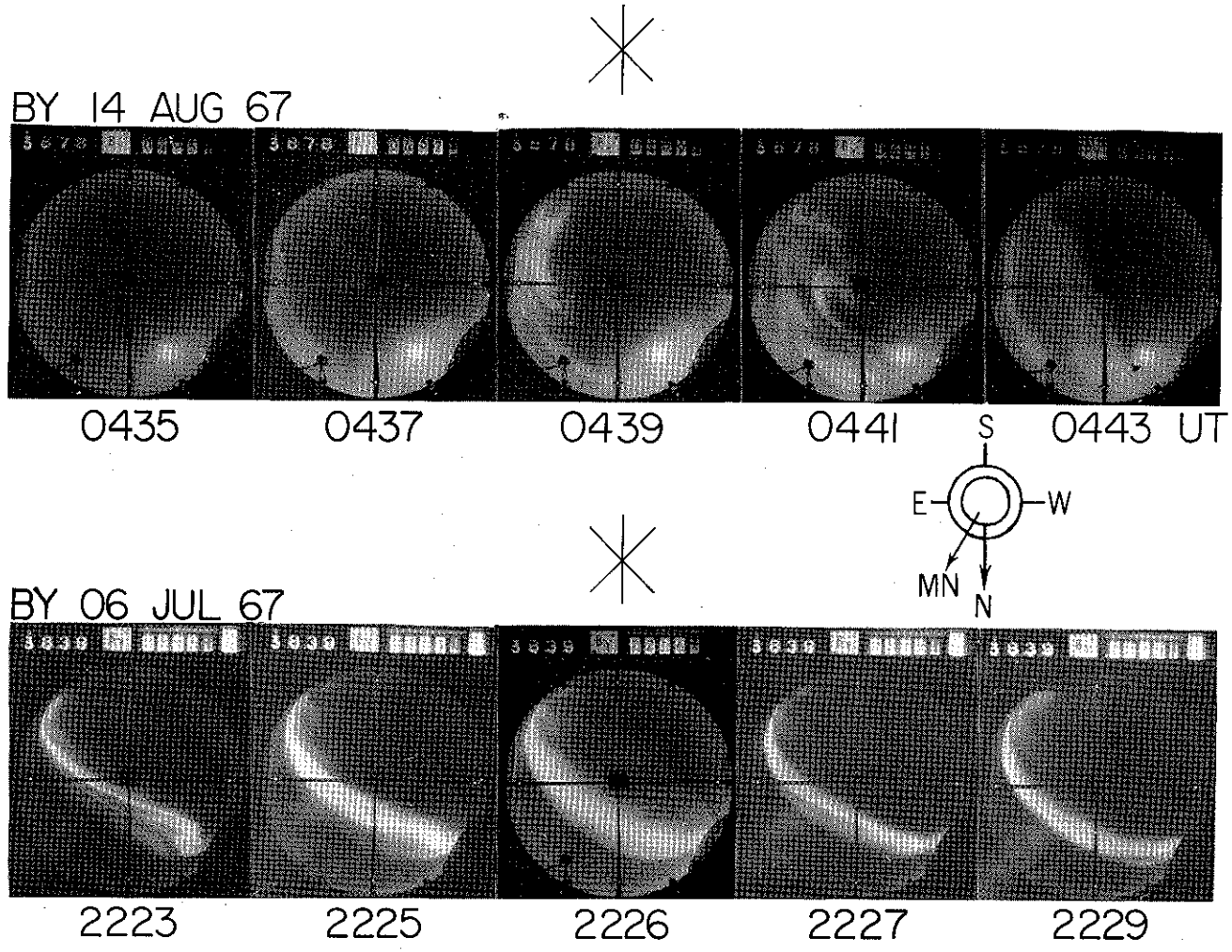

FIGURE 4.1. BYRD STATION ALL-SKY CAMERA PHOTOGRAPHS. (above) 0435-0443 UT on 14 August 1967. (below) 2223-2229 UT on 6 July 1967. Asterisks: fast hissler occurrence.

in VLF hiss intensity over background noise in the 2-4 kHz, 11-13 kHz, and 31-38 kHz bands (Figure 2.1).

The direction of the interplanetary magnetic field (IMF) was southward at 0439 UT, and had been southward for at least 83 minutes prior to 0439. Observation of the IMF was made by the Ames Research Center magnetometer aboard satellite Explorer 33 which was outside the magnetosphere at the time [D. Colburn, personal communication, 1974]. In some theories of the magnetosphere southward orientation of the IMF is essential for the storing of magnetic energy in the tail of the magnetosphere (in the still-controversial "growth" phase of substorms) prior to its subsequent release in the expansion phase of substorms [Roederer, 1974]. Akasofu, et al [1973] have presented a somewhat different theory in which there is no "growth" phase associated with a southward orientation of the IMF, but instead there is a steady general equatorward motion of the auroral oval during periods of southward IMF and that substorms, which are assumed to occur randomly within these periods, are observed or not by various high-latitude magnetic and auroral observatories depending on whether the auroral oval has moved to their vicinity. The August 14, substorm is not inconsistent with this model, but is inconsistent with models that associate substorm expansion phases with southward turnings of the IMF (with delays of 40 minutes to 1 hour). IMF orientation was not used as a selection criterion in this study.

An isolated long hissler occurred during the expansion phase of this substorm. Its commencement followed the fast hisslers by about 22 s. It decreased in frequency from 13 kHz to 7 kHz in 1 s, then stabilized at a center frequency of 7 kHz until it faded out about 2-1/2 s later. Its bandwidth was 1-2 kHz and it was about as intense as the most intense

preceding fast hissler. This is the only example known to the author of an association between the two kinds of hissler, and this association is of note because of the rarity of isolated long hisslers, which commonly occur in groups.

Byrd Station "correlation" charts like that in Figure 2.1 provided the geophysical data from which the selection of events was made. Table 1 lists the criteria met by the substorm events selected for examination.

TABLE 1. SELECTION CRITERIA FOR SUBSTORM N-2 PHASE.

PARAMETER	CRITERION
30 MHz Relative Ionospheric Opacity	$\geq$ .50 db increase
Magnetometer H component	$\geq$ 30γ negative bay
558 mμ Aurora Intensity	increase
Micropulsation N-S component	$\geq$ 6 db increase
31-38 kHz VLF hiss intensity	$\geq$ 10 db increase above background
11-13 kHz VLF hiss intensity	$\geq$ 6 db increase above background
2-4 kHz VLF hiss intensity	$\geq$ 6 db increase above background

The table lists 7 simultaneous criteria characterizing an N-2 phase, and deemed adequate for examination were all events satisfying any 5 of the 7 criteria. The criteria identifying N-2-like phases were specified somewhat differently than was done by Morozumi and Helliwell. ELF (2-40 Hz) data were not recorded, so the presence of ELF bursts was not a requirement. The 558 mμ data cam from a coruscatometer (sensitive to .01-1 Hz variations in auroral light intensity) viewing a cone of 4^{o}

half-angle about the zenith, while Morozumi and Helliwell's had come from an all-sky photometer. Other differences existed. Nevertheless the events selected are as distinctive as Morozumi and Helliwell's N-2 phases. In the author's opinion the number of events in this interval that they would have designated N-2 that the author did not, and vice versa, is a small fraction of the 24 chosen. It was required for the purposes of this study that the event commence during a recorder on period. This requirement eliminated 5 events. Table 2 lists the N-2 events chosen for investigation. Figure 4.2 shows the time distribution of the substorm N-2 phases. The 19 events are indicated in the figure by a vertical solid line corresponding to the time of commencement. The dashed lines correspond to the commencement of the August 14, event (c) and to a September 18, 1971 fast hissler event (d) to be described in Chapter 5. The extended lines correspond to the events in which fast hisslers occurred. By "auroral midnight" is meant the time at which the sub-solar point is on the great circle through Byrd Station and the center of the southern auroral zone, and is nearer the latter. Morozumi and Helliwell found N-2 phases clustered within a few hours of auroral midnight, as did the author, with a single (non-hissler) exception. Fast hisslers occurred in two events prior to auroral midnight and in two events subsequent to auroral midnight.

The tape-recorded VLF data were played back at the speed at which they had been recorded, and aurally monitored. The monitoring included an interval from at least 10 minutes before to at least 10 minutes after each N-2 phase commencement as determined from the "correlation" charts. Fast hisslers were heard in two of the recordings, at 0554 UT on June 24, 1967 and at 2226 UT on July 6, 1967. These data were subsequently spectrum

TABLE 2. SUBSTORM N-2 PHASE EVENTS 16 JUNE - 17 JULY 1967.

	Time of Occurrence (UT)	30 MHz Relative Ionospheric Opacity Increase (db)	Magnetometer H component bay (γ)	558 mμ Aurora Intensity (+ designates increase)	Micropulsation N-S component (db increase)	31-38 kHz VLF Hiss Intensity (db increase)	11-13 kHz VLF Hiss Intensity (db increase)	2-4 kHz VLF Hiss Intensity (db increase)
	18 JUN 0356	.13	no data	+	10	14	11	8
	18 JUN 0519	1.69	no data	+	20	18	16	15
	21 JUN 0318	.23	0	+	29	24	16	14
	21 JUN 0402	.35	-20	+	14	12	15	12
	22 JUN 0416	.11	-60	+	18	18	12	10
a)	24 JUN 0554*	1.08	-280	+	18	12	6	10
	27 JUN 0015	2.22	-260	+	> 20	> 20	> 18	17
	27 JUN 0523	5.25	-480	+	20	20	8	0
	30 JUN 1818	2.36	-30	+	20	0	0	10
	03 JUL 0247	.60	-30	+	19	20	> 18	19
	03 JUL 0318	.74	-110	+	> 14	20	15	20
	04 JUL 0429	.94	-200	+	12	20	10	5
b)	06 JUL 2226*	1.48	-80	no data	2	30	10	16
	06 JUL 2248	2.09	-40	no data	9	32	> 17	20
	07 JUL 0225	2.15	-230	no data	8	23	18	19
	07 JUL 0300	1.07	-120	no data	6	10	13	16
	11 JUL 0052	.50	-240	+	8	16	5	0
	13 JUL 0454	2.58	-90	+	23	16	18	> 22
	14 JUL 0329	.62	-80	+	> 15	14	> 19	> 19
c)	14 AUG 0439* (1967)	1.45	-380	+	23	14	8	8
d)	18 SEP 0135* (1971)	no data	-320	no data	(decrease)	16	13	23

* = Fast hisslers observed

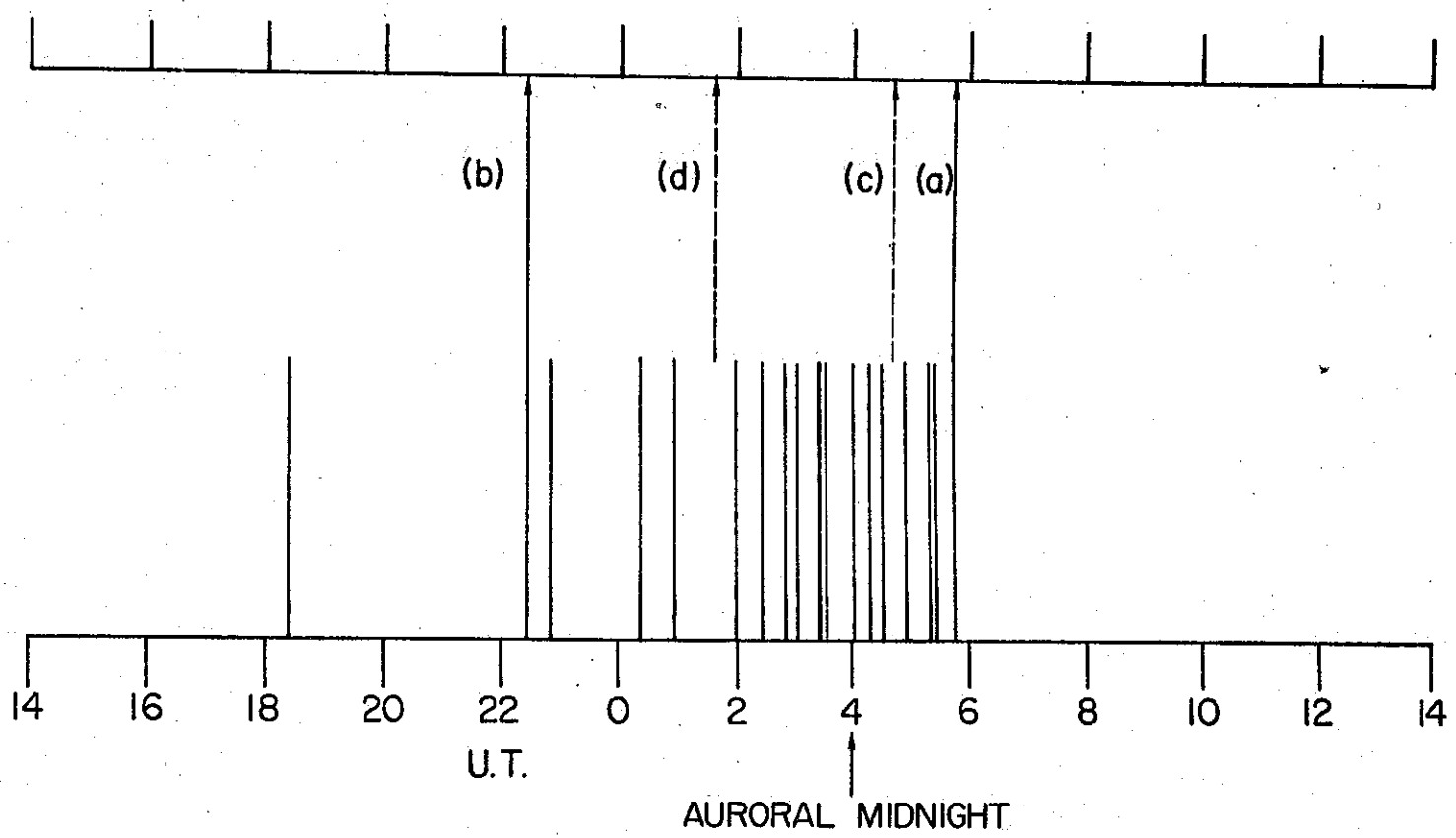

FIGURE 4.2. DIURNAL DISTRIBUTION OF SUBSTORM N-2 (BREAKUP) PHASES, 16 JUNE - 17 JULY 1967. Extended arrows: fast hissler occurrence.

analyzed by a Rayspan analyzer. Spectra of these fast hisslers are shown in Figure 4.3a,b. Included for comparison are fast hissler spectra from the August 14, event (c) and the September 18, 1971 event (d). (The reader should, in comparing these spectra, keep in mind that the frequency and time scales differ for the different events, as indicated, and that the darkening of the display is proportional to the power spectral density only within a particular spectrum. The dynamic range available in this form of display is orders of magnitude less than is recorded on the original tapes and Rayspan level settings must be adjusted individually for each tape-recorded event, as was done here.) Although the June 24, and July 6, fast hisslers in absolute terms were more intense than those observed on August 14, the "background" noise, consisting of steady and impulsive hiss, was relatively even more intense, rendering the hisslers less sharply defined. The fast hisslers occurred in intervals of less than about one minute, with only one such interval per substorm.

The interplanetary magnetic field was southward at the time of the June 24, fast hissler occurrence and had been southward since a northward-to-southward turning at 0435 UT, 79 minutes previous. The comments made above about the relationship of IMF to substorm expansion phases and hisslers apply equally here. IMF orientation was not measured by Explorer 33 for July 6, on which date the satellite was in the vicinity of the magnetopause or inside it.

Frequency vs time delay curves parametric in altitude of origin were fitted to these hisslers as to the hisslers discussed in the previous chapter. "Noses" or non-extremal frequencies of earliest arrival were observed in the hisslers labeled 1 and 2 in the June 24, event (Figure 4.3a). Nose frequencies were 5 kHz and 6.5 kHz, respectively. These

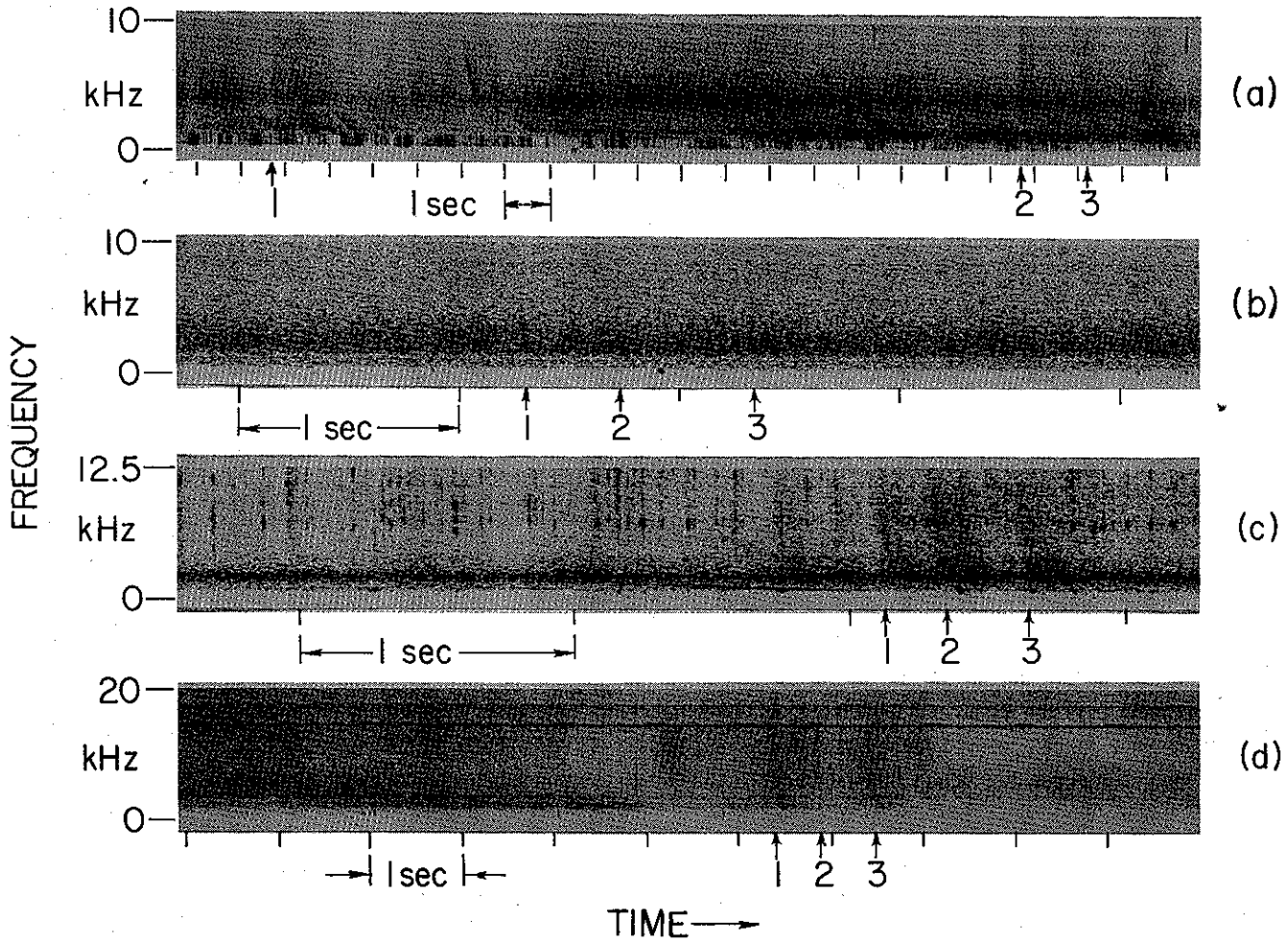

FIGURE 4.3. RAYSPAN DYNAMIC SPECTRA OF FAST HISSLERS. a) 0554 UT on 24 June 1967. b) 2226 UT on 6 July 1967. c) 0439 UT on 14 August 1967. d) 0135 UT on 18 September 1971.

hisslers could be fit with frequency-time curves with altitudes of origin sufficiently high to match the observed nose frequencies.

For a given altitude of origin, the calculated nose frequency of a fast hissler (under the assumptions of the model presented in the previous chapter) is a relatively more slowly varying function of plasma frequency along the path of propagation than is propagation delay time at the nose frequency. Under the assumption that the plasma frequency along the magnetic field line is that given by the Lim and Laaspere model, the nose frequency of a fast hissler originating at 25,600 km is 8.5 kHz and the propagation delay time at the nose is 0.23 s. Increasing the plasma frequency by a factor of 1.4 (doubling the electron density) everywhere along the field line increases the nose frequency by only 0.1 kHz, or about 1%, but it increases the propagation delay time at the nose by .08 s or 37%. Figure 3.6 shows the nose frequency as a function of altitude of origin for the assumed model, but the relation is in error by only 1% for models of the ionosphere-magnetosphere in which the plasma frequency is multiplied (or divided) by a constant factor 1.4 everywhere. Altitudes of origin for the fast hisslers found in this investigation have been estimated by use of the nose frequency when that has been observed; on lower-frequency dispersion otherwise. Under the above assumptions the fast hisslers labeled 1, 2, and 3 in Figure 4.3b originated at 9400 km, 3900 km, and 1800 km respectively. Errors in these estimates are difficult to judge but might be 20-25%. These are the least dispersed hisslers yet observed. The power spectral density of hissler 1 (taken as an example) was 9.7×10^{-16} $Wm^{-2}Hz^{-1}$ in the frequency band 2-4 kHz. All-sky camera photographs were taken during this event (see Figure 4.1, bottom panel). The photographs show a single moderately bright latitudinally aligned arc

that appears somewhat broader at 2226 UT than before or after that time, but is not otherwise differently structured. A uniform equatorward drift is evident from 2223 UT to 2229 UT.

The hissler labeled 3 in the June 24, event (Figure 4.3a) showed no nose up to its highest frequency, 9 kHz. This indicated an altitude of origin not greater than 25,000 km. However, the dispersion at lower frequencies is greater than can result from propagation from 25,000 km altitude to the ground through no more ionization than is assumed in the Lim and Laaspere model. Both the lack of a nose and the lower-frequency dispersion can be accounted for with an ionosphere-magnetosphere model in which the plasma frequency at each point along the magnetic field line is twice that of the Lim and Laaspere model. With this assumption the altitude of origin is estimated as 21,000 km. The altitudes of origin of hisslers 1 and 2 of the June 24, event are estimated from their 5 kHz and 6.5 kHz nose frequencies as 30,000 km and 28,000 km respectively. The peak power spectral density of the most intense fast hissler of this event, the one labeled 2, was 7.5×10^{-17} $Wm^{-2}Hz^{-1}$ in the frequency range 2-4 kHz and 1.3×10^{-16} $Wm^{-2}Hz^{-1}$ in the frequency range 11-13 kHz.

Power spectral densities observed in these auroral hiss emissions range from 7.5×10^{-17} to nearly 10^{-15} $Wm^{-2}Hz^{-1}$, almost two orders of magnitude greater than in the fast hisslers reported in the August 14, event. For comparison, the peak power spectral densities reported by Jørgensen [1968] for Byrd Station auroral hiss were 10^{-16}, 5×10^{-16}, and 2×10^{-15} $Wm^{-2}Hz^{-1}$ in the 1-2, 2-4, and 11-13 kHz bands respectively. Thus these hisslers approach in intensity the maximum steady hiss intensity at Byrd Station. The volumes of the source regions required for incoherent Cerenkov radiation from precipitating auroral electrons are even larger

than that calculated by Taylor [1973] for the August 14, hisslers, which was found in the previous chapter to be too large for consistency with the assumed model. Taylor found also that Cerenkov radiation at these frequencies would propagate with wave normal angles greater than 89^{o}, although wave normal angles less than 12^{o} are necessary for penetration through the ionosphere.

None of the fast hisslers observed in this investigation is morphologically inconsistent with the assumption that they originate as undispersed noise pulses at fixed points on auroral zone field lines.

V. FAST HISSLERS WITH NON-EXTREMAL FREQUENCIES OF EARLIEST ARRIVAL

Rayspan spectra of fast hisslers extending up to the highest upper cutoff frequency yet observed, 18 kHz, are shown in Figure 4.3d. These hisslers occurred at 0135 UT on September 18, 1971 at Byrd Station. Geophysical data for this event have been included in Table 2. In contrast to the data whose spectra are shown in lines (a), (b), and (c), of Figure 4.3, these data were received with the under-snow loop antenna at Byrd Station, rather than by the horizontal dipole at Byrd VLF substation. For the purposes of this study the principal difference between the broadband data tape-recorded at Byrd Station and at Byrd VLF substation is a lower signal-to-noise ratio in the former in the range of hissler frequencies, because of the somewhat wider bandwidth recorded at Byrd Station. The "fields of view" of the two VLF observatories overlap by over 98%, an estimate based upon the 500 km "viewing radius" of an observatory and the 13-km separation.

Figure 4.3d indicated that the hisslers were less intense than a preceding emission of "steady" hiss which had ended about 3 s prior to the hisslers. Peak power spectral densities could be measured in three bands, for hissler 1. The peak power spectral densities were 3×10^{-17} Wm^{-2} Hz^{-1} at 1-2 kHz, 1×10^{-16} $Wm^{-2}Hz^{-1}$ at 2-4 kHz, and 4×10^{-16} $Wm^{-2}Hz^{-1}$ at 11-13 kHz. These intensities are somewhat less than those measured for the hisslers discussed in the previous chapter. All-sky camera photographs taken at Byrd Station at this time show no aurora in a clear sky [M. J. Neale, personal communication, 1973]. This event occurred during an interval of substorm activity but an N-2 phase was not in progress at this time. These hisslers were noted first by visual inspection of the data

[J. Yarbrough, personal communication, 1973].

A common 8.5 kHz nose frequency, or non-extremal frequency of earliest arrival was observed in these hisslers. This corresponds to an altitude of origin of 25,600 km. Half the electron gyrofrequency (the upper frequency limit for ducting) at this altitude is 7.2 kHz, indicating that frequency components of the hissler above 7.2 kHz are nonducted for some portion of the propagation path above 17,000 km where half the electron gyrofrequency is 18 kHz, the observed upper cutoff frequency (see Figure 3.4).

In Chapter 4 was summarized the result of test calculations showing that for a fixed altitude of origin, the nose frequency of a fast hissler is affected proportionately much less ($\Delta f_n/f_n = +1\%$) than is the time delay at the nose ($\Delta t_n/t_n = +37\%$) by a uniform doubling of the electron density. This is closely analogous to the corresponding relationships for nose whistlers [Helliwell, 1965]. In Chapter 3 a qualitative explanation was given for the calculated result that the nose frequency of fast hisslers exceeds half the electron gyrofrequency at the point of origin. Reference was made to a study of nose whistlers by Carpenter [1968] who had found a somewhat different behavior for nose whistlers: the nose frequencies is less than half the electron gyrofrequency at all points of the propagation path, including the equatorial crossing where the altitude is a maximum and the electron gyrofrequency is a minimum. This difference in behavior should serve as a point of caution against drawing the analogy between nose hisslers and nose whistlers too far. In Chapter 3 the proposed model for fast hisslers assumed an impulsive source like those known to be sources of whistlers (lightning, nuclear blasts). However, the source is assumed to be not at the ground or in the ionosphere

but at altitudes of the order of one to several earth radii and for propagation from these sources many of the relationships to nose whistler propagation break down. In the assumed model the invariant latitude of the propagation is not variable, but is taken to be fixed, and equal to the invariant (magnetic) latitude of Byrd Station, -71°. The nose frequency of the fast hisslers is a function of the altitude of origin along the fixed magnetic field line through Byrd Station (see Figure 3.6).

Current models of magnetosphere configuration predict that magnetic field lines originating at low magnetic latitudes on the earth's surface are almost always "closed," that is, that these field lines are connected to the earth at both ends; that field lines originating near the north and south magnetic poles on the earth's surface are almost always "open" or connected to the interplanetary magnetic field; and that field lines originating at middle latitudes on the earth's surface are sometimes "closed" and sometimes "open" depending on whether the magnetospheric dawn-to-dusk convection electric field is relatively weak or strong. Roederer [1974] discusses some of these magnetosphere models in more detail than will be presented here: the reader is referred to Roederer's article for a broader look at the magnetosphere. Field-aligned ducts of enhanced ionization which carry whistler-mode energy in interhemisphere propagation can exist only on "closed" field lines. "Knee" whistlers [Carpenter, 1963] or whistlers propagating outside the plasmapause (in steady state, the outer limit of closed equipotential contours in the magnetosphere) are not an exception to this rule, as these whistlers are carried by ducts being refilled from below by F-region ionization subsequent to emptying of the ducts to interplanetary space during intervals of temporary "opening." Observation of fast hisslers at a ground station

should not, therefore, be regarded as evidence that the field line through that station is either open or closed, since the propagation is assumed to take place entirely within the magnetic hemisphere of observation.

Ducting is expected to figure much less prominently in the propagation of fast hisslers than of whistlers. Interhemisphere propagation of whistlers requires that the Poynting vector (the local ray direction) rotate through an angle of $\sim 270^{\circ}$ along the path of propagation. Without the density gradients believed to exist at the boundaries of ducts, the wave normal vector, initially field-aligned, would rotate in the same sense but would gradually lag behind the rotation of the Poynting vector until by the time the conjugate region is reached, the wave normal angle is greater than 89°. At the lower boundary of the conjugate ionosphere the angle of incidence of the whistler wave exceeds the critical angle for total internal reflection, the whistler reflects, and is not observed on the ground. Ducts provide density gradients that cause whistlers to undergo many small-angle reflections during propagation. These reflections have the effect of limiting the excursions of the wave normal vector away from the magnetic field direction to a few degrees or tens of degrees. At the lower boundary of the conjugate ionosphere the wave normal is within a few tens of degrees of vertically downward, Snell's Law is satisfied at the boundary, and the wave passes through to the ground where the whistler is observed. On the magnetic field line through Byrd Station, the direction of the magnetic field rotates through only $\approx 30^{\circ}$ between 15,000 km altitude and the ionosphere. Taylor's [1973] ray-tracing calculations show that, even in the absence of ducts, the wave normal

vector of a 12 kHz wave originating at 15,000 km altitude lags behind the Poynting vector by only 6^{o} (its rotation is 24^{o}) in propagation down to the lower boundary of the ionosphere. The angle of incidence falls within the range of angles satisfying Snell's Lwa, and the wave can pass through to the ground. The lag is roughly proportionately smaller, at lower frequencies.

These considerations should apply equally well to long hisslers should their sources be found to lie at comparable altitudes.

VI. AN ALTERNATIVE MODEL OF FAST HISSLER GENERATION: FIELD-ALIGNED "CLOUDS" OF PRECIPITATING AURORAL ELECTRONS

Precipitating electrons that strike the upper atmosphere at high latitudes and cause auroral light emissions have energies of about 1 keV to many tens of keV. Electrons of energies in this range have velocities comparable to the phase and group velocities of auroral hiss VLF waves in the magnetosphere. Cerenkov radiation from precipitating auroral electrons (electrons that strike the atmosphere and lose their kinetic energy) has appealed to many authors as a possible source mechanism for the generation of auroral hiss largely because the Cerenkov condition $\mu\cos\theta = c/v_{\parallel}$ is met by copious quantities of electrons for frequencies and wave normal angles characteristic of the whistler mode of propagation. (μ is the wave refractive index, given by Eq. (3.1); θ is the wave normal angle relative to the static magnetic field, c is the speed of light and $v_{\parallel}$ is the component of particle velocity parallel to the static magnetic field.) A review of theoretical papers treating Cerenkov radiation as a source mechanism for auroral hiss was given in Chapter 1. A common feature of all the papers is the assumption that energetic electrons emit wave energy at all points of their trajectories, and that all the emitted energy propagates to the ground, in ducts or otherwise. Thus Jørgensen [1968], for example, in his calculations of auroral hiss intensities at the ground included the contributions from electrons as high as 26,000 km above the earth. These assumptions are made necessary because the radiation from a single electron is very weak, and is sharply peaked in intensity at a frequency that is dependent, through the electron plasma frequency and gryofrequency, on altitude.

In Chapter 3 an almost "structureless" model of fast hissler generation was presented. This model assumed that the fast hisslers originated as undispersed noise pulses at fixed points on high-latitude field lines and propagated longitudinally (with zero wave normal angle) to the ground, where they were observed. A systematic search through broadband VLF data disclosed more examples of fast hisslers. Although some of these had noses (unlike the August 14, hisslers) none of the newly found hisslers was inconsistent with the simple model, nor the conclusions that were drawn from it.

The next least structureless model of fast hissler generation assumes, as before, emission at all frequencies simultaneously from point sources, but in this model the sources are assumed to be moving downward along the Byrd Station field line with constant velocity. Since the range of velocities chosen corresponds to electron energies in the range 5-50 kev, the sources will be referred to as "clouds" of precipitating electrons or "electron clouds," although protons of energies 9-90 MeV would possess the same range of velocities. Because, to the author's knowledge, protons of these energies have not been found to be correlated with auroral light emissions nor with auroral hiss, no further consideration will be given them. The assumption is made that one cloud is associated with each hissler; that at each point of the cloud's trajectory it emits hiss in the frequency range bounded below by 2 kHz and bounded above by 0.9 times the local electron gyrofrequency or 20 kHz, whichever is lower; that the cloud begins its trajectory at 30,300 km altitude and ends it at 12,300 km altitude and travels with constant velocity between those altitudes; and that the emitted wave energy propagates longitudinally to the ground and its wave refractive index is given by the Lim and Laaspere

[1972] ionosphere-magnetosphere model (same as that used in Chapter 3). Some of these assumptions are arbitrary but their consequences are sufficiently clear that the effect of modifying them will be evident at least qualitatively.

Figure 6.1 shows the plot in frequency-time coordinates of the fast hissler produced by a 50 keV cloud. The resemblance to Figure 3.4 is more than coincidental. Coordinate scales were chosen for Figure 6.1 to maximize the resemblance. The hissler is shown as the superimposition of discrete contributions from each of the altitudes indicated in Figure 3.4. The individual curves that make up the sum are the same as in Figure 3.4, but the time separation between the curves in this figure is now no longer simply the group propagation time between the respective altitudes; the time separation is now the group propagation time between the respective altitudes minus the time required for the cloud to traverse the difference in altitudes. The cloud travels at velocity v_c given by

$$v_c = c[1-(1+E/m_0c^2)^{-2}]^{1/2} . \qquad (6.1)$$

E is the electron kinetic energy and $m_0 = 511$ keV/c^2 is the electron rest mass. For E = 50 keV, the cloud velocity v_c is 1.24×10^5 km/s. It can be seen that the curves are compressed into a smaller region of the frequency-time plane than the curves in Figure 3.4. The curves at 23,400 km altitude and above do not cross, because the cloud velocity exceeds the group velocities at those altitudes, but at 21,300 km and below the curves begin to cross each other because the cloud velocity equals the group velocities at certain frequencies below 20 kHz and altitudes below 21,300 km. There is a "piling up" of curves behind the dotted curve that outlines the sharp "leading edge" of the hissler.

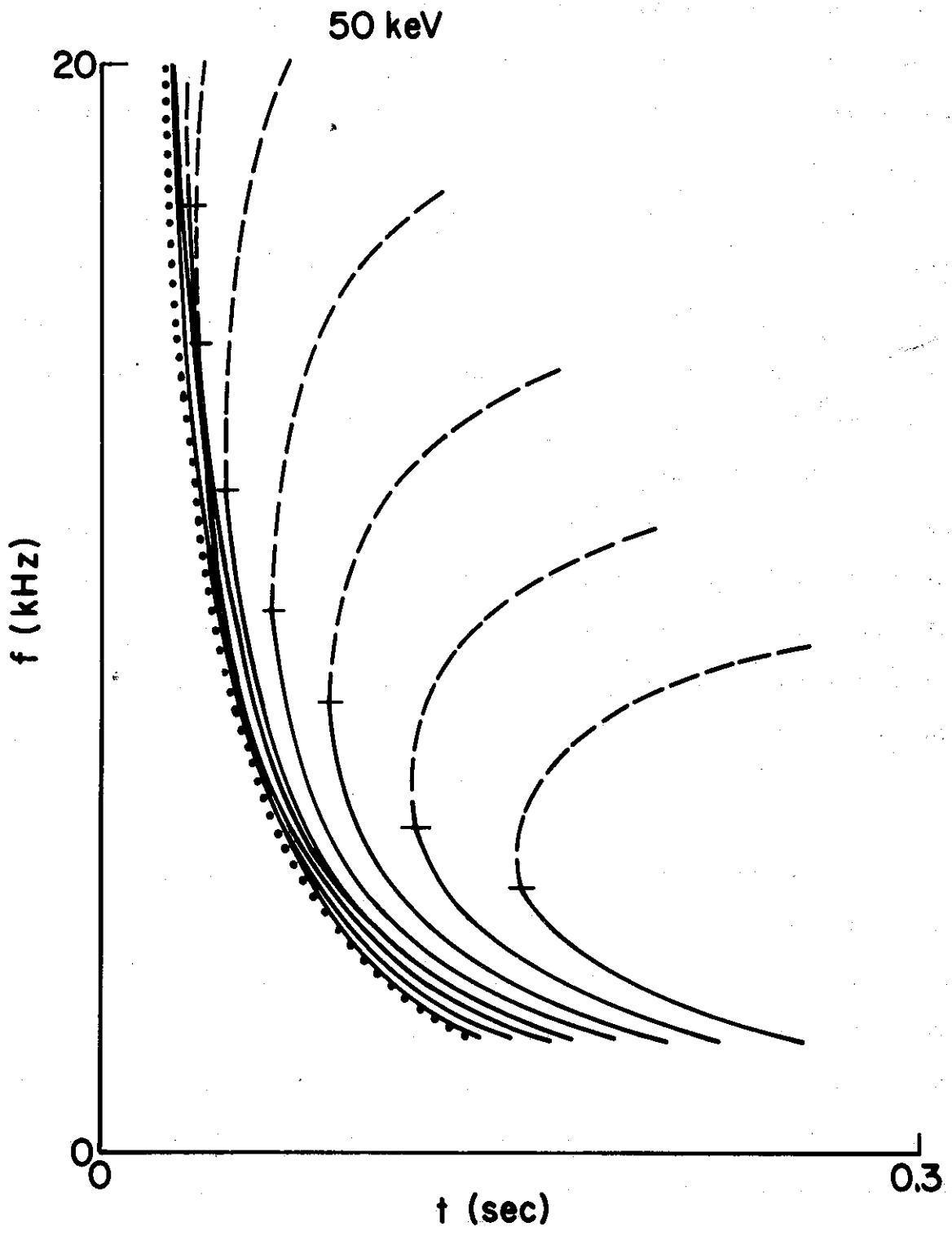

FIGURE 6.1. FAST HISSLER PRODUCED BY 50 keV ELECTRON "CLOUD."

As in Chapter 3, the dashed portions of the curves correspond to frequencies above half the electron gyrofrequency at the altitude of origin.

The reader is asked to visualize two regions of the frequency-time plane. The first region contains only the solid portions of the curves in Figure 6.1. It is bounded on the early side by the dotted curve at the leading edge, above by 20 kHz, on the late side by an imaginary curve through the cross-hatch marks and the 30,300 km altitude curve, and below by 2 kHz. Within the outline of this region (which will be designated as the "ducted" region) is contained all the energy radiated by the cloud in the whistler mode and which propagates down to the ground at half the local electron gyrofrequency or less. The second region contains both the solid and the dashed portions of the curves in Figure 6.1. It is bounded on the late side by an imaginary curve through the upper ends of the dashed portions of the curves and by the dashed portion of the 30,300 km altitude curve above the cross-hatch mark, by the solid portion below; the other boundaries are the same as for the "ducted" region. This region will be designated as "nonducted" even though some portions of the curves within it could represent either ducted or nonducted propagation. Within the outline of the "nonducted" region is contained all the energy radiated by the cloud in the whistler mode and which propagates down to the ground, regardless of whether the propagation is ducted or not. The "ducted" region narrows from 126 ms wide at 2 kHz to 7 ms wide at 20 kHz, while the "nonducted" region flares from 126 ms wide at 2 kHz to 260 ms wide at 10 kHz, then narrows to 46 ms wide at 20 kHz. Neither shape matches well the observed duration of fast hisslers, which to first approximation is independent of frequency (Figure 3.1). Although the figure does not show this effect directly, the "piling up" of curves at the early side of

the region represents what might be termed a "caustic" in the frequency-time plane that would be manifest as a sharp leading edge in the fast hissler spectrum. In contrast, the trailing edge would not possess this sharpness.

In Figure 6.2 are the curves making up a fast hissler produced by a 20 keV electron cloud ($v_c = 8.15 \times 10^4$ km/s). The frequency and time scales in this and the subsequent two figures are the same as in Figure 6.1. The curves at 23,400 km altitude and above do not cross, as was the case for these curves in the previous case, but are closer together because v_c does not exceed the wave group velocities by as much. At 21,300 km altitude and below a reversal begins to take place, as the cloud velocity begins to be exceeded by the wave group velocities. Lower-latitude curves arrive at the ground successively later. As in the previous figure, the dotted curve outlines the sharp leading edge of the hissler, which is almost vertical near 20 kHz. "Ducted" and "nonducted" regions in the frequency-time plane can be visualized for this example as for the previous one. The "ducted" region varies in width from 46 ms at 2 kHz down to 28 ms at 20 kHz, with secondary extrema between: 30 ms at 4 kHz and 46 ms at 9 kHz. It is less variable in width than the "ducted" region of the 50 keV cloud, but more variable than observed fast hisslers. The "nonducted" region has the same shape below 5.3 kHz, but above that frequency flares rapidly to 202 ms at 10 kHz, then narrows gradually to 28 ms at 20 kHz.

Figure 6.3 shows the curves making up a fast hissler produced by a 10 keV electron cloud ($v_c = 5.8 \times 10^4$ km/s). This figure shows the reversal described as for the previous case taking place at even the highest altitude, 30,300 km, at frequencies below 4 kHz, and at progressively

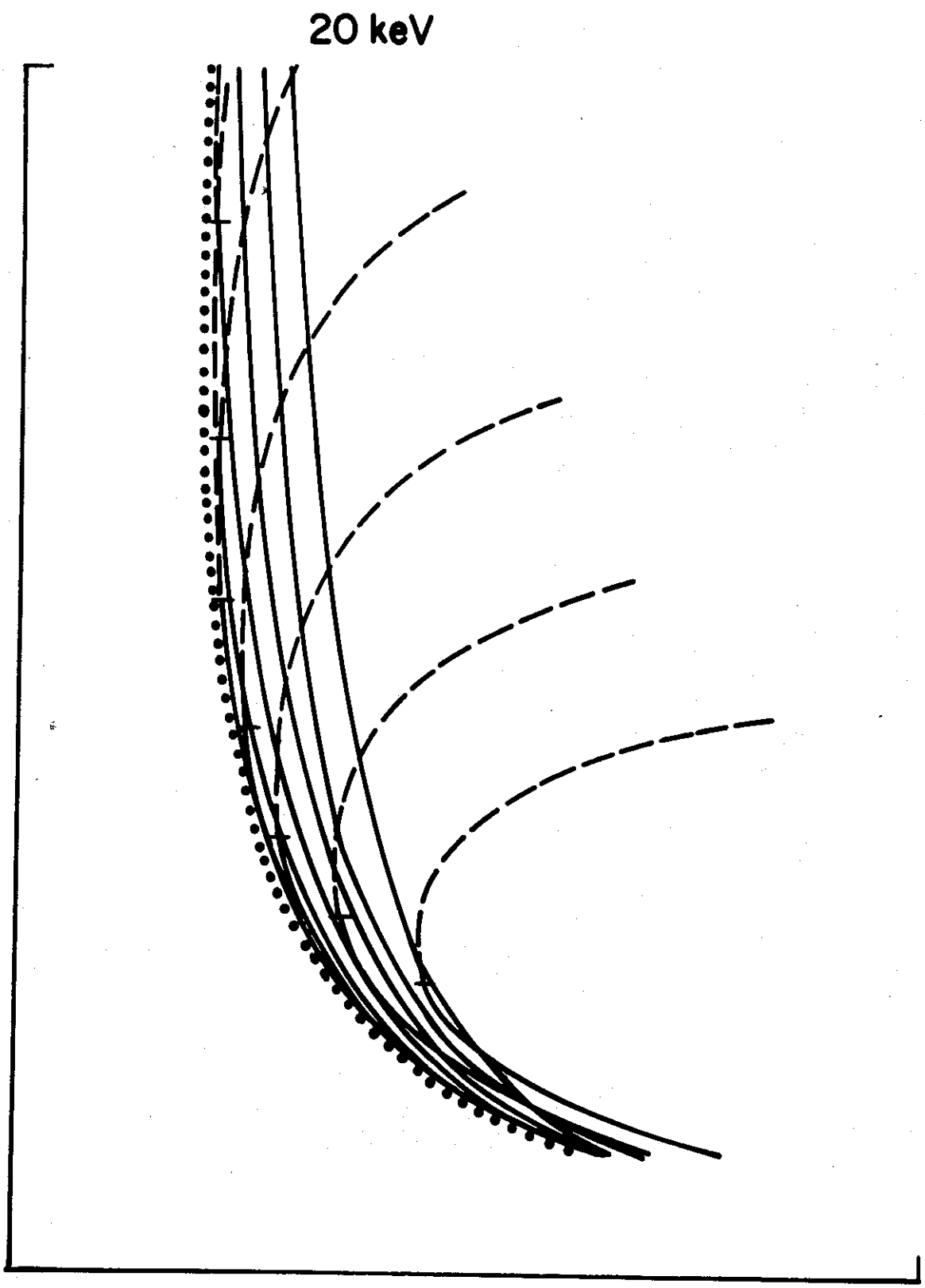

FIGURE 6.2. FAST HISSLER PRODUCED BY 20 keV ELECTRON "CLOUD."

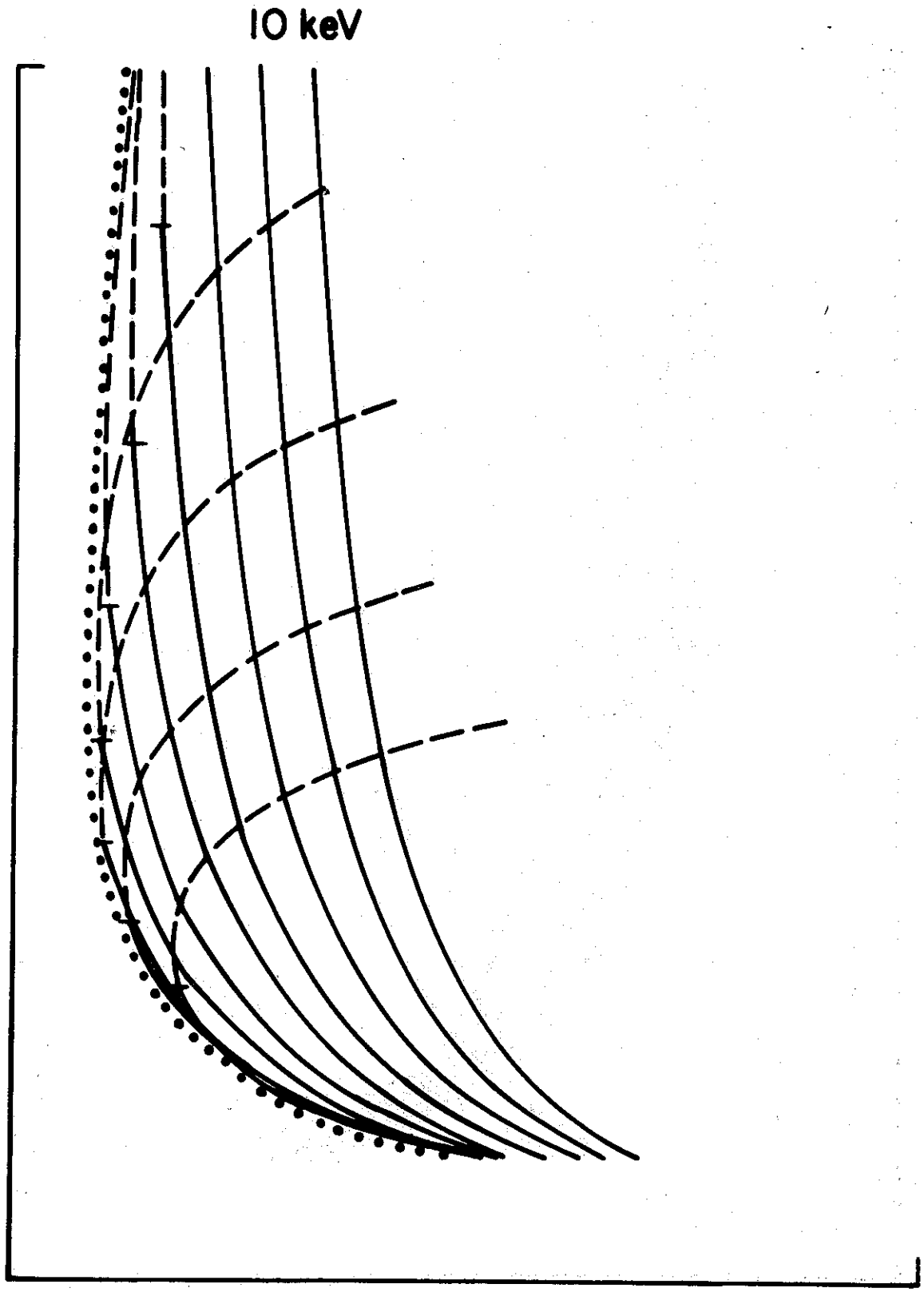

FIGURE 6.3. FAST HISSLER PRODUCED BY 10 keV ELECTRON "CLOUD."

higher frequencies at lower altitudes. At this energy even the highest altitude curve contributes to the sharp leading edge of the hissler, again outlined by the dotted curve. The "ducted" and "nonducted" regions that can be visualized almost coincide, as most of the upper portions of the high altitude curves are crossed by low altitude curves. The "nonducted" portions of the curves contribute to the leading edge above about 9-12 kHz. The leading edge leans back to later arrival times at frequencies above 10 kHz, creating a "nose" that is blunter than the noses of the curves that contribute to its shape. The "ducted" region widens from 56 ms at 2 kHz to 111 ms at 7.4 kHz, then narrows to 49 ms at 20 kHz. The "nonducted" region has the same shape up to 9 kHz, widens to 153 ms at 10 kHz, and narrows to 66 ms at 20 kHz.

Almost complete reversal in the order of the altitude curves has taken place in Figure 6.4, representing the fast hissler from a 5 keV electron cloud ($v_c = 4.2 \times 10^4$ km/s). Only the nonducted portions of the curves cross. For this case, the leading edge of the hissler has a significantly different shape depending on whether the "ducted" or "nonducted" regions of the frequency-time plane correspond to an actual hissler. In both cases, however, the leading edges lean back above 5.6 kHz, creating noses that again, are blunter than the noses of the curves that contribute to their shape. The leading edges of the hisslers may not be as sharply defined as in the 50, 20, and 10 keV examples. The "ducted" region is quite wide-209 ms at 2 kHz, 244 ms at 4.8 kHz, and 77 ms at 20 kHz, and the "nonducted" region is wider yet at frequencies above 4.8 kHz, where its shape differs from that of the "ducted" region: its width is 126 ms at 20 kHz.

The general trend with energy is clear. At electron energies above

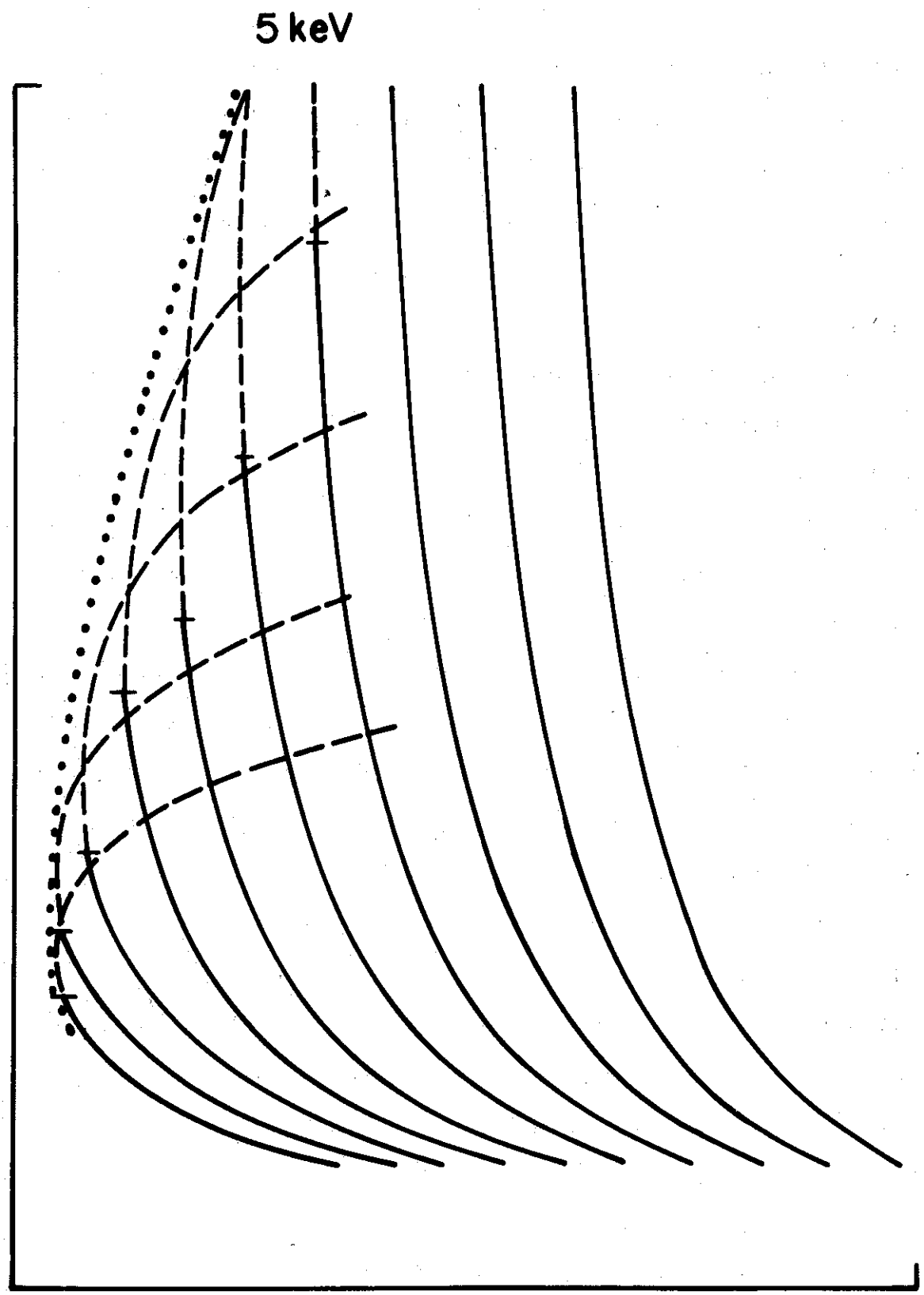

FIGURE 6.4. FAST HISSLER PRODUCED BY 5 keV ELECTRON "CLOUD."

50 keV, the arrangement of frequency-time curves approaches a configuration very similar to that in Figure 3.4 (but not identical with it because of the relativistic constraint $v_c < c$). At electron energies below 5 keV, the arrangement of frequency-time curves with respect to time of arrival is reversed and the spacing between the curves increases as the energy decreases. A sharp leading edge is present in both the "ducted" regions and the "nonducted" regions of the frequency-time plane for the fast hisslers assumed to be associated with electron clouds of energies 50 keV down to 10 keV. The detailed amplitude spectrum of fast hisslers is not predicted by this model but the absence of "caustic" curves (in the frequency-time plane) on the trailing edges of the "ducted" and "nonducted" regions leads one to expect longer "fall times" than "rise times" of the hiss bursts produced by electron clouds of these energies. The effect of including contributions to the fast hisslers from altitudes outside the range considered here would be to broaden them in time and to make the hissler duration as a function of frequency more uniform if contributions from lower altitudes are added, more irregular if contributions from higher altitudes are added. If this model is extended to frequencies below 2 kHz, it predicts increasing time delay for all electron cloud energies, but if the model is extended to frequencies above 20 kHz, it predicts decreasing time delay only for an energy of 50 keV, and then only up to a nose. For energies 20 keV and below it predicts increasing time delays.

For none of the energies considered do either the "ducted" nor "nonducted" regions possess the uniformity of duration at all frequencies found in fast hisslers. One effect not considered above has been that of non-zero pitch angle α, defined as the angle between the electrons'

momentum vector and the static magnetic field. It has been assumed that the pitch angle is zero and the electrons move with constant velocity down the field line. If however the initial pitch angle at 30,3000 km altitude is not zero then conservation of the first adiabatic invariant $p_\perp^2/B$, where $p_\perp$ is the perpendicular component of the particles' momentum, implies that the particles progressively lose their downward momentum as they encounter increasing static magnetic field B. The increase of B from 30,300 km to 12,300 km altitude is sufficient to bring to a halt electrons with initial pitch angles of 22^o or larger. The effect of this deceleration would be to increase the time delays of the frequency-time curves at lower altitudes, relative to those at higher altitudes. To first order the effect would be like extending the zero-pitch-angle calculations considered above to lower final altitudes, which as already mentioned would broaden the fast hisslers and make their durations more uniform as a function of frequency.

Observed fast hisslers can be compared directly with predictions based on the model presented in this chapter. Observed fast hisslers differ in their dynamic spectra, "dispersion," rise and fall times, durations, and (when present) nose frequencies, but the following have held generally: Durations are less than 200 ms and are independent of frequency; rise and fall time of a given fast hissler are about the same (one possible exception to this may be hissler 1 in Figure 4.3a, which appears to have a sharper leading edge than trailing edge) and are in the range 20-50 ms; nose frequencies are 5 kHz and above. None of the predictions of this chapter fits all these requirements simultaneously. The "ducted" 20 keV hissler, for instance, has a minimum width comparable to that of the briefer fast hisslers observed, but has a sharp leading

edge, unlike observed fast hisslers. A better fit to the shapes of observed fast hisslers in the frequency-time plane is obtained by suitably choosing a single curve in Figure 3.4 and broadening it in time by an amount equal to the observed duration of the hissler. Something similar to this might be effected within the framework of the moving-source model presented in this chapter by suitably manipulating the dynamic spectrum associated with each altitude. It is not clear, however, in what direction to proceed with such extensions to the model to maintain consistency with the data.

Among conclusions drawn from the fixed-source model presented in Chapter 3, various modifications are necessary for the moving-source model. These are relatively subtle except for modifications in the last section of Chapter 3, concerning power spectral densities near the source. A spacecraft VLF receiver in the path of the moving source would observe a rapidly increasing wave amplitude as the source approached, a peak as the source passed the spacecraft, and a rapidly decreasing (or zero) wave amplitude afterward. In some circumstances the fast hisslers might have a sharper leading edge as observed by the spacecraft than by a ground receiver.

VII. COMPARISON OF FAST HISSLERS WITH PURE NOISE IMPULSES

In previous chapters frequency-time space has been treated as if it were possible to put within any limited region of it infinitely many distinct "frequency-time curves" or trajectories. Implicit in the discussion of the "ducted" and "nonducted" regions defined in Chapter 6 was the assumption that these regions could in some sense be "filled" with an infinite continuum of "frequency-time" curves of which the curves in the figures were only a few examples. Strictly, this is not possible. The error Δf in a frequency measurement and the error Δt in a simultaneous time measurement made on the same signal are related by the uncertainty principle

$$\Delta f \cdot \Delta t \gtrsim 1 \ . \qquad (7.1)$$

There are no "points" in frequency-time space; only unit cells of (dimensionless) area 1. A signal can be characterized by the area of frequency-time space it occupies. If the signal is of fixed duration and bandwidth, this area is denoted the "time-bandwidth product" of the signal. This area is equal to the number of unit cells the signal occupies. The shapes of the unit cells are established by the instrument or technique used to analyze the signal. The Fourier transform establishes rectangular unit cells whose axes are parallel to the frequency and time axes of the space. The fast Fourier transform, which is a variant of the Fourier transform, acquires its speed at the cost of a certain loss of flexibility which limits the time dimension of the rectangle to some integral power of 2 times the basic sampling period τ of the analyzing instrument. The frequency dimension is determined accordingly.

The axes of the unit cell need not be oriented parallel to the frequency or time axes. The author has experimented with transforms based on the sine and cosine functions of the Fourier transform, but with a quadratic term in t included in the functions' arguments, thus: $\sin 2\pi(Ft + F't^2 + \phi)$, $\cos 2\pi(Ft + F't^2 + \phi)$. These functions have the effect of tilting the time-like axis of the unit cell so that it has a slope $2F'$ relative to the time axis. Depending on the choice of which samples are included in the sampling interval for each unit cell, the frequency-like axis of the unit cell can be parallel to the frequency axis as for the Fourier transform or have either a positive or negative "slope" relative to the frequency axis. The length of the sampling interval $\delta t = n\tau$, where τ is the basic sampling period and n is an integer, is related to the slope F' of the time-like axis by the requirement that the sine-like and cosine-like functions above be orthogonal on the unit cell, that is,

$$\int_{t=0}^{t=n\tau} \sin 2\pi(Ft + F't^2 + \phi) \cos 2\pi(Ft + F't^2 + \phi)\, dt = 0 . \qquad (7.2)$$

If $\delta F(=1/\delta t)$ is the separation in frequency of adjacent unit cells, and F is an integral multiple of δF, it follows that

$$F' = \frac{1}{2}(\delta F/\delta t) = \frac{1}{2(\delta t)^2} = \frac{1}{2n^2\tau^2} , \qquad (7.3)$$

so that F' is limited to a set of discrete values that depend on the basic sampling period τ. The transform based on these functions has a resolution equal to that of the Fourier transform, however, the author has not been able to exhibit a "fast" version of this transform--"fast" having the meaning here that the number of repeated arithmetic operations increases with n, the number of independent data points analyzed, more

slowly than n^2 (the fast Fourier transform requires $\sim n \log_2 n$ repeated arithmetic operations). The periodicity of the sine and cosine functions which makes possible certain simplifications in arithmetic for the fast Fourier transform is absent here.

Other transforms, such as those based on Haar and Walsh functions, also have a resolution equal to that of the Fourier transform, but they do not have a simple geometrical interpretation in frequency-time space as do the transforms discussed above. Geophysical phenomena seem not to occur as Haar or Walsh functions, which therefore are not as directly applicable to geophysics; however, the Haar and Walsh transforms do have fast versions.

It is possible that every transform has, at least potentially, a fast version; however no general meta-algorithm now exists which can produce a fast version of the transform based upon an arbitrarily chosen set of spanning orthogonal functions. Should such a meta-algorithm be developed it would open to view the exciting prospect of rapidly analyzing natural phenomena with orthogonal mathematical functions most suited to the phenomena, perhaps even derived from data itself; rather than by functions having only the distinction that their transform is fast. Such a development might bring about within the field of computer science the kind of radical reorientation of techniques described by Kuhn [1970].
It should be pointed out that the sequence of mathematical operations performed in computer fast Fourier transform routines depends only on the periodicity of the sine and cosine functions, and not on any of the intrinsic symmetries of these functions. Any transform based on some other set of periodic orthogonal mathematical functions, square waves for example, has a fast version obtained simply by replacing the coefficient

matrix of the Fourier transform with that of the other orthogonal mathematical functions. This transform could then be performed with $\sim n \log_2 n$ mathematical operations. Perhaps the absolute lower limit on the number of operations required for a transform is even less than the order of $n \log_2 n$.

The difference in dynamic spectrum analysis techniques can be revealed by graphic displays of their output. In Figures 7.1 and 7.2 are shown enlarged views of the same hissler data (August 14, 1967) given in Figure 3.1. The difference between the analog (Rayspan, Figure 7.1) and digital (fast Fourier transform, Figure 7.2) displays is more apparent on close inspection than from a distance. Figure 7.3 shows the details of the 3-level (0,1,5) digital display employed to generate Figure 7.2. What appears to the eye at a distance to be a uniform gray tone is seen at close range to be an irregular pattern of light and dark. This pattern agrees in detail in the Rayspan and fast Fourier transform displays and is not an artifact of the method of analysis. The Rayspan display appears somewhat more continuous partly because of the extended spot of the oscilloscope in the recording apparatus and partly because consecutive frequency scans of the instrument overlap. The two display techniques are comparable in resolution.

Fast hisslers are composed of VLF radio noise. This is made evident by their point-to-point intensity variations in frequency-time space, which is visually comparable to the "speckle pattern" produced by laser light [Collier et al., 1971]. Figure 7.4 is a photograph of the "speckle pattern" produced by coherent light from a helium-neon laser. Collier et al., show that if the intensity of the speckle pattern results from the superimposition of randomly phased waves of scattered amplitudes,

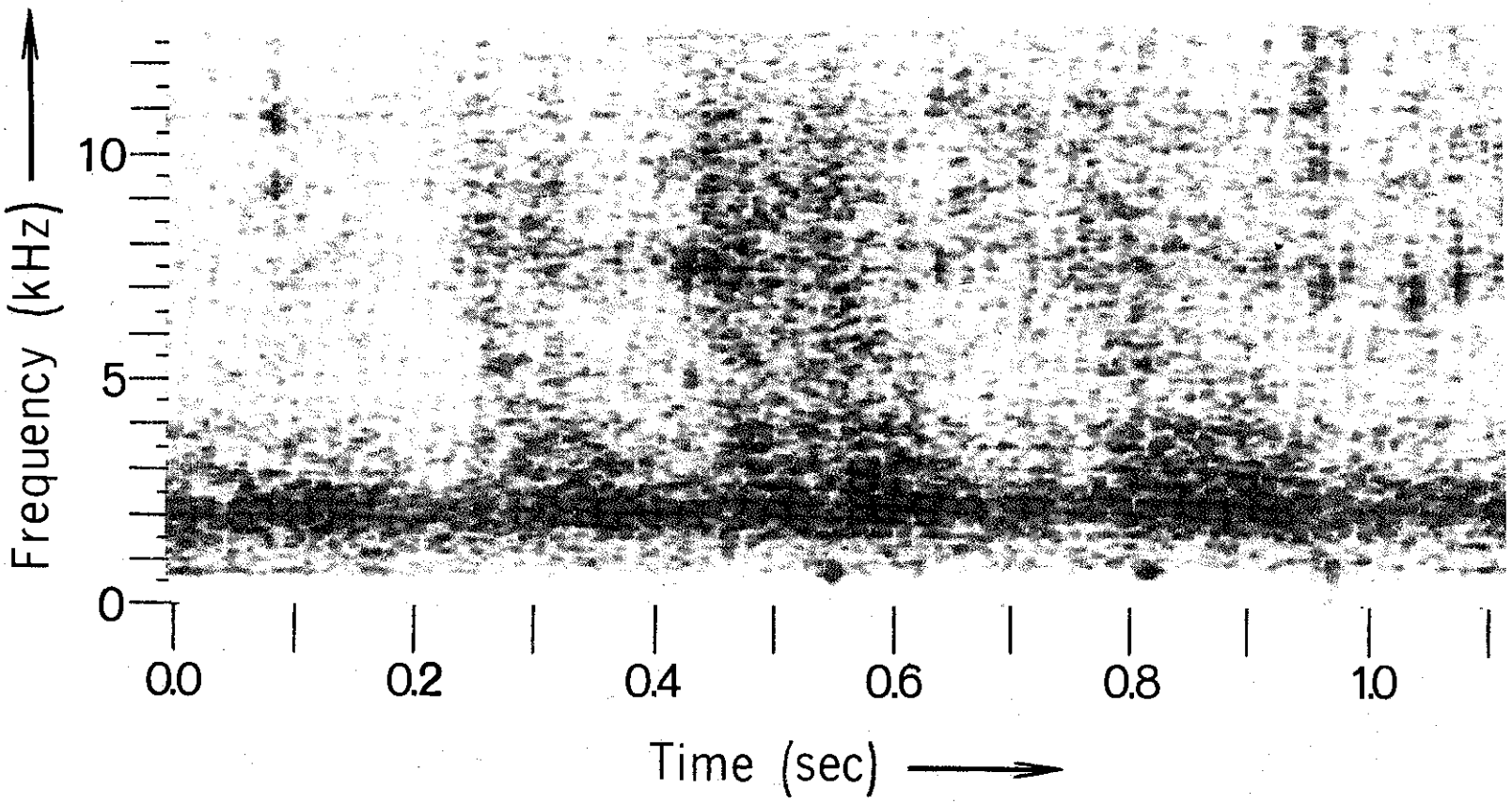

FIGURE 7.1. RAYSPAN DYNAMIC SPECTRA OF FAST HISSLERS. 0439 UT on 14 August 1967.

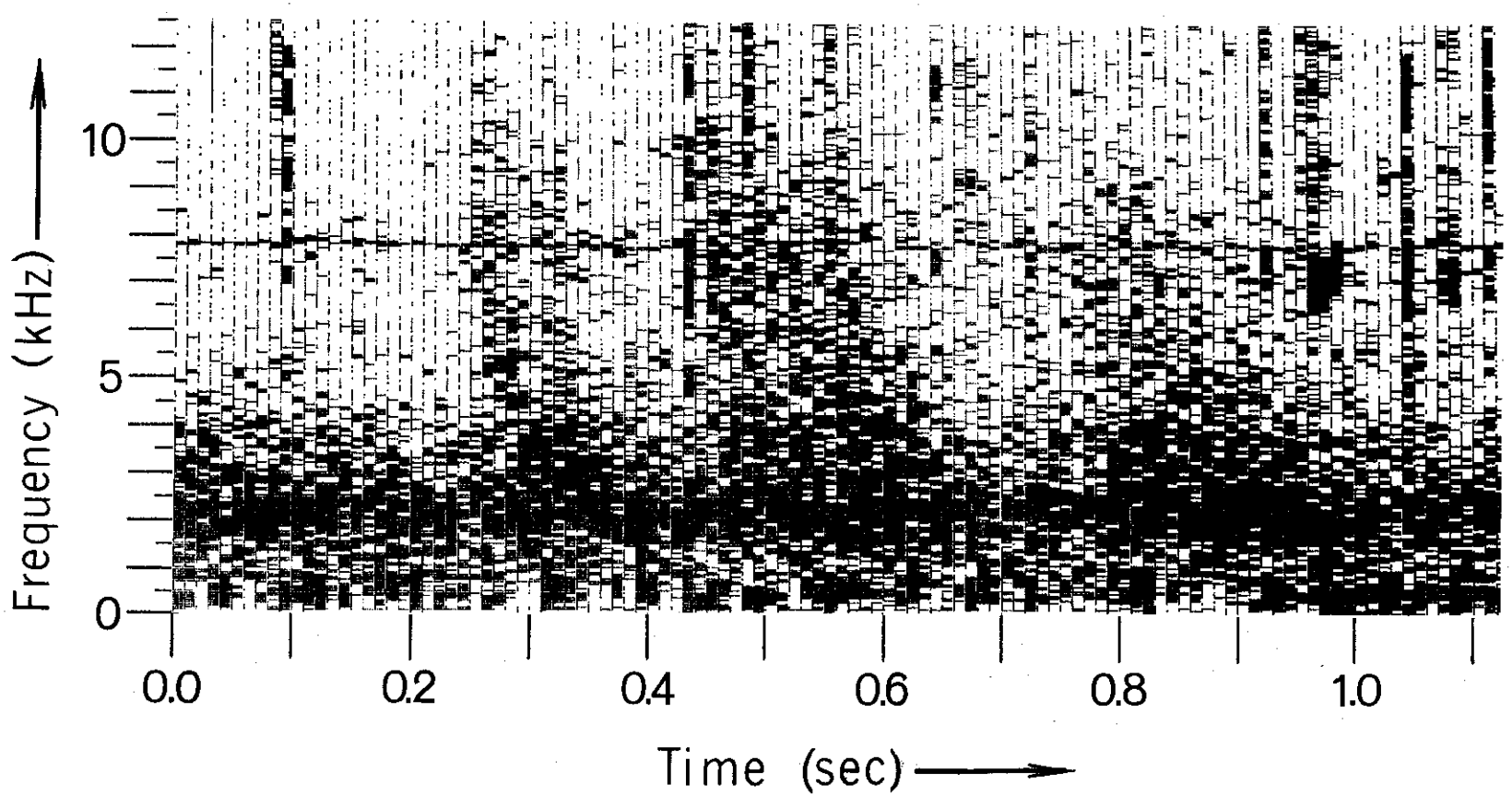

FIGURE 7.2. FAST FOURIER TRANSFORM DYNAMIC SPECTRA OF FAST HISSLERS (SAME DATA AS FIGURE 7.1).

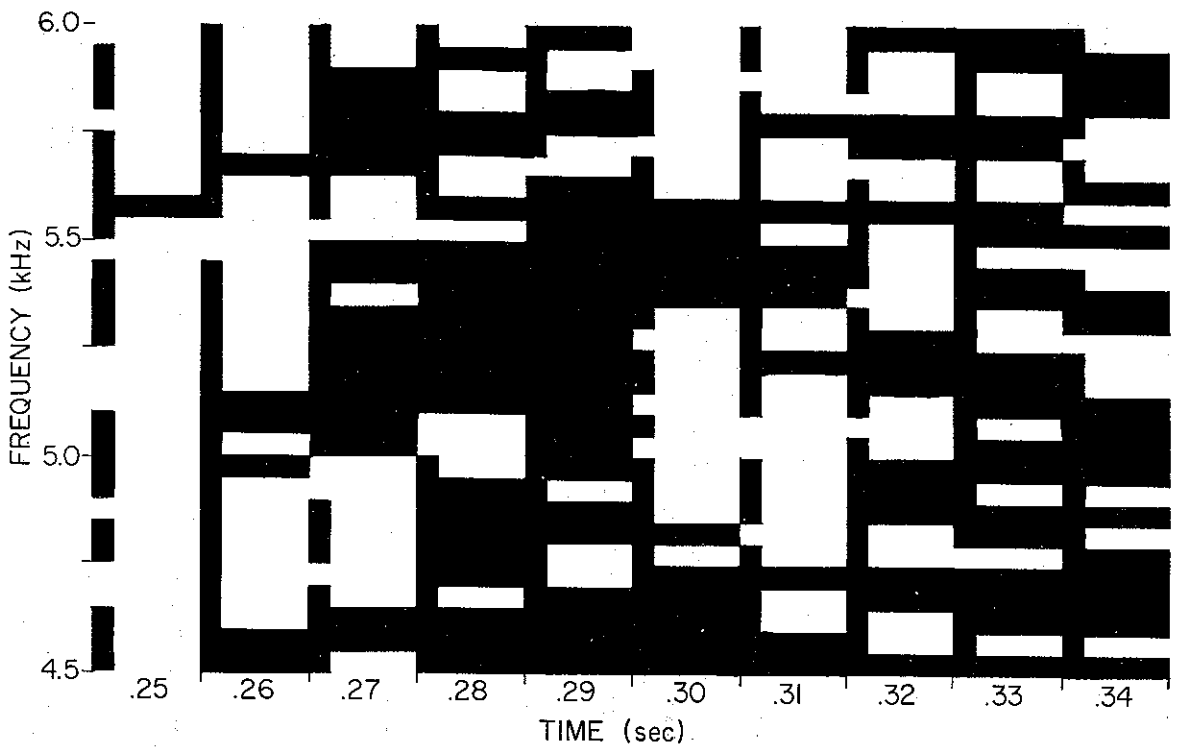

FIGURE 7.3. DETAILS OF 3-LEVEL (0,1,5) DIGITAL DISPLAY TECHNIQUE EMPLOYED TO GENERATE FAST FOURIER TRANSFORM DYNAMIC SPECTRA.

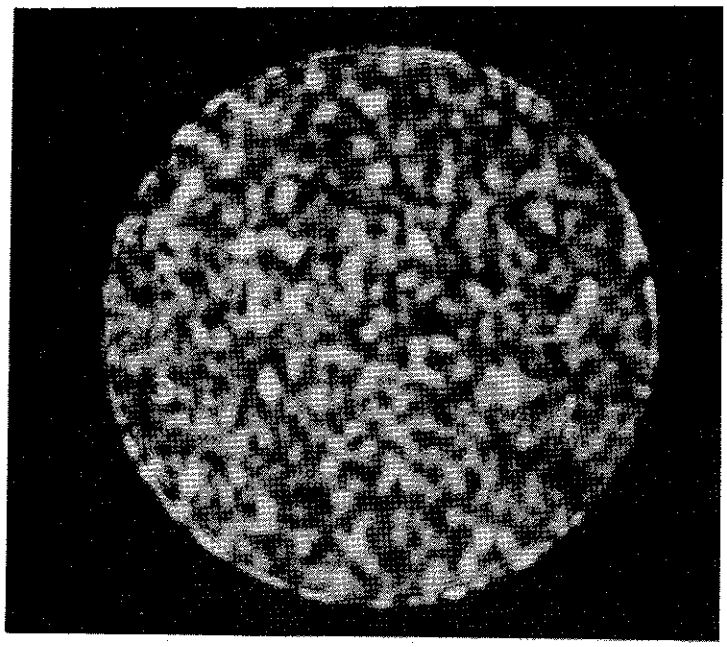

FIGURE 7.4. TWO-DIMENSIONAL COHERENT LIGHT SPECKLE PATTERN. Helium-neon laser.

then the amplitudes of the resultants have a Rayleigh distribution and the root-mean-square of the intensity fluctuations F is related to the mean intensity $\bar{I}$ by

$$F \equiv [\overline{(I-\bar{I})^2}]^{1/2} = [\overline{I^2}-\bar{I}^2]^{1/2} = \bar{I} . \qquad (7.4)$$

Quoting the above-mentioned authors, "Therefore the ratio of the root-mean-square of the intensity fluctuations to the mean intensity is one." If the sources of fast hisslers are composed of large numbers of individual oscillators, radiating independently in frequency and randomly in amplitude and phase, then (in a region of frequency-time space in which fast hissler intensity is approximately constant) the intensity distribution of fast hissler waves should have the same characteristic. This hypothesis was tested in a study whose results are presented in this chapter.

It was decided, somewhat arbitrarily, that the hypothesis be tested on the August 14, 1967 fast hisslers and that the requirement of approximately constant intensity would be met by taking samples from "rectangles" 1 kHz tall by 30 or 40 ms wide in the frequency-time plane, arrayed along the highest-intensity "ridges" of the hisslers (Figure 7.5). In Figure 7.5, "rectangles" A_3 to A_{11} (the subscript refers to the lower boundary frequency), B_3 to B_{10}, and Q_1 were 30 ms wide, and "rectangles" C_3 to C_{10} were 40 ms wide. The arrow in the box labeled "W" points to a barely-visible whistler to be discussed below. The "rectangles" contain 30 or 40 unit cells, however, the number of amplitude values a calculated by the fast Fourier transform program is twice the number of unit cells, or 60 or 80 respectively, because the data were "windowed" by a $\cos^2$ window and the frequency scans were overlapped by half. All the amplitude values from each "rectangle" were included in the calculation of the ratio

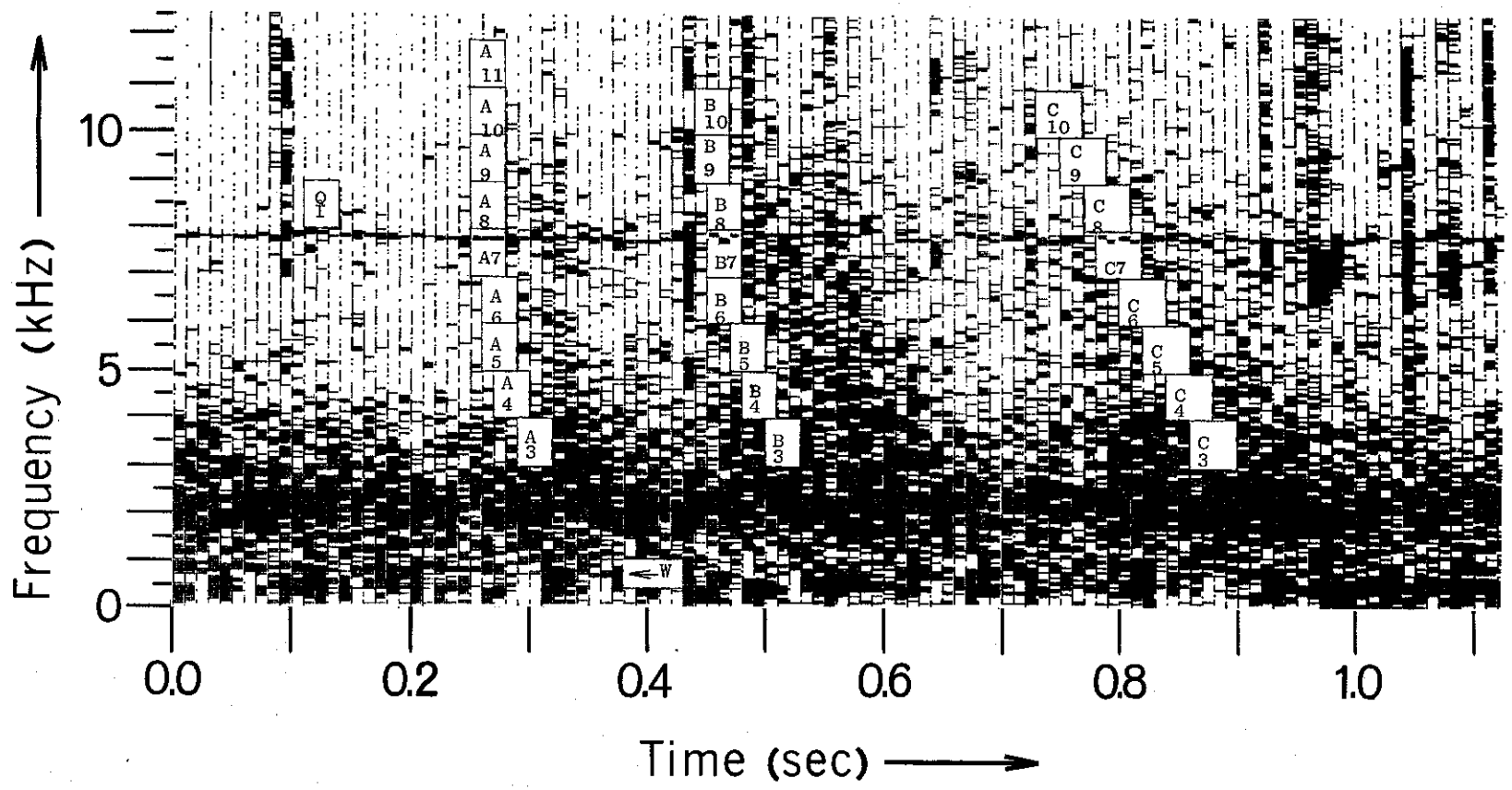

FIGURE 7.5. DATA SELECTION FOR NOISE FLUCTUATION TO MEAN INTENSITY RATIO CALCULATIONS.

$R = F/\bar{I}$ (Table 3) and the amplitude values were scaled in "bins" to produce the amplitude histograms in Figures 7.6 - 7.9. Exceptions were "rectangles" A_7, B_7, and C_7 from which two amplitude values from each frequency scan "contaminated" by the signal from the Navy fleet transmitter NAA at 7.8 kHz were eliminated from the calculations. (A separate calculation was done on the amplitudes of NAA in the frequency scans 1-113 inclusive. The NAA signal, originally 17.8 kHz, has been "aliased" down to $f_A = 7.8$ kHz $= f_N - f_{NAA}$, where $f_N = 25.6$ kHz is the Nyquist or sampling frequency.)

The ratios R have been tabulated in the fourth column of Table 3. All the ratios for the fast hisslers fall in the range $1.000 \pm .250$ and 72% fall in the range $1.000 \pm .100$. More of the ratios are less than 1.000 than are greater than 1.000, but the statistical significance of this is not known to the author. Barring this tendency, however, the ratios are consistent with a "pure-noise" interpretation.

Histograms drawn from the numbers of amplitude values in the "bins" are given in Figures 7.6 - 7.9. Superimposed on each histogram is a continuous curve of the function $p(a) = Ka \exp(-a^2/\sigma^2)$ (the Rayleigh distribution) with K and σ chosen so as to equalize the area under the curve and the mean, respectively, to those of the histogram. It can be seen that each histogram roughly matches the shape of the curve, and as a increases the last non-empty "bin" occurs at about 3 times the mean amplitude (where the curve is falling rapidly toward its asymptotic value of 0).

The same ratio calculation was performed for "rectangle" Q_1 containing background hiss, the sferic in Scan 10 at .09 s, the whistler indicated in Figure 7.5 by the arrow, and the NAA keydown transmission

TABLE 3. RATIOS OF ROOT-MEAN-SQUARE INTENSITY FLUCTUATIONS TO MEAN INTENSITIES.

Type of signal	Denoted in Figure 7.5 by	Number of amplitudes a	$R(=F/\bar{I}=F/\bar{a}^2)$
Hissler	A_{11}	60	1.059
"	A_{10}	60	0.905
"	A_9	60	1.021
"	A_8	60	0.968
"	A_7	54	0.898
"	A_6	60	0.931
"	A_5	60	0.861
"	A_4	60	0.916
"	A_3	60	0.895
"	B_{10}	60	1.030
"	B_9	60	1.083
"	B_8	60	0.846
"	B_7	54	1.086
"	B_6	60	0.932
"	B_5	60	0.941
"	B_4	60	0.974
"	B_3	60	1.098
"	C_{10}	80	0.995
"	C_9	80	0.902
"	C_8	80	0.959
"	C_7	72	0.829
"	C_6	80	0.919
"	C_5	80	0.763
"	C_4	80	0.989
"	C_3	80	0.893
Background hiss	Q_1	60	1.265
Sferic	(Scan 10 at .09 s)	251	2.154
Whistler	W	38	0.796
NAA Key-down transmission	7.8 kHz (see text)	224	0.671

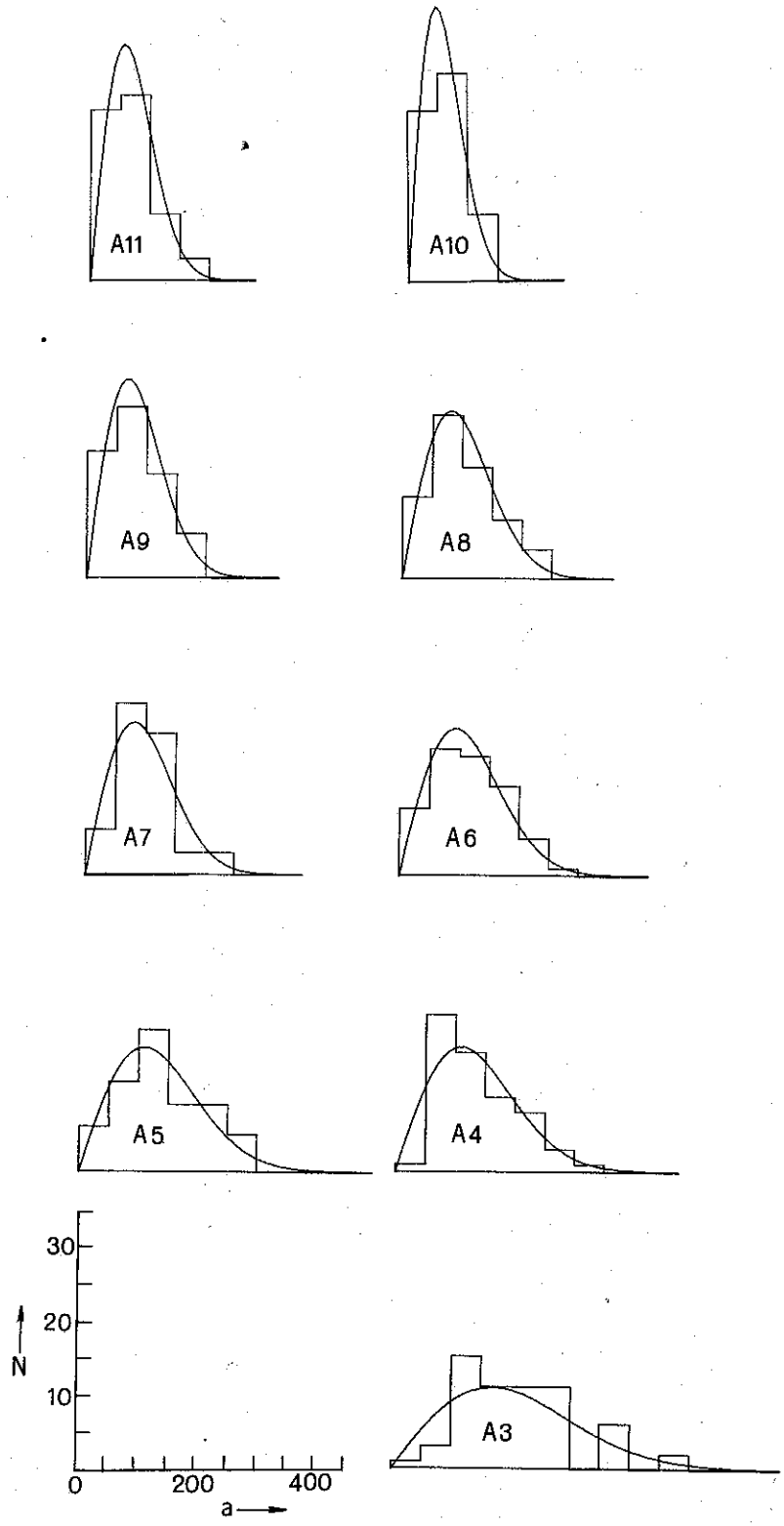

FIGURE 7.6. AMPLITUDE HISTOGRAMS A_3-A_{11}.

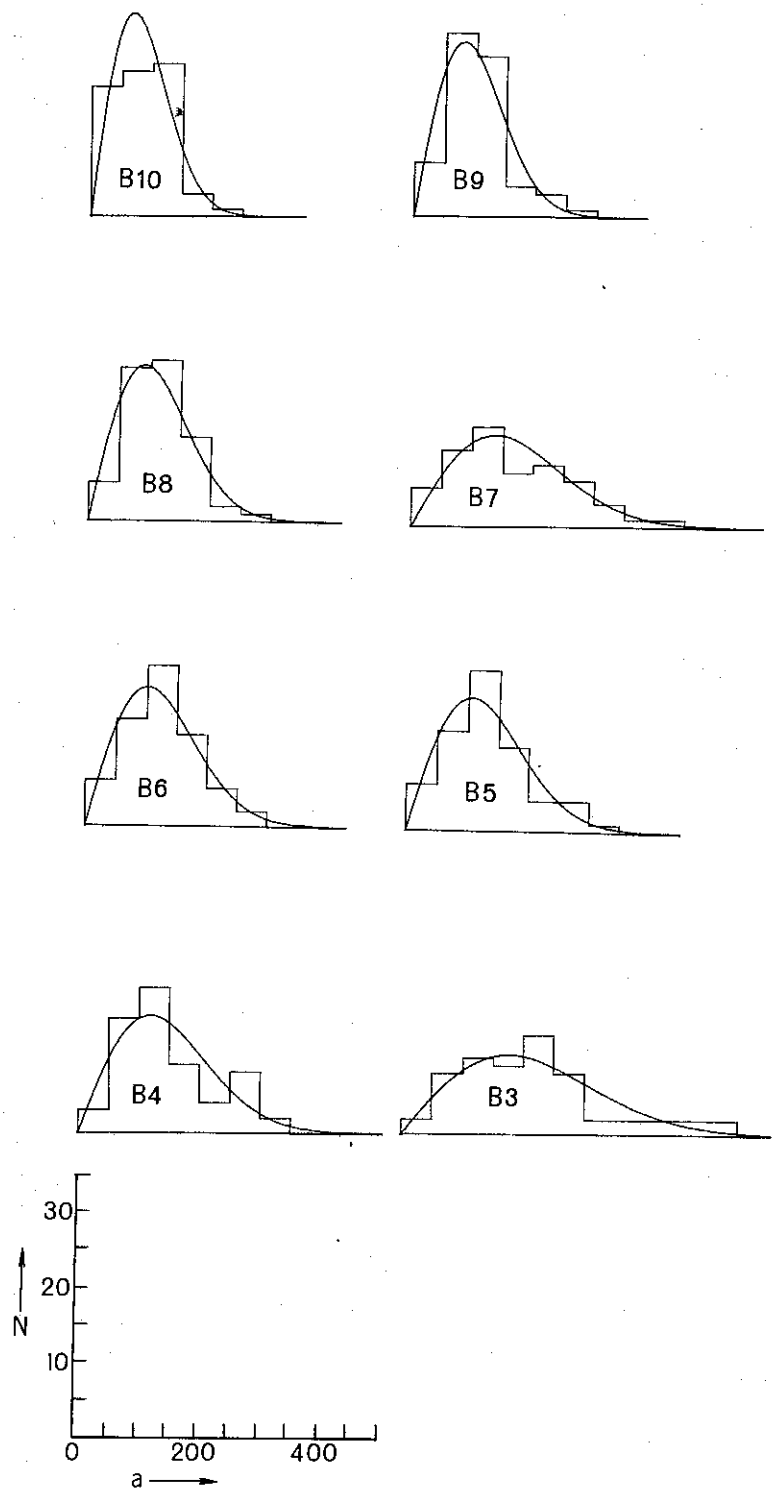

FIGURE 7.7. AMPLITUDE HISTOGRAMS B_3 - B_{10}.

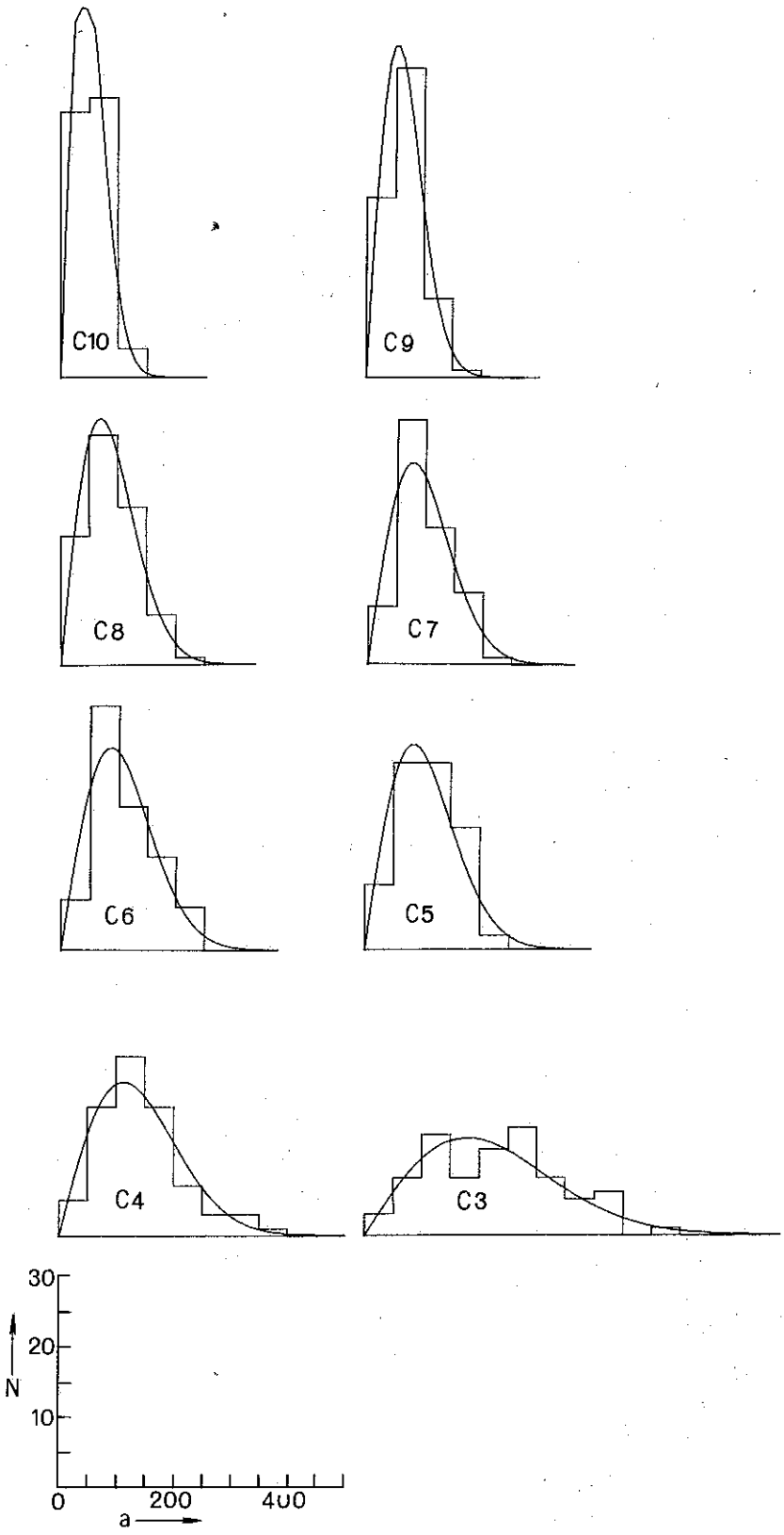

FIGURE 7.8. AMPLITUDE HISTOGRAMS C_3- C_{10}.

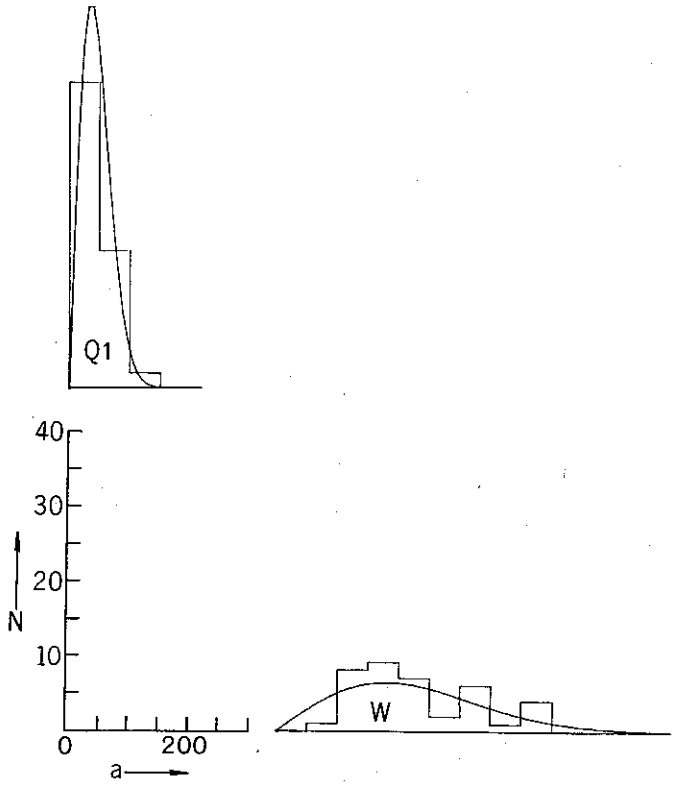

FIGURE 7.9. AMPLITUDE HISTOGRAMS W, Q_1.

observed at 7.8 kHz. Table 3 shows the results of these calculations. With the exception of the whistler, these signals have fluctuation to mean intensity ratios that fall outside the 1.000±.250 limits that include all the fast hissler ratios. The whistler's ratio, 0.796, is moderately low but not significantly so. The NAA keydown transmission has a ratio well above 1, probably because the Scan 10 amplitude distribution is bimodal (it contains both the sferic signal above 6 kHz and the steady hiss signal below 4 kHz). The background hiss ratio is also well above 1, but the reason for this is unknown. Histograms and Rayleigh distribution curves for the whistler W and background hiss Q_1 amplitude distributions are given in Figure 7.9.

It has been shown above that the ratio of intensity fluctuations to mean intensity is quite close to the theoretical ratio of 1.0. While this has been shown to be true for fast hisslers, it should also hold for a wide range of VLF phenomena, including steady and impulsive hiss; but as has also been shown, some VLF signals have fluctuation to mean intensity ratios significantly different from 1.0. It is of interest to attempt to predict the intensity fluctuation to mean intensity ratios for VLF phenomena that have not as yet had this ratio calculation performed on them. A signal that is constant in amplitude will, of course, have $R = F/\overline{I} = 0$. This would be the case for VLF signals received from nearby transmitters, locally induced power-line harmonics, and so forth.

Helliwell and Crystal [1973] have predicted, for some forms of VLF emissions produced by wave-particle cyclotron interactions, an almost precisely exponential growth in intensity with time, through several e-foldings of intensification. The ratio R can be calculated for a signal

with this type of intensity variation. Consider a signal whose intensity varies as

$$I(t) = I_0 \exp(\alpha t) \tag{7.5}$$

from t=0 to t=T. Then

$$\bar{I} = \frac{1}{T}\int_0^T I(t)\,dt = \frac{1}{T}\int_0^T I_0\exp(\alpha t)\,dt = \frac{I_0}{T}\,\frac{(\exp(\alpha T)-1)}{\alpha} \tag{7.6}$$

and

$$F = \left[\frac{1}{T}\int_0^T (I(t)-\bar{I})^2 dt\right]^{1/2} = \left[\frac{1}{T}\int_0^T (I(t))^2\,dt - \bar{I}^2\right]^{1/2} \tag{7.7}$$

$$= \left[\frac{1}{T}\int_0^T I_0^2\exp(2\alpha t)\,dt - \bar{I}^2\right]^{1/2}$$

$$= \left[\frac{I_0^2}{\alpha T}\left\{\frac{1}{2}(\exp(2\alpha T)-1) - \frac{(\exp(\alpha T)-1)^2}{\alpha T}\right\}\right]^{1/2}.$$

The ratio $R = F/\bar{I}$ with F and $\bar{I}$ given by Eq. (7.7) and Eq. (7.6) respectively can be evaluated at two limits representing extreme cases.

Case 1. $\alpha T \ll 1$. Physically this represents a situation in which the signal grows in intensity very little during the interval when it is observed. For this case we find $R \Rightarrow (\alpha T)^{1/2}$ in the limit $(\alpha T) \Rightarrow 0$, which is in accord with our expectation that R approach 0 in the limit of zero signal intensity variation.

Case 2. $\alpha T \gg 1$. Physically this represents a situation in which the signal grows in intensity many e-foldings during the interval when it is observed. For this case we find $R \Rightarrow (\alpha T/2)^{1/2}$ in the limit $(\alpha T) \rightarrow \infty$. This is a less obvious result, since it predicts that the variations in intensity can exceed the mean intensity itself and, in fact,

the ratio can become arbitrarily large as the ratio of observing interval to e-folding time ($1/\alpha$) increases.

In both cases if the signal consisted of the superimposition of numbers of emissions whose intensity variations were given by Eq. (7.5), the ratio R would be closer to 1 than for single emissions of the same type.

For emissions of the type discussed by Helliwell and Crystal the root-mean-square intensity fluctuation to mean intensity ratio can therefore be either greater than 1 or less than 1 depending on whether the observing interval is short or long compared to the e-folding time of the growth in intensity.

VIII. POTENTIAL DOUBLE LAYERS AS AN ENERGIZATION MECHANISM FOR AURORAL ELECTRONS

Because of the association of VLF hiss at high latitudes with the occurrence of aurora, the assumption is usually made that the current of energetic (1 keV to a few tens of keV) electrons that strikes the atmosphere and produces the aurora is also the source of the hiss. Certainly the power suffices: In the brightest auroras as much as 10^{-3} Wm^{-2} of beam power is being converted to light emission, while the auroral hiss power (assuming the generous bandwidth of 100 kHz) is at maximum only about 10^{-7} Wm^{-2}. The results reported in Chapters 3, 4, and 5, and to a lesser extent Chapter 6, lead naturally to the question whether the auroral electrons can be accelerated to their observed energies in regions of the magnetosphere that are small in dimension compared to their altitudes. In laboratory plasmas carrying dc currents, potential double layers are often observed to form when the current exceeds a certain threshold. Double layers are sites where the energy injected into the plasma as the charge supplied at the anode-cathode potential difference is converted to the kinetic energy of "beam" electrons and ions accelerated in the layers. The number of such double layers present increases with current, but the thickness of each does not. This remains small compared with cathode and anode separation and inter-layer spacing. In this chapter the applicability of the theory of potential double layers to the acceleration and deceleration of auroral electrons is investigated.

Potential double layers are local density depletion regions in current-carrying plasmas. Conditions relating to their presence in the ionosphere are discussed in an article by Block [1972]. In a companion

article Carlqvist [1972] discusses the process of their formation from rarefaction instabilities. Double layers are laminar, that is, they are flat and their lateral extent is many times their thickness. Double layers are invariably perpendicular to the direction of current flow in the plasmas they are immersed in. In magnetized plasmas the current flow is parallel to the magnetic field, and therefore the double layers cut across field lines. In the double layers there is a substantial deviation from quasi-neutrality; however, the electric charge per unit area (integrated through the thickness) is very close to zero because the positive surface charge density on one "face" of the double layer is very nearly equalled in magnitude by the negative surface charge density on the other face. This is the origin of the name "double layer" applied to the phenomenon. The electric field within the double layer is directed along the thickness, and is sufficiently large that the potential difference across the layer is of the order of kT/e or larger, even though the thickness is only one to several Debye lengths $\lambda_D=(kT_e/4\pi N_e e^2)^{1/2}$, where T_e is the electron temperature, as distinct from the plasma temperature $T = (T_e + T_{ion})/2$, k is Boltzmann's constant, N_e is the electron number density, and e is the electron charge. In the ionosphere where N_e is in the range 10^4 to 10^6 cm^{-3} and $T_e \approx 10^3$ K, the Debye length is in the range 10^{-1} to 1 cm. The Debye length increases with altitude but is only about 10 to 100 cm at 10^4 km altitude. (The Debye length is conventionally described as the shielding distance of an isolated charge immersed in a plasma, or in other words the distance over which deviations from charge neutrality can be sustained without the input of energy against neutralization by the thermal motion of the plasma particles.) Consequently the probability of observing directly a double layer with a

spacecraft experiment is quite small, but on the other hand indirect effects of double layers might be more clear cut than those of phenomena with a greater extension in space.

A rocket experiment that may have detected indirectly the presence of ionospheric double layers was performed by Albert and Lindstrom [1970]. Their particle detector, launched into an aurora, measured the energy and pitch angle of electrons with 1 keV and one-half degree resolution, respectively. Two kinds of structure were observed which were interpreted as resulting from the presence of double layers on the field lines through the rocket. One structure, a trough in the pitch angle distribution at about 80^{o} pitch angle, was interpreted as resulting from the downward acceleration by a 500-1000 volt double layer of nearly mirroring electrons (electrons whose pitch angle was about 90^{o} prior to their double-layer acceleration). The double layer was said to be a few hundred kilometers or less above the rocket. The interpretation of the trough was recognized as ambiguous, however: with both the double layer altitude and potential drop as adjustable parameters the pitch angle distribution could have been equally adequately fit by a model with a single, 9 kV double layer at 1 R_e (= 6370 km) altitude. The latter would have supplied 90% of the electron energy. The other structure, multiple energy-dependent peaks in the pitch angle distribution, were interpreted with less ambiguity as resulting from double layers at 250, 270, and 280 km altitude. There was a potential difference of 160 volts across each of the upper layers and 80 volts across the lowest double layer. The peaks in the pitch angle distributions from which the interpretations were made persisted about 18 seconds. In each of the cases studied the electric field in the layer was deduced to have been directed upward (accelerating

electrons downward). No structure of the type discussed would have resulted from downward-directed double layers.

It should be pointed out that even for the double layers associated with the pitch angle peaks there remains an ambiguity which the data can not resolve. Two sufficiently closely spaced double layers with potential differences V_2 each will produce the same pitch angle distribution at the detector as a single double layer at the same average altitude, with the potential difference $V_1 = 2V_2$. The same is true of a more general aggregation of double layers (of both orientations) whose overall potential difference is V_1, if the thickness of the aggregation is sufficiently small. This can be understood through the following considerations (based upon the calculations of Albert and Lindstrom [1970]): Assume that electrons of energy W_1 are spiralling along a magnetic line of force of strength B_1 at a pitch angle, or angle between the velocity vector and the magnetic field, denoted by α_1, when an electrostatic double layer with an accelerating voltage V is encountered. The direction of acceleration is such as to increase the parallel component of the electrons' velocity. We assume that the "first adiabatic invariant" or the quantity $\mu = W_\perp/B$, is conserved, where $W_\perp$ is the portion of the total electron kinetic energy due to the component of velocity perpendicular to the magnetic field. After the electrons cross the double layer, they continue to travel along the field line to a point where the field may have a different value, B_0. The electron energy at this point is

$$W_0 = W_1 + V .$$

The electron pitch angle α_0 at this point can be calculated assuming the constancy of the first adiabatic invariant:

$$\frac{W_1 \sin^2\alpha_1}{B_1} = \frac{W_0 \sin^2\alpha_0}{B_0}$$

Then

$$\sin^2\alpha_0 = \frac{B_0}{B_1}\,(1-V/W_0)\,\sin^2\alpha_1 \ . \qquad (8.1)$$

The assumption made here is that the magnetic field variation across the double layer is zero or negligibly small compared to the magnetic field change between point 1 and point 0, or B_1-B_0. If the magnetic field changes gradually from B_1 to B_0 between point 1 and point 0, the assumption is equivalent to the assumption that the thickness of the double layer is small compared with the distance from point 1 to point 0. No assumption is made about the details of the acceleration process itself, only that the electron total energy is increased from W_1 to W_1+V without changing the first adiabatic invariant in the process. Since double layer thicknesses are less than a meter, while in the magnetosphere at least 1700 km altitude increase is required for a factor of 2 decrease in B, it is clear that existing techniques are not precise enough to distinguish between a single double layer and an aggregation of many closely spaced but distinct double layers. The conclusions drawn from particle data by Albert and Lindstrom are, therefore, not inconsistent with the presence of double layers as they suggested, but are insufficient to determine that single double layers, multiple double layers, or some other mechanism of generation of parallel dc electric fields, produce the observed pitch angle distributions.

Albert and Lindstrom's electron spectra were nearly monoenergetic. That was considered to be a strong indication that the primary process for energizing the electrons involves electrostatic fields rather than

stochastic processes. This hypothesis is not altered by the conclusions we have reached above.

Double layers grow from inhomogeneities in a current-carrying plasma. Carlqvist [1972] predicts that the growth takes place in two distinct stages. In the first stage, the overall potential drop remains zero while a plasma density dip grows. Particles that are accelerated out of the growing dip remain in its vicinity. Only when the plasma density in the dip is too tenuous to carry the full current does charge begin to accumulate on opposite sides of the dip, a simple double layer form, and the particles crossing the double layer acquire a kinetic energy increment. These particles can travel large distances from where they are accelerated.

Carlqvist's theory does not include the details of the process by which a simple double layer develops out of the plasma density dip. The time scale of this process may be given approximately by a semi-empirical theory based upon the observed formation times of double layers in laboratory plasmas, which is tens of milliseconds in air-filled discharge columns. The appropriate scaling factor is the ratio of the Debye length in the magnetosphere to that in laboratory plasmas (since the double layer thickness is closely related to the Debye length), divided by the ratio of the respective ion thermal velocities. If the ion temperatures are equal (which is assumed) the ion thermal velocities vary inversely as the square root of the mean ion mass, which is assumed to be 1 (amu) for the magnetosphere and 28 for laboratory plasmas. The thermal velocity ratio with these assumptions is 5.3. The ratio of Debye lengths is in the ratio of ~ 10 to ~ 100, so the formation time of magnetospheric double layers might take from the order of 40 milliseconds to 200 milliseconds or 1 second.

This time is somewhat longer than the observed rise times of fast hisslers, but only moderately so. The range does include part of the range of rise times.

Another, more subtle aspect of Carlqvist's theory is that, being one-dimensional, it does not predict the lateral extent of the double layer. It was mentioned above that double layers are many times wider than they are thick. In fact, in laboratory plasmas the double layers usually extend across the whole width of the discharge in both lateral dimensions, as if the average unconfined double layer width were very large compared to the diameter of the discharge tubes usually employed. Even when no constrictions are placed within the discharge tube and the double layers appear and disappear at random locations along its length, the formation of a particular double layer is nearly simultaneous at all points on its lateral extent. Departures from simultaneity are a small fraction of the time required for formation. If the double layer has no precursor-that is, if the double layer itself establishes, through an instability mechanism, the conditions for its lateral expansion-then the lower limit to the time required for the establishment of a complete double layer is the time required for the wave of expansion to propagate across the current-carrying region. Carlqvist's theory comprises neither a precursor mechanism nor a wave of lateral expansion and therefore is incomplete. If the precursor mechanism or wave of lateral expansion takes place through the means of lateral transport of ions at their thermal velocities, then the estimates made above on the time required for development of magnetospheric double layers must be increased by a factor which is the ratio of double layer lateral extent to the thickness. This would imply a time of many seconds to minutes for the development. There is,

however, no direct experimental evidence of this means of expansion, which has the theoretical difficulty of requiring that the thermal ions be beamed in a very small range of angles close to the perpendicular to the current. Such beaming is not implicit in the one-dimensional double layer theory.

Finally, double layer theory does not predict the potential drops across double layers, although Carlqvist does present some calculations of the relationship between double layer thickness and potential drop. If one can be measured, the other can be computed. Neither quantity, however, has been measured in single magnetospheric or ionospheric double layers. It is not possible to make as precise a prediction of potential drop by the combination of empirical measurements made on double layers in laboratory discharge tubes, and "similarity transformations" [Alfvén and Fälthammar, 1963] as was done above to predict the rise times of magnetospheric double layers. The reason is that the potential drop is not directly derived from quantities that scale unambiguously in similarity transformations. The potential drop may be most directly determined by any one of the following: the applied electric potential; ionization potentials of the neutral constituents; the electron temperature; the ion temperature; or some as yet undetermined quantity. (Of course, ionization potentials do not "scale" at all, but the relative concentration of various neutral constituents may affect the importance in some sense of the particular ionization potentials.)

Existing potential double layer theory has been found to be incomplete in its formulation, lacking as it does the ability to predict the lateral spatial extent of a magnetospheric double layer, the time required for the lateral spreading of an incipient double layer, and the potential drop.

It has been shown also in this chapter that existing experimental evidence that has been interpreted as indicating the presence of ionospheric double layers is consistent with alternate interpretations as well. Extrapolated values of the development time of double layers (taking laboratory plasma parameters as the basis for extrapolation) are in the same range as the rise times of fast hisslers, which are $\sim 20 - \sim 50$ ms. This extrapolation does not take into account the time required for lateral expansion, since that is unknown. In regard to the applicability of double layers to the generation of the fast hisslers, double layer theory itself does not provide for the collective organization of electron perpendicular velocities into at least partial coherency. This velocity organization is required, because incoherent radiation by the Cerenkov mechanism, as was pointed out in the Introduction, has been found to be insufficient to account for auroral hiss at these frequencies. It must be concluded that the existing knowledge, theoretical and experimental, of double layers is insufficient to permit an unambiguous association of them with fast hisslers, or in fact with any form of auroral hiss.

IX. SCIENTIFIC CONCLUSIONS AND SUGGESTIONS FOR FURTHER WORK

In this chapter the conclusions reached in each of the previous chapters are summarized, and the scientific contribution in each chapter is placed in proper perspective in relation to the work as a whole. In addition, suggestions are made for further research on topics which follow immediately from the work in that chapter. In the final part of this chapter the attempt is made to describe how this work relates to areas of current interest in the scientific community, and to suggest the initiation of new fields of scientific research.

Chapter 1 contained a history of auroral hiss observations and compared the four most recent attempts in the literature to calculate theoretically the incoherent Cerenkov radiation emitted by precipitating (descending) auroral electrons exceeding the whistler mode phase velocity. It was concluded that common to all the calculations, which do differ in detail, the single-electron emission spectrum was sharply peaked at a frequency characteristic of altitude, that the peak frequency decreased with altitude, and that the calculated intensities were not sufficiently high to account for the observed emissions. Since fast hisslers are a form of auroral hiss which approaches in intensity the maximum intensity of steady hiss that has been observed at Byrd Station, it is concluded that incoherent Cerenkov radiation does not account for fast hisslers.

It is suggested that further theoretical effort be directed toward the primary emission mechanism, rather than toward refining the incoherent Cerenkov model. This is a departure from the approach that has been taken in the four most recent attempts to calculate the incoherent Cerenkov radiation. It is unfortunate that the wave-particle interaction model of

Helliwell and Crystal [1973], which so successfully predicts many features of whistler mode wave growth and wave-particle resonance in the magnetosphere, is not applicable to the present case, in which the waves are observed to be emitted in the same sense (downward) relative to the thermal plasma as the velocity of the precipitating electrons which are their source of energy. (The Helliwell-Crystal model requires counter-streaming waves and electrons in order that the wave frequency, which must be less than the electron gyrofrequency in the rest frame of the thermal plasma, be Doppler-shifted up to the electron gyrofrequency in the frame of the streaming energetic electrons.) It is suggested further that a possible candidate for the primary emission mechanism is wave-particle interactions in the Gendrin condition, in which the wave group velocity and the longitudinal components of the wave phase velocity and particle velocity are simultaneously equal (proposed by Helliwell, personal communication, 1973).

Chapter 2 described the equipment complement used in the present study. The observations were performed at Byrd Station, Antarctica in the southern auroral zone. That equipment recorded signals in the frequency range 0-20 kHz but was not specifically designed to discriminate short rise time signals such as fast hisslers with rise times shorter than 50 ms. All the events reported here were found by examination of the recordings at Stanford University.

In Appendix A is described an experiment performed at Byrd Station which involved the transmission of very low frequency waves from the Byrd longwire substation to the polar orbiting satellite OGO 2. Two unresolved questions, which warrant (at least) further theoretical study, remain: 1) What is the cause of the deep and rapidly varying signal fading

that occurred even when the satellite was most nearly overhead at the transmitter site? 2) Why does the tendency for the oppositely polarized waves to be received at distinctly different signal levels persist even when the satellite is well outside the region where the initial ray directions from transmitter to satellite are within 45^{o} of the local zenith?

The initial fast hissler observation at Byrd Station was described in Chapter 3. It was found that the simplest assumption consistent with the experimental data is that the fast hisslers originate as undispersed noise pulses at fixed altitudes on the Byrd Station field line. That assumption originates entirely from consideration of ground-based very low frequency data. Fast hisslers have not yet been observed in satellite data. Investigation of the phenomenon can not be regarded as complete without a comparison of satellite and ground fast hissler data, preferably simultaneous data. A search for fast hisslers in satellite data should be seriously considered as the next stage of the investigation of the phenomenon. Power spectral densities of fast hisslers as a function of frequency and time at various altitudes should be compared, in order to test the basic assumption of this chapter.

Chapter 4 concerned a systematic search for fast hisslers in continuous tape recorded very low frequency data from Byrd Station, Antarctica, from June and July, 1967. The search concentrated on the expansion phase of magnetospheric substorms, of which 19 met criteria established for the search. Two fast hissler events occurred. The phenomenon is now known to occur at times other than the expansion phase of substorms, but has not been observed in magnetically quiet conditions. All the fast hisslers found were (at least) morphologically consistent with the assumption that

they originated as undispersed noise impulses at fixed altitudes on auroral zone magnetic field lines. The direction of the interplanetary magnetic field in the vicinity of the earth was continuously southward for 79 minutes prior to one of these fast hissler events (and for a longer interval prior to the 14 August event), lending support to magnetosphere dynamics models which do not require a northward to southward turning of the interplanetary magnetic field one hour or less prior to a substorm expansion phase. A southward interplanetary magnetic field causes the auroral oval to move in the equatorward sense, and for these two events the auroral oval was equatorward of Byrd Station. Thus the hisslers were generated on tail-like or open magnetic field lines. Altitudes of origin of fast hisslers from 1800 km to 30,000 km were inferred. Should a data set of great extent become available, an effort should be made to establish the statistics of fast hissler dispersion and intensity.

Fast hisslers with noses or non-extremal frequencies of earliest arrival were described in Chapter 5. This was an isolated event, discovered fortuitously. Statistical inferences can not be drawn from it, only the conclusion that fast hisslers with noses occur. In Chapter 3 it had been pointed out that the existence of a nose implies (under the same set of assumptions established in that chapter) that at least part of the propagation from source to receiver is nonducted. Various methods have been developed by other workers for distinguishing between ducted and nonducted whistler-mode signals detected by satellite-borne very low frequency receivers. These methods might be modified and extended to apply to the study of fast hisslers, in order to test the conclusion on ducting drawn from the assumptions and observations. This should be an

integral part of any investigation of the occurrence of the phenomenon in satellite data.

An alternative model of fast hissler generation was investigated in Chapter 6. There it was assumed that the sources were moving down auroral-zone field lines with velocities corresponding to various electron kinetic energies from 5 keV to 50 keV. Less precise matching between observed fast hissler shapes and predicted shapes was found, than with the fixed point source model. Satellite fast hissler data, should it exist, would be more appropriate for distinguishing between these models than would ground data. The particular differences in prediction of the models should be specified prior even to the initiation of a search for satellite fast hisslers. It is suggested that the particular effects of extending the frequency range, altitude range, and distribution of pitch angles be calculated theoretically as an integral part of the specification.

In Chapter 7, what is believed by the author to be a novel method of distinguishing pure noise pulses from coherent or partially coherent signals was presented, and applied to the case of fast hisslers. The criterion assumed was that the ratio of intensity fluctuations to mean intensity fall in the range from 0.75 to 1.25, for data blocks corresponding to 30 or 40 contiguous unit cells in the frequency-time plane. Pure noise was assumed to fall within this range. The fast hisslers were found to be pure noise. This method is only partially complete, as no specification about phase randomness has been made. It is suggested that this method be refined by the inclusion of criteria for phase randomness. Further, since it has been applied to signals which have undergone some whistler mode dispersion, the criterion for phase randomness should be applied to the signal at the source, rather than at the receiver. In

practice this may be somewhat complex to implement.

Potential double layers as an energization source for auroral electrons were investigated in Chapter 8. It was concluded that potential double layer theory has not yet reached the stage where specific predictions about double layers at fast hissler altitudes (1800-30,000 km) are possible. Most important goals of development of double layer theory, which is warranted at this time, are to establish both necessary and sufficient conditions for the establishment of double layers (should they exist) and to make quantitative predictions on the rise times and lateral extent of these density irregularities.

The relationship of fast hisslers, or more generally of all forms of auroral hiss, to the occurrence of "high-pass noise" (so designated by Dunckel et.al. [1970]; referred to as "terrestrial kilometric radiation" by Gurnett [1974]) as observed on satellite radio wave receivers, is not known. High-pass noise has been found to correlate closely with AE (auroral electrojet) index, which is the usual criterion for worldwide substorm occurrence, and has been found to occur simultaneously with discrete aurora. Although the frequency range of high-pass noise (20 kHz to at least 100 kHz) does not overlap that of fast hisslers, the altitude range of its generation may do so. An experiment to investigate a correlation if any between the two phenomena is strongly urged, as it may shed light on the mechanism of generation of both phenomena. High-pass noise is the closest terrestrial analogue to Jovian decametric radiation, which is known to be associated with the motion of the natural satellite Io through the Jovian magnetosphere, producing what might be termed a "continuous substorm."

The author has investigated the possibility of a correlation between various very low frequency hiss phenomena and the simultaneous occurrence of short rise time auroral phenomena. The results of this investigation are unclear, and the details of that investigation will not be presented here. It can be stated unequivocally that auroral hiss occurs in conjunction with visible aurora, but that not all visible aurora is accompanied by hiss.

Individual electrons, radiating independently and incoherently, do not emit sufficient energy to account for the intensity of auroral hiss. Collective organization of the transverse component of the electrons' velocities must occur, in order to produce the transverse currents which radiate electromagnetic waves. The scale size of this collective organization is probably at least as large as the wavelength of electromagnetic waves used to probe the ionosphere in incoherent backscatter (Thomson scatter) experiments, since the density irregularities that scatter these waves are half a wavelength in depth (0.05-0.50 m) and have not been observed to have anomalously large (significantly greater than thermal) amplitudes.

That auroral light emissions can be produced by precipitation of electrons that have been accelerated from altitudes above the ionosphere, but relatively distant from the equatorial plane, has been known for some years. In addition the long hissler emission is known by its occurrence at high latitude stations, to originate on magnetic field lines that do not even cross the equatorial plane. If the interpretation of fast hisslers presented in this work is correct--and experiments to unambiguously test this interpretation have been proposed in Chapter 3--these emissions for

the first time provide a method for measuring the altitude of generation of auroral hiss at these frequencies, which is found to be in the range 1800 - 30,000 km.

APPENDIX A. ELLIPTICALLY POLARIZED RADIO TRANSMISSION AT 9 kHz FROM BYRD VLF SUBSTATION, ANTARCTICA TO SATELLITE OGO 2

Introduction. On 25 September 1967 radio signals at 9 kHz in various modes of elliptical polarization were transmitted from the Byrd VLF substation in Antarctica. The polar orbiting satellite OGO 2 received the signals as it passed close to the magnetic zenith at Byrd Station. Since only the "whistler" or right-hand circularly polarized mode propagates through the ionosphere at this frequency, I expected the right-elliptically polarized transmission to be received more strongly at the satellite than the linearly polarized transmission, and the latter more strongly than the left-elliptically polarized transmission (all three at approximately the same radiated power). Relative strengths at the satellite were in the expected order, although it has been necessary to take into account the different characteristics of the East-West and North-South elements of the turnstile transmitting antenna employed. These differences in characteristics were overlooked when the experiment was originally conceived.

Antenna. The transmitting antenna was made up of two long dipoles of "RG17" cable core: 0.46 cm diameter copper wire encased in 1.73 cm diameter polyethylene insulation. One dipole, 33.5 km long, was aligned parallel to the magnetic meridian; the other, 17 km long, was perpendicular to it. The dipoles were fed at their midpoints, at Byrd VLF substation, Antarctica, latitude 80°S, longitude 120°W. The dipoles had been constructed by laying out the insulated cable on the surface of the Antarctic ice cap, locally 2164 m thick. Subsequent snow accumulation had buried them to a depth of about one meter when the experiment was performed.

This depth was well over 10 times the outer diameter of the insulation.

Transmitters. Two VLF transmitters were employed simultaneously in the experiment. A solid state transmitter operated continuously at 50 kW at 9 kHz into the 33.5 km dipole. A one-turn current transformer picked off the waveform from one leg of the 33.5 km dipole and fed it through an adjustable phase shifter and switching circuit to a tube-type linear amplifier operated at 15 kW into the 17 km dipole. A second one-turn current transformer, identical to the first but linked to one leg of the 17 km dipole, picked off the waveform from it. This waveform was compared in phase with that from the longer dipole on an oscilloscope, to facilitate setting the relative phase between the dipole currents. On the (incorrect) assumption that the far-field radiation patterns of the dipoles were identical up to a 90^{o} rotation about the vertical axis, the phase was adjusted so that the driving currents were in quadrature.

Three modes of polarization were provided by the switching circuitry: "Left-hand elliptical," with the transmitters operating in quadrature, West leading North; "right-hand elliptical," also with the transmitters operating in quadrature, but with West lagging North; and linear, with only the solid state transmitter operating. These modes of polarization were switched manually in the sequence linear, "left," linear, "right," a complete cycle taking about 10 seconds, with roughly equal dwell times on each mode in sequence.

Data Acquisition. It has been expected on the basis of a preliminary calculation that even though the tube-type transmitter power was only 30% that of the solid state transmitter, the three modes of polarization should have distinctly different levels in the telemetry returned from the OGO

satellite. Tape recordings of the telemetry were made at Byrd Station in order to permit subsequent quantiative measurement of the effect. Two tape tracks were recorded simultaneously. Track One held voice announcement, time ticks, and the VLF signal received by a 6.5 m × 19.7 m copper pipe loop receiving antenna buried below the snow surface. Track Two held broadband VLF satellite telemetry. The telemetry receiving site and the copper-pipe loop antenna were at Byrd Station, 20 km east of the transmitting site.

The OGO 2 satellite was in near circular polar orbit at about 1100 km altitude. It received radio signals in the frequency range 250-12,500 Hz through a 3 m diameter single turn circular loop. The broadband signals were amplified and log-compressed, then used to frequency-modulate the 400.85 MHz telemetry carrier wave. Absolute amplitude information in the broadband VLF signals was almost completely suppressed by the log compressor. A voltage-controlled-oscillator circuit whose frequency varied with the logarithm of the broadband signal amplitude was in operation in the receiver during the experiment, but its absolute calibration had drifted an unknown amount since pre-launch calibration [Roy Stehle, personal communication, 1972]. Nevertheless relative amplitude information has been extrated from the broadband data, as will be explained below.

Figure A.1 is a plot of the ground track of OGO 2 in relation to Byrd Station during the experiment, based on the master ephemeris supplied by NASA. Drawn to scale is the transmitting antenna. The small crosses indicate the intersections of the southern latitude circles 74^{o}S - 84^{o}S with the west longitude meridian 120^{o}W.

Steady hiss was received by the satellite throughout the time of the transmission. This hiss was broadband but most intense below 5 kHz.

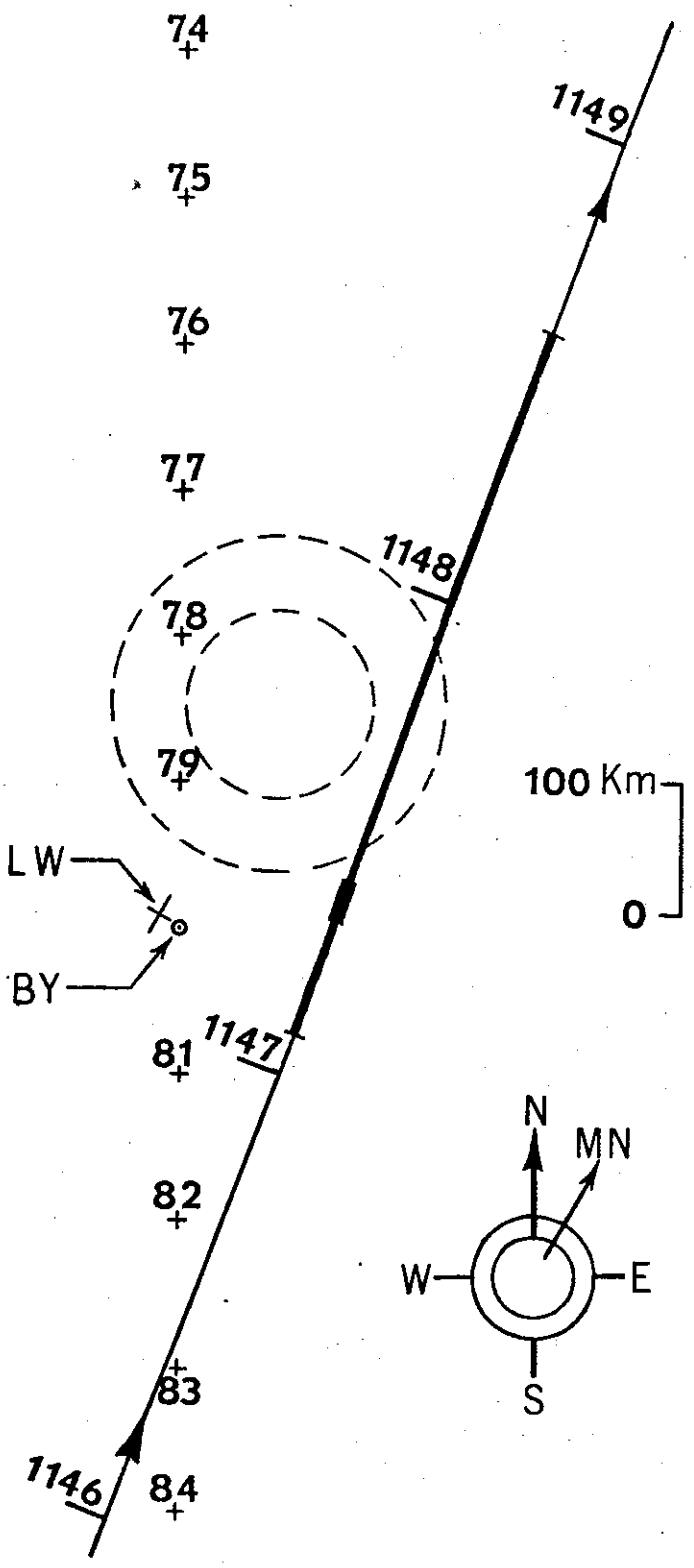

FIGURE A.1. GROUND TRACK OF OGO 2 RELATIVE TO BYRD STATION, ANTARCTICA, 25 September 1967.

Transmissions began at 1145:10 UT and ended at 1152:27 UT. On a rayspan frequency-time spectrogram (bandwidth 32 Hz) of the telemetry the signal first emerged briefly out of the hiss background at 1145:50. At this moment the satellite was 60^{o} above the southern horizon, rising toward the zenith. The signal emerged again and was received continuously at 1147:05, just after the satellite passed its maximum elevation. At that moment it was 11^{o} from the magnetic zenith above the transmitter, and approaching it. The signal continued to increase in amplitude at the satellite, until it exceeded the level of the integrated hiss in the band from 1147:19 until 1147:24. This was indicated by the deep and rapid fading of the hiss on the rayspan record (because of the receiver's log compression) and by the frequency of the voltage controlled oscillator, which showed a maximum total signal strength (artificial plus natural). The satellite passed 3^{o} from the magnetic zenith at 1147:35. By 1148:35 when the satellite had moved to 17^{o} from the magnetic zenith, the 9 kHz signal amplitude had fallen off to the point where its rayspan record began to show gaps. As the satellite continued toward the northern horizon the 9 kHz signal faded out for the last time at 1148:50. I have indicated the interval of continuous signal reception in Figure A.1 by broadening the trace. I have doubly broadened the trace to indicate the five seconds of maximum signal. Frequency-time spectra for two intervals in this pass are given in Figure A.2.

Quantitative amplitude information was extracted from the tape recording by playing back the broadband telemetry track through a narrow-band filter tuned to 9 kHz, detecting the envelope of the filtered signal, and recording the detected voltage on a strip chart. The same was done with the ground VLF tape track in order to obtain timing information.

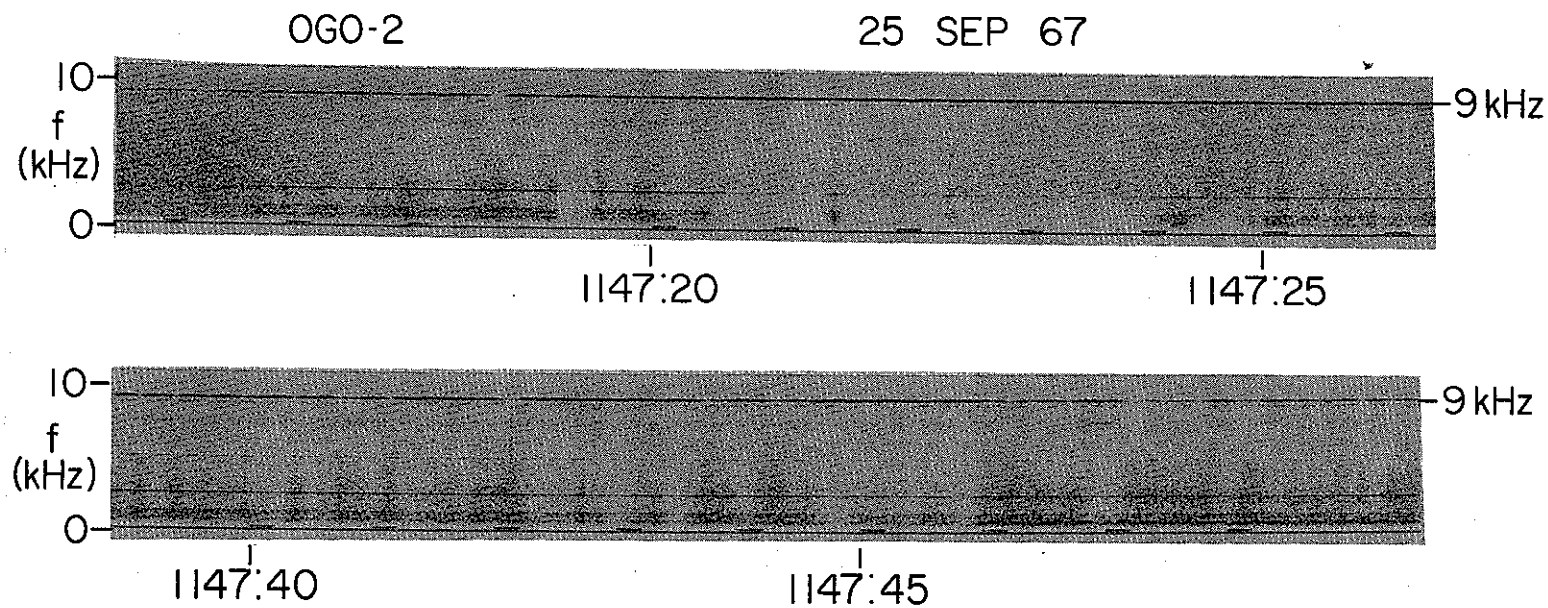

FIGURE A.2. FREQUENCY-TIME SPECTRA FOR TWO INTERVALS DURING THIS PASS.

Each of the three modes of polarization had its own distinct amplitude "signature" on the simultaneously recorded ground VLF track. The ground signal amplitude was a maximum for the "right elliptical" mode, and a minimum for the "left elliptical" mode. This phenomenon, incidentally, has yet to be explained.

The most prominent feature of the 9 kHz signal as observed in the satellite telemetry was its random, deep fading, sometimes nearly down to noise level. Fading cycles were most pronounced at 1-2 Hz. This occurred because of the log compressor circuit in OGO 2 because natural hiss was present simultaneously throughout the transmission. This circuit had a "small-signal suppression" characteristic: the smaller of two simultaneously present signals was suppressed on output some 4-6 db relative to the larger signal. The transition from "small-signal" to "large-signal" took place gradually over an input relative dynamic range of 6 db. Thus a variation in 9 kHz signal strength from 3 db below noise level to 3 db above noise level appeared as a 15 db increase of the 9 kHz signal in the broadband telemetry. Rapid variation of this kind was observed especially in the post-maximum interval from 1147:35 to 1148:25 (see Figure A.2). An "average" signal amplitude was computed for each interval of transmission of the three polarization modes. Only the relationships between these values have been considered here in detail. The amplitude of the detected signal was measured on the strip chart at 0.1 second intervals and the "average" amplitude was computed as the sum of the samples taken during each transmission interval. The shortest transmission interval was 1.3 second; the longest, 3.9 seconds. Propagation delay from transmitter to receiver is estimated to have been $\lesssim$ 60 ms and has been neglected. These average amplitudes have been plotted as a

bar graph in Figure A.3. The horizontal axis represents time, and the vertical axis represents relative amplitude in arbitrary units. Each bar stands for one interval of transmission with a particular mode of polarization. Its length is the average amplitude during the interval. The prominent feature of this data is the very pronounced variation of relative amplitude, despite the averaging that has been done. Most "left elliptical" transmissions tend to be stronger than the "right elliptical" transmissions immediately preceding and following them, but this tendency is somewhat obscured by fading.

The data were further smoothed by employing the linear transmission amplitudes as an indicator of longer-period fading. This was effected by dividing each of the elliptical transmission amplitudes by the mean of the first immediately preceding and following linear transmission amplitudes. In Figure A.4 is a bar graph showing the result of this procedure performed on the 10 complete switching cycles between 1147:04 and 1148:36, the interval of maximum signal. The linear transmissions separating the elliptical transmissions are represented by bars of uniform length 1.0. The elliptical transmissions are represented by bars of lengths proportional to the smoothed values. The "left-hand elliptical" values, mean $1.15 \pm .28$, are greater than the "right-hand elliptical" values, mean $.73 \pm .18$. The former range from .74 to 1.64, with only four (of tens) less than 1.0; the latter range from .50 to 1.01, with only one (of ten) greater than 1.0. These relative values confirm what had already been noted upon aural monitoring of the telemetry tape, immediately subsequent to the experiment. "Left-hand elliptical" transmissions were distinctly heard to be weaker than linear transmissions, and those in turn weaker than "right-hand elliptical" transmissions.

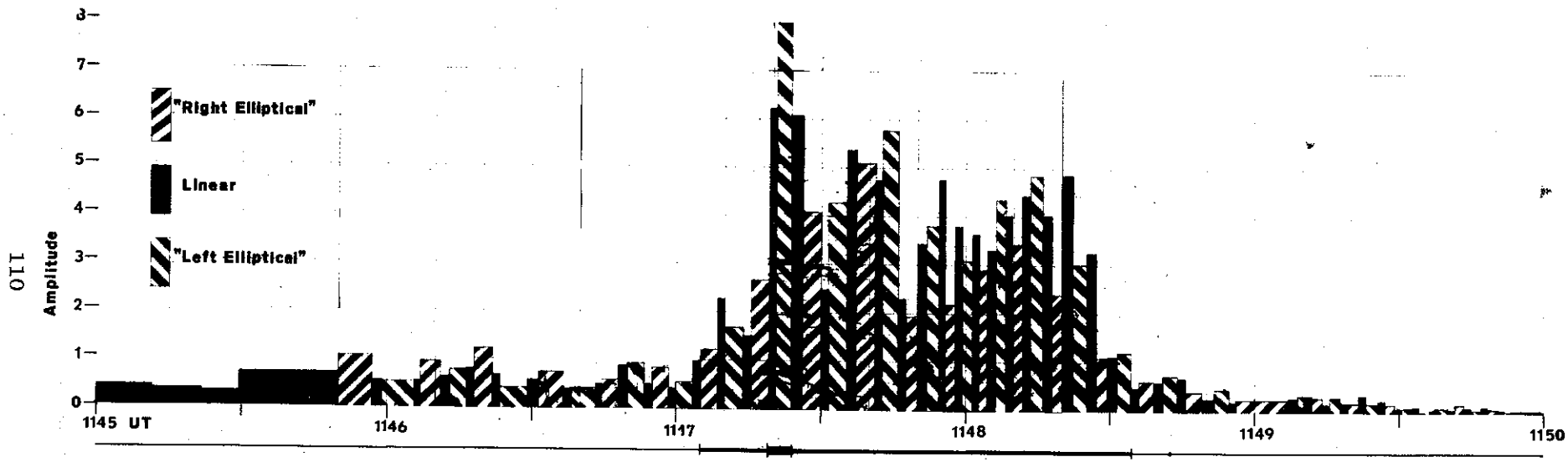

FIGURE A.3. AVERAGED AMPLITUDE OF 9 kHz SIGNAL OBSERVED ON OGO 2.

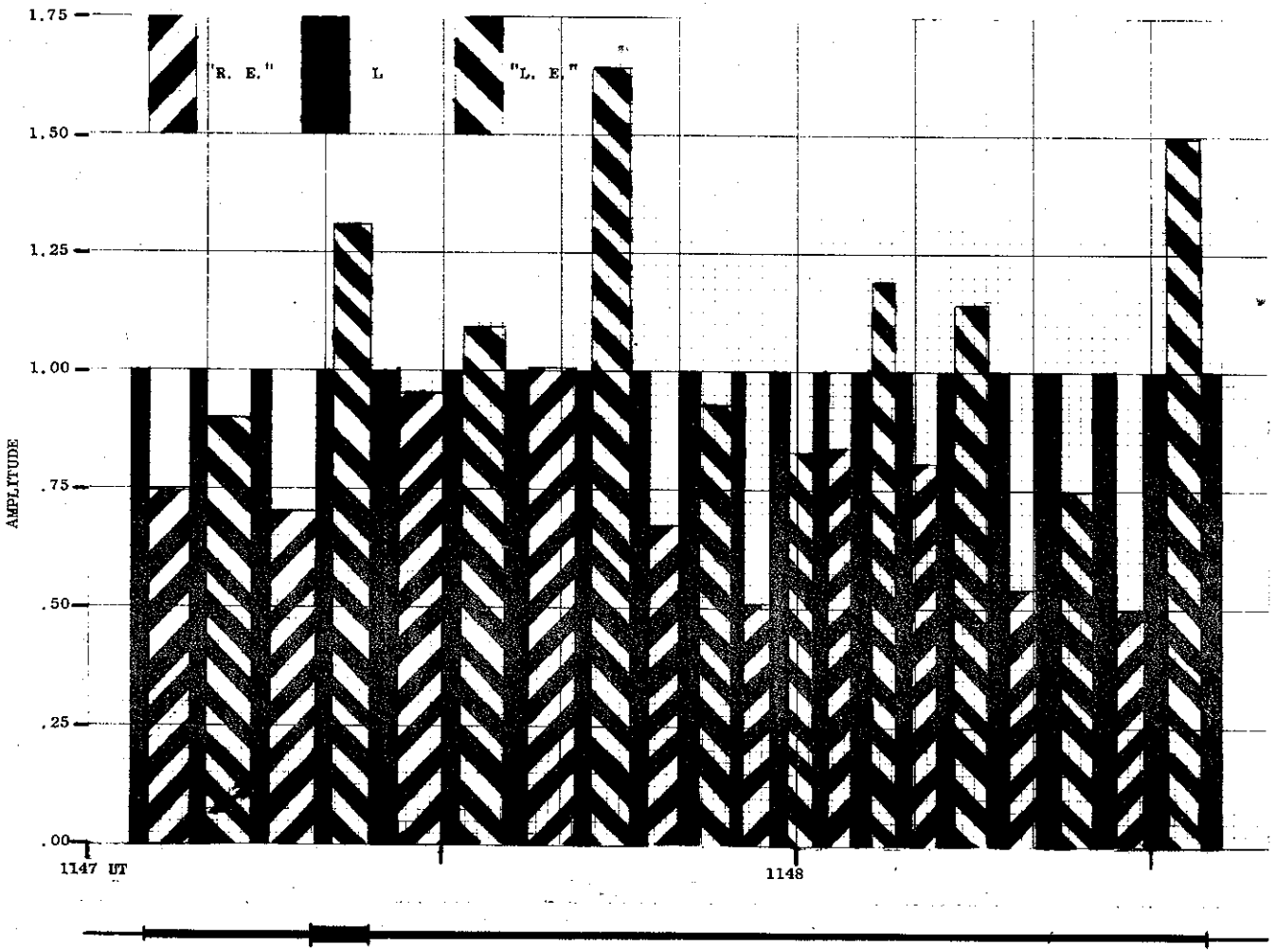

FIGURE A.4. AVERAGED AMPLITUDE OF 9 kHz SIGNAL OBSERVED ON OGO 2 NORMALIZED TO PRECEDING AND FOLLOWING "LINEAR" AMPLITUDE.

This was contrary to the original conception of the experiment, which did not take into account the asymmetry of the antenna under 90^{o} rotation. The experimenters rechecked the equipment and confirmed its proper functioning.

Interpretation of Experimental Results. Propagation of the signal to the satellite is not in a straight line. When the plasma frequency and electron gyrofrequency are both large compared with the signal frequency, the signal arrives at the satellite from a direction that is less than 19^{o} from the direction of the local magnetic field. The range of possible arrival directions lies in a cone whose half-angle may be much smaller than 19^{o}. A typical ray path from transmitter to satellite is a dog leg. The lowest portion of the ray path is a straight line from the transmitter to the base of the ionosphere at about 70 km. The ray path curves sharply as it enters the ionosphere, bending toward the magnetic field direction. It then curves slightly as it passes through the D, E, and F regions of the ionosphere, but remains within 19^{o} of the magnetic field direction all the way to the satellite. Two hypothetical rays launched from the antenna in different directions diverge in the troposphere, and continue to diverge after entering the ionosphere, but most of their divergence between transmitter and satellite takes place below the ionosphere. In Figure A.1 the inner dashed circle, of radius 70 km, is the ground projection of the circle that, at satellite altitude (1147 km at 1147.0 UT) encloses those rays launched at angles 45^{o} or less from the zenith, if ionospheric divergence is neglected. Similarly, the outer circle, of radius 129 km, is the ground projection of the circle that encloses those rays launched at angles of 45^{o} or less from the zenith, when the effect of ionospheric divergence is included. The

ionospheric model is that of Helliwell [1965, p. 63] for night time. Both dipole antenna patterns peak at the zenith, according to Guy et al. [1966, p. 90] whose contribution to the understanding of the results of this experiment will be discussed further below. In Figure A.3 it can be seen that the interval of maximum signal at the satellite was a few seconds prior to the passage of the satellite through the outer 45^{o} circle. The tendency of the "left elliptical" transmissions to be received more strongly than the "right elliptical" persisted when the satellite had passed through and was well outside the 45^{o} circle even though the ratio of the normalized (to the vertical) far-field antenna patterns of the two dipoles remains within 33% of 1.0 only at zenith angles less than 45^{o} [Guy et al., 1966, Figure 3.9].

It is possible to satisfactorily account for the unexpected reversal in order of relative amplitudes as resulting from the difference in lengths of the N-S and E-W dipole elements. Clearly if the antenna had been symmetric under 90^{o} rotation about the vertical, the E-W and N-S components of the waves radiated by it would have had the same relative phase as the relative phase of the feed point currents. What is to be determined is how much these symmetries are affected by a difference in dipole lengths.

Guy et al. [1966] theoretically predicted the characteristics of long horizontal dipole antennas buried in polar ice. They assumed antenna elements of copper wire encased in low-loss dielectric material (specifically, "RG17" cable core) buried in snow or ice at a depth not less than ten wire diameters, but small compared to the polar cap thickness. They included end effects in their calculations. During the construction of the 33.5 km dipole used in this experiment they measured its current distribution characteristics. They were able to do this at both 17.1 km

and 33.5 km lengths, since the dipole was constructed symmetrically, from the center outward. They found close agreement with their prediction. I have applied their results directly here.

One prediction made by them is that at VLF in a long dipole, the current $I(x)$ as a function of the distance x from the feed point varies like the current in a lossy transmission line. Letting $I(0)$ = current at feed point, k = free space wave number, and $2L$ = dipole length, to a good approximation

$$\frac{I(x)}{I(0)} \cong \frac{\sin(\xi_0 k(L-|x|))}{\sin(\xi_0 kL)} \qquad (A.1)$$

An $e^{i\omega t}$ time dependence is assumed. Here ξ_0 is the complex-valued propagation constant, a function of dipole wire conductivity, dipole insulation dielectric constant and thickness, and ice cap temperature, density, and chemical purity. The work cited includes extensive tables of ξ_0 vs frequency for "RG17" cable core antennas buried in ice or snow with various physical characteristics and temperatures, including those found at Byrd Station, Antarctica. Mean temperature there is $-28.2^{\circ}C$. Some typical values of ξ_0 at 9 kHz are:

(A) Solid pure ice, $-28.2^{\circ}C$ $\xi_0 = 2.091-i0.845$

(B) Pure snow, $-28.2^{\circ}C$, density 0.6 g/cm^3, maximum measured value of dielectric constant $\xi_0 = 1.692-i0.411$

(C) Pure snow, $-28.2^{\circ}C$, density 0.6 g/cm^3, minimum measured value of dielectric constant $\xi_0 = 1.579-i0.262$

(D) Surface snow, Byrd Station, Antarctica $\xi_0 = 2.398-i0.857$

Given the current distribution $I(x)$ in the dipole it is possible to exhibit a closed-form solution as an integral for the wave fields at a general point in the far-field region. For present purposes it suffices

to determine the fields at a point vertically above the dipole at a height r. I assume that only the right-hand circularly polarized component of an elliptically polarized wave normally incident on the ionosphere from below propagates.

Define a coordinate system with the origin at the antenna center, x axis along the 33.5 km dipole (aligned with the magnetic meridian), x increasing northward, y axis along the 17 km dipole, y increasing westward, and z axis vertical, z increasing upward.

The radiation electric field due to the 33.5 km dipole with an input power P_x has an x component only, given by

$$E_x = \frac{i60}{r}\sqrt{\frac{2P_x}{R_x}}\, e^{i(\omega t - kr)} f_x \qquad (A.2)$$

where

$$f_x = \frac{1}{2}(1-\mathcal{R}_v)k \int_{-L_x}^{L_x} \frac{I_x(s)}{I_x(0)}\, ds \qquad (A.3)$$

The subscript x refers to the 33.5 km dipole. R_x is the resistive component of the input impedance and $\mathcal{R}_v$ is the reflection coefficient for a 8 kHz plane wave vertically incident on the surface of the ice.

Similarly, the radiation electric field due to the 17 km dipole with an input power P_y has a y component only, given by

$$E_y = \frac{i60}{r}\sqrt{\frac{2P_y}{R_y}}\, e^{i(\omega t - kr)} f_y \qquad (A.4)$$

where

$$f_y = \frac{1}{2}(1-\mathcal{R}_v)k \int_{-L_y}^{L_y} \frac{I_y(s)}{I_y(0)}\, ds \qquad (A.5)$$

The subscript y refers to the 17 km dipole.

The integrals in Eqs. (A.3) and (A.5) can be performed at once, using the approximation in Eq. (A.1). The result of the integration for Eq. (A.3) is:

$$k \int_{-L_x}^{L_x} \frac{I_x(s)}{I_x(0)}\, ds = \frac{2 \sin(\xi_0 k L_x)}{\xi_0} \qquad (A.6)$$

For the special case of vertical propagation, Eq. (A.6) is exact also for the more accurate expression from which the approximation in Eq. (A.1) is derived. If into the factor here called K are collected those factors common to Eqs. (A.2) and (A.4), namely $\frac{i60}{r} e^{i(\omega t - kr)} \frac{1}{2} (1-\mathcal{R}_v)k$ we obtain the result

$$E_x = KE'_x = K\left(\sqrt{\frac{2P_x}{R_x}} \frac{\sin(\xi_0 k L_x)}{\xi_0}\right) \qquad (A.7)$$

$$E_y = KE'_y = K\left(\sqrt{\frac{2P_y}{R_y}} \frac{\sin(\xi_0 k L_y)}{\xi_0}\right) \qquad (A.8)$$

Dipole impedances were measured on 26 June 1967, three months before the experiment was performed. Antenna breaks were repaired on 20 July. Prior to repairs, R_x was 613 Ω, R_y was 690 Ω. I have used these values as the post-repair values are unavailable. The value of kL_x at 9 kHz is 3.159 and the value of kL_y at the same frequency is 1.612.

Using $P_x = 50$ kW and $P_y = 15$ kW it is found for the four cases A, B, C, and D described earlier that the relative values of E_x and E_y are:

(A)	Solid ice	$E'_x = 0.834-i0.969$	$E'_y = -0.102+i0.136$
(B)	Pure snow, max. diel. constant	$E'_x = -0.303-i0.313$	$E'_y = 0.039+i0.090$
(C)	Pure snow, min. diel. constant	$E'_x = -0.316-i0.117$	$E'_y = 0.071+i0.059$

(D) Surface snow, Byrd $E'_x = 1.190-i0.087$ $E'_y = -0.146-i0.146$

Phases are referred to the phase of $I(0)$, at the respective feed points.

Figure A.5 shows the relative phases and amplitudes of E_x and E_y as vectors in the complex plane for the four cases considered. Although the specific values of E'_x and E'_y depend quite strongly on the assumed properties of the ice cap material, in each case the relative phase angle between E'_x and E'_y exceeds 90^o. This phase difference is solely a consequence of the inequality of the dipole lengths. If both dipoles had been fed with the same current $I(0)$, in the far-field region above the dipoles the E-W and N-S components of the wave would have been nearly opposite in phase. In the transmission experiment described here the dipoles were not, however, fed with the same current. $I_y(0)$ was adjusted to be in quadrature with $I_x(0)$. But the difference in dipole characteristics introduced an unintended additional phase shift, so that the radiation fields were approximately in quadrature, but with the "wrong" sense. Consequently the "right elliptical" wave above the antenna contained both right circular and left circular components, but predominantly the latter. Similarly the "left elliptical" wave consisted principally of the right circular component.

Only the right circular component couples into the whistler mode in the ionosphere. The left circular component is totally reflected at the base of the ionosphere. Using the notation of Smith and Brice [1964] it is possible to represent the circularly polarized components of a wave in terms of its x and y components by

$$\mathcal{E}_l = (\mathcal{E}_x + i\mathcal{E}_y)/\sqrt{2} \qquad \text{(Right)} \qquad \text{(A.9)}$$

(A) Solid Ice

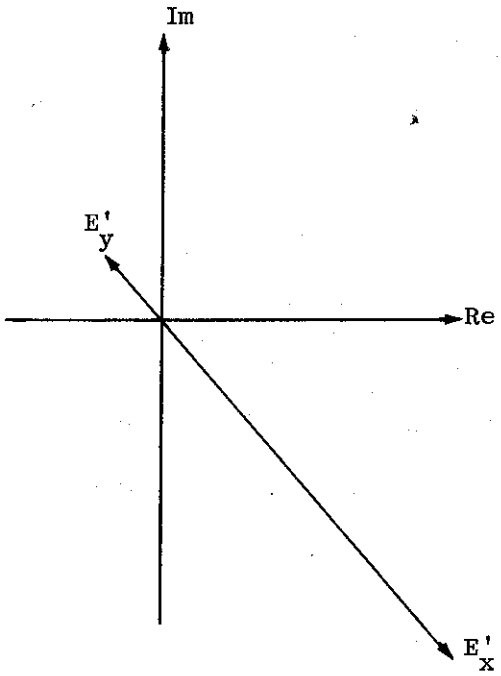

(B) Snow, maximum properties

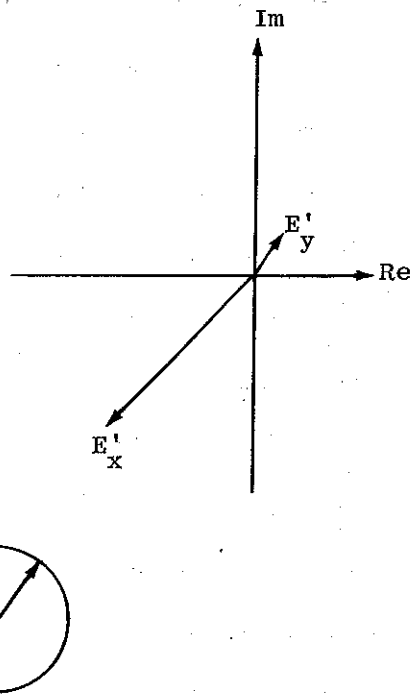

(C) Snow, minimum properties

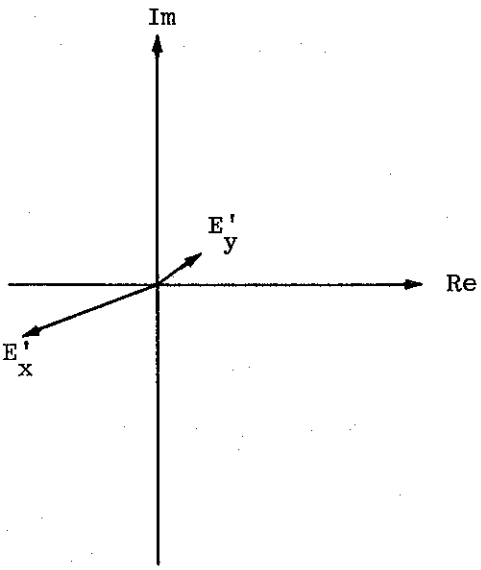

(D) Surface Snow, Byrd Station

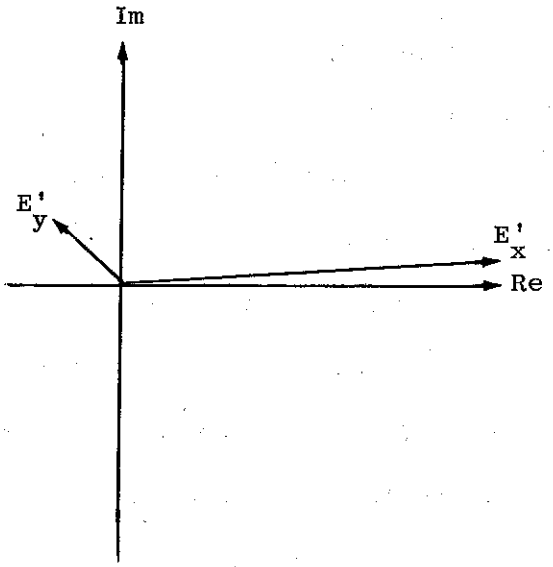

FIGURE A.5. RELATIVE VECTOR AMPLITUDES OF ELECTRIC FIELDS E'_x AND E'_y.

$$\mathcal{E}_{-1} = (\mathcal{E}_x - i\mathcal{E}_y)/\sqrt{2} \qquad \text{(Left)} \qquad \text{(A.10)}$$

Here both $\mathcal{E}_x$ and $\mathcal{E}_y$ are referred to a common phase, that of the current in the 33.5 km dipole. That is, $\mathcal{E}_x = E'_x$, and $\mathcal{E}_y = -ipE'_y$, where $p = 0, 1,$ or -1 depending on whether the transmission is linear, "right elliptical," or "left elliptical," respectively.

The amplitude of the right circular component is

$$|\mathcal{E}_1| = \left(\left\{\mathrm{Re}(\mathcal{E}_x) - \mathrm{Im}(\mathcal{E}_y)\right\}^2 + \left\{\mathrm{Im}(\mathcal{E}_x) + \mathrm{Re}(\mathcal{E}_y)\right\}^2\right)^{1/2}/\sqrt{2}$$

$$= \left(\left\{\mathrm{Re}(E'_x) + \mathrm{Re}(E'_y)\right\}^2 + \left\{\mathrm{Im}(E'_x) + \mathrm{Im}(E'_y)\right\}^2\right)^{1/2}/\sqrt{2}$$

Although in the experiment considered here $|\mathcal{E}_y|$ was small compared to $|\mathcal{E}_x|$, because the 17 km dipole compared to the 33.5 km dipole was both a less efficient radiator at 9 kHz and was fed with less power, its relative phase had a significant effect on the value of $|\mathcal{E}_1|$, as shown in Table A.1. It can be seen that any of the four cases A, B, C, or D is compatible with the results of the polarization experiment.

The satellite data indicated that the 9 kHz transmitted signal was comparable in strength to, and briefly stronger than, the integrated natural hiss in the band 0.3 - 12.5 kHz. We can roughly estimate (without resort to ray tracing) the signal strength to be expected in a near-overhead pass as follows: The efficiency or ratio of radiated power to input power, of the 33.5 km dipole is 5.30×10^{-2} and that of the 17.1 km dipole is 4.56×10^{-2}. Maximum radiated power in the right circular mode is 301 W. Of this power, 41.0% or 123 W is radiated at zenith angle less than 45° [Guy, et al., 1966, Figure 3.9]. If all the power radiated at zenith angle less than 45° is transmitted to satellite altitude and

TABLE A.1. RELATIVE ELECTRIC FIELD STRENGTHS IN THE WHISTLER MODE IN RADIO WAVES EMITTED BY CROSSED DIPOLES ON POLAR ICE CAPS.

Substrate Material	$\mathcal{E}_{1_p}$	$\frac{\mathcal{E}_{1_p}}{\mathcal{E}_{1_0}}$
(A) Solid pure ice		
p = 1 "Right elliptical"	.78	.87
p = 0 Linear	.90	1.00
p = -1 "Left elliptical"	1.02	1.13
(B) Pure snow, max. diel. constant		
p = 1	.24	.79
p = 0	.31	1.00
p = -1	.37	1.21
(C) Pure snow, min. diel. constant		
p = 1	.18	.75
p = 0	.24	1.00
p = -1	.30	1.26
(D) Surface snow, Byrd Station		
p = 1	.76	.90
p = 0	.84	1.00
p = -1	.95	1.12
(E) Present experimental result		
p = 1		.73±.18
p = 0		1.0
p = -1		1.53±.28

uniformly illuminates a 129 km radius circle the power density P in that circle is 2.36×10^{-9} Wm^{-2}.

Jørgensen [1968] found the auroral hiss spectral intensity measured by OGO 2 at 9 kHz to range from 2×10^{-17} $Wm^{-2}Hz^{-1}$ to 10^{-13} $Wm^{-2}Hz^{-1}$. The broadband receiver bandwidth on OGO 2 was 12.2 kHz. A flat auroral hiss spectrum with the power spectral density at 9 kHz in the range observed by Jørgensen would have a total power density in the receiver bandwidth of 2.44×10^{-12} Wm^{-2} to 1.22×10^{-8} Wm^{-2}.

Conclusions. It has been possible to account for the unexpected result of the polarization experiment, namely, that "left elliptically" polarized radio waves seem to excite the whistler mode more strongly than linearly polarized waves, and that the latter in turn seem to excite the whistler mode more strongly than "right elliptically" polarized. The phases of the waves in the radiation fields of the two longwire dipoles relative to their driving currents have been calculated, and their difference exceeds 90^{o}. The effect of this in the experiment described here was to transform a "left elliptical" transmission at the antenna feed into a right elliptically polarized wave in the far field. The right circularly polarized component of this wave coupled into the whistler mode and was received by the OGO 2 satellite. It was received at greater strength than the right circularly polarized component of a linearly polarized wave transmitted at approximately the same power, which in turn was received at a greater strength than the right circularly polarized component of a left elliptically polarized wave transmitted at approximately the same power.

I have argued that in the post-maximum portion of the satellite pass the auroral hiss was within a few decibels of the 9 kHz signal

strength, estimated above as 2.36×10^{-9} Wm^{-2}. While this value lies within the range I have based upon Jørgensen's result, I have not been able to measure the auroral hiss power density present directly. A direct measurement of auroral hiss power density would have been desirable because the 9 kHz signal strength in the post-maximum interval could have been measured by comparison with the auroral hiss. The signal maximum at 1147:19 - 1147:24 may have been evidence of magneto-ionospheric ducting between the transmitter and OGO 2.

APPENDIX B. FAST HISSLER PLOTTER PROGRAM

Fast hissler "trajectories" in frequency-time space are plotted by a Hewlett-Packard Model 9810 Calculator-Plotter programmed with the program listed below. Whistler-mode group delays from selected altitudes to the ground as a function of frequency are integrated for field-aligned propagation along an auroral-zone magnetic field line. The parameters (plasma frequency, gyrofrequency) used for this integration are those given by the light lines in Figure 3.3. These parameters are generated in subroutines C and E, respectively from constants stored, prior to running, in machine absolute locations ØØ1 through ØØ6 and Ø11 through Ø13. The values of these constants used to generate the curves in Figure 3.4 and Figures 6.1 through 6.4 are as follows: Plasma frequency model: ØØ1, -2.00; ØØ2, 2.30×10^{9}; ØØ3, -0.48; ØØ4, 5200; ØØ5, 800; and ØØ6, 240. Gyrofrequency model: Ø11, 6370; Ø12, -2.97; Ø13, 3.45×10^{14}. The plasma frequency model can be increased or decreased by a constant factor k (as was done for selected runs in this work) by multiplying by k both of the constants stored in machine absolute locations ØØ2 and ØØ4.

Each sequentially numbered line in the program listing contains, in order, 3 codes. The first is the machine absolute location of the program instruction; the second is the mnemonic or abbreviation for the keystroke generating the instruction (CLR = clear, GTO = go to, LBL = label, CNT = continue, EEX = enter exponent, XTO = value in X register transferred to specified location, STP = stop, CLX = clear X register, UP = value in X register transferred to Y register, XFR = value in specified location transferred to X register, "X = Y" = test of equality,

DN = value in Y register transferred to X register, S/R = subroutine/return, XEY = interchange contents of X and Y registers, XSQ = value in X register is replaced by its square, RUP = values in all temporary registers are transferred to next higher register, H = value in X register is replaced by that value raised to value in Y register, END = program terminates), and the third is the machine code for that instruction.

In operation the program pauses once for operator input. Input is an integer n, $0 \leq n \leq 24$, which specifies the altitude of the fast hissler source through the formula altitude = $(301 + 50(n^2+n))$ km. (This somewhat complex altitude specification represents a three-way compromise among coding complexity, running time, and accuracy.) The frequency range of the calculation in this program is 20 kHz (which can be altered by changing program instructions $\phi 3\phi\phi$ through $\phi 3\phi 5$) and the time duration is .5 sec (which can be altered by changing program instructions $\phi 266$ through $\phi 27\phi$). Program running time depends on n. For $n=0$, the running time is about 30 seconds, most of which is plotting time; for $n=24$, the running time is about 20 minutes, most of which is calculating time. The program can be altered without great difficulty to produce printed rather than plotted output. It was printed output that made possible the accurate nose frequency comparisons discussed in Chapter 4.

Program instructions and data are stored in separate sets of machine locations, thus there is no conflict between program instruction $\phi\phi\phi\phi$--CLR and the data stored in location $\phi\phi\phi$.

HISSLER PLOTTER

```
0000--CLR---20
0001--GTO---44
0002--LBL---51
0003-- A ---62
0004--LBL---51
0005-- M ---70
0006--CNT---47
0007--CNT---47
0008--CNT---47
0009--CNT---47
0010--CNT---47
0011-- 2 ---02
0012-- . ---21
0013-- 9 ---11
0014-- 9 ---11
0015-- 7 ---07
0016-- 9 ---11
0017--EEX---26
0018-- 0 ---00
0019-- 3 ---03
0020--XTO---23
0021-- 0 ---00
0022-- 0 ---00
0023-- 0 ---00
0024--CLX---37
0025--STP---41
0026--XTO---23
0027-- 7 ---07
0028--LBL---51
0029-- F ---16
0030--CLX---37
0031--XTO---23
0032-- 0 ---00
0033-- 1 ---01
0034-- 0 ---00
0035-- 3 ---03
0036-- 0 ---00
0037-- 1 ---01
0038--XTO---23
0039-- 0 ---00
0040-- 9 ---11
0041-- UP---27
0042--LBL---51
0043-- G ---15
0044--XFR---67
0045-- 7 ---07
0046-- UP---27
0047-- 1 ---01
0048-- + ---33
0049--XFR---67
0050-- 1 ---01
0051-- 6 ---06
0052--X=Y---50
0053--GTO---44
0054--LBL---51
0055-- N ---73
0056--CNT---47
0057--CNT---47
0058--CNT---47
0059--CNT---47
0060--CNT---47
0061--CNT---47
0062-- DN---25
0063-- DN---25
0064--GTO---44
0065--S/R---77
0066--LBL---51
0067-- C ---61
0068--YTO---40
0069-- 1 ---01
0070-- 5 ---05
0071--GTO---44
0072--S/R---77
0073--LBL---51
0074-- E ---60
0075--YTO---40
0076--DIV---35
0077-- 1 ---01
0078-- 5 ---05
0079--XFR---67
0080-- 0 ---00
0081-- 0 ---00
0082-- 8 ---10
0083--XEY---30
0084--DIV---35
0085--CNT---47
0086--CNT---47
0087--CNT---47
0088--CNT---47
0089--CNT---47
0090--YTO---40
0091-- 1 ---01
0092-- 4 ---04
0093--XFR---67
0094-- 1 ---01
0095-- 5 ---05
0096--XSQ---12
0097--XTO---23
0098-- 1 ---01
0099-- 5 ---05
0100--RUP---22
0101-- 1 ---01
0102--RUP---22
0103--DIV---35
0104-- 1 ---01
0105-- - ---34
0106-- DN---25
0107--DIV---35
0108--YTO---40
0109-- 6 ---14
0110--DIV---35
0111--XFR---67
0112-- 1 ---01
0113-- 4 ---04
0114--DIV---35
0115--DIV---35
0116-- + ---33
0117-- + ---33
0118-- 2 ---02
0119--DIV---35
0120--XFR---67
0121-- 0 ---00
0122--DIV---35
0123-- 6 ---14
0124-- UP---27
0125--XFR---67
0126-- 1 ---01
0127-- 4 ---04
0128--XSQ---12
0129-- + ---33
0130-- DN---25
0131-- r ---76
0132--DIV---35
0133--XFR---67
0134-- 1 ---01
0135-- 6 ---06
0136-- X ---36
0137--YTO---40
0138-- + ---33
0139-- 1 ---01
0140-- 0 ---00
0141--CNT---47
0142-- UP---27
0143-- 1 ---01
0144-- + ---33
0145--YTO---40
0146-- 0 ---00
0147-- 1 ---01
0148-- 6 ---06
0149-- 1 ---01
0150-- 0 ---00
0151-- 0 ---00
0152-- X ---36
0153-- - ---34
0154--YTO---40
0155-- + ---33
0156-- 9 ---11
0157--XFR---67
0158-- 9 ---11
0159-- UP---27
0160--GTO---44
```

```
0161--LBL---51
0162-- G ---15
0163--LBL---51
0164-- E ---60
0165--XTO---23
0166-- b ---14
0167--XFR---67
0168-- + ---33
0169-- 0 ---00
0170-- 1 ---01
0171-- 1 ---01
0172-- UP---27
0173--XFR---67
0174-- 0 ---00
0175-- 1 ---01
0176-- 2 ---02
0177--XEY---30
0178-- H ---74
0179--XFR---67
0180-- X ---36
0181-- 0 ---00
0182-- 1 ---01
0183-- 3 ---03
0184-- UP---27
0185-- b ---14
0186--S/R---77
0187-- 0 ---00
0188-- 0 ---00
0189-- 0 ---00
0190-- 0 ---00
0191-- 0 ---00
0192-- 0 ---00
0193-- 0 ---00
0194-- 0 ---00
0195-- 0 ---00
0196-- 0 ---00
0197-- 0 ---00
0198-- 0 ---00
0199-- 0 ---00
0200-- 0 ---00
0201-- 0 ---00
0202-- 0 ---00
0203-- 0 ---00
0204-- 0 ---00
0205-- 0 ---00
0206-- 0 ---00
0207-- 0 ---00
0208-- 0 ---00
0209-- 0 ---00
0210-- 0 ---00
0211-- 0 ---00
0212-- 0 ---00
0213--LBL---51
0214-- C ---61
0215--XTO---23
0216-- b ---14
0217--XFR---67
0218-- 1 ---01
0219-- UP---27
0220-- b ---14
0221-- H ---74
0222--XFR---67
0223-- X ---36
0224-- 2 ---02
0225-- UP---27
0226--XFR---67
0227-- 3 ---03
0228-- UP---27
0229-- b ---14
0230-- H ---74
0231--XFR---67
0232-- X ---36
0233-- 4 ---04
0234--XEY---30
0235-- DN---25
0236-- + ---33
0237-- b ---14
0238-- UP---27
0239--XFR---67
0240-- 0 ---00
0241-- 5 ---05
0242-- + ---33
0243-- DN---25
0244--DIV---35
0245-- b ---14
0246-- UP---27
0247--XFR---67
0248-- 0 ---00
0249-- 6 ---06
0250-- - ---34
0251-- DN---25
0252-- X ---36
0253-- b ---14
0254--S/R---77
0255--LBL---51
0256-- N ---73
0257-- 8 ---10
0258-- 0 ---00
0259-- 0 ---00
0260--XFR---67
0261-- X ---36
0262-- 0 ---00
0263-- 0 ---00
0264-- 8 ---10
0265-- UP---27
0266-- 2 ---02
0267-- 0 ---00
0268-- 0 ---00
0269-- 0 ---00
0270-- 0 ---00
0271--XFR---67
0272-- X ---36
0273-- 0 ---00
0274-- 1 ---01
0275-- 0 ---00
0276--FMT---42
0277-- DN---25
0278-- 0 ---00
0279-- . ---21
0280-- 5 ---05
0281--XTO---23
0282-- - ---34
0283-- 0 ---00
0284-- 0 ---00
0285-- 8 ---10
0286-- 1 ---01
0287--XTO---23
0288-- 0 ---00
0289-- 1 ---01
0290-- 6 ---06
0291--GTO---44
0292--LBL---51
0293-- F ---16
0294--STP---41
0295-- 0 ---00
0296-- 0 ---00
0297-- 0 ---00
0298--LBL---51
0299-- A ---62
0300-- 1 ---01
0301-- 9 ---11
0802-- . ---21
0303-- 9 ---11
0304-- 9 ---11
0305-- 9 ---11
0306--XTO---23
0307-- 0 ---00
0308-- 0 ---00
0309-- 8 ---10
0310-- 1 ---01
0311--XTO---23
0312-- 0 ---00
0313-- 1 ---01
0314-- 6 ---06
0315-- 1 ---01
0316--EEX---26
0317-- 6 ---06
0318--FMT---42
0319-- DN---25
0320--GTO---44
0321--LBL---51
0322-- M ---70
0323--END---46
```

REFERENCES

Akasofu, S.-I., P. D. Perreault, F. Yasuhara, and C.-I. Meng, Auroral substorms and the interplanetary magnetic field, J. Geophys. Res., 78, 7490, 1973.

Albert, R. D. and P. J. Lindstrom, Auroral-particle precipitation and trapping caused by electrostatic double layers in the ionosphere, Science, 170, 1398, 1970.

Alfvén, H. and C.-G. Fälthammar, Cosmical Electrodynamics, Oxford University Press, Oxford, England, 1963.

Allcock, G. McK., C. K. Branigan, J. C. Mountjoy, and R. A. Helliwell, Whistler and other very-low-frequency phenomena associated with the high-altitude nuclear explosion on July 9, 1962, J. Geophys. Res., 68, 735, 1963.

Bell, T. F., Wave particle gyroresonance interactions in the earth's outer ionosphere, Tech. Rept. No. 3412-35, Radioscience Lab., Stanford Electronics Labs., Stanford University, Stanford, Calif., 1964.

Block, L. P., Potential double layers in the ionosphere, Cosmic Electrodynamics, 3, 349, 1972.

Brice, N., Magnetosphere and high latitude ionospheric disturbance phenomena, in Physics of the Magnetosphere, R. L. Carovillano, J. F. McClay, and H. Radoski (eds.), D. Reidel Publishing Co., Dordrecht, Holland, 1968.

Burton, E. T. and E. M. Boardman, Audio-frequency atmospherics, Proc. IRE, 21, 1476, 1933.

Carlqvist, P., On the formation of double layers in plasmas, Cosmic Electrodynamics, 3, 377, 1972.

Carpenter, D. L., Whistler evidence of a "knee" in the magnetospheric ionization density profile, J. Geophys. Res., 68, 1675, 1963.

Carpenter, D. L., Ducted whistler-mode propagation in the magnetosphere; a half-gyrofrequency upper intensity cutoff and some associated wave growth phenomena, J. Geophys. Res., 73, 2919, 1968.

Carpenter, D. L., N. Dunckel, and J. F. Walkup, A new very-low-frequency phenomenon: whistlers trapped below the protonosphere, J. Geophys. Res., 69, 5009, 1964.

Collier, R. J., C. B. Burckhardt, and L. H. Lin, Optical Holography, Academic Press, New York, 1971.

Dinger, H. E. and W. E. Garner, Whistler observations in connection with nuclear explosions, J. Geophys. Res., 68, 5641, 1963.

Duncan, R. A. and G. R. Ellis, Simultaneous occurrence of sub-visual aurorae and radio noise bursts on 4.6 kc/s, Nature, 183, 1618, 1959.

Dunckel, N., B. Ficklin, L. Rorden, and R. A. Helliwell, Low-frequency noise observed in the distant magnetosphere with OGO 1, J. Geophys. Res., 75, 1854, 1970.

Ellis, G. R. A., Low frequency radio emission from aurorae, J. Atmos. Terr. Phys., 10, 302, 1957.

English, H. W. and A. R. W. Hughes, An attempt to explain satellite observations of high latitude VLF hiss in terms of generation by incoherent Cerenkov radiation, Paper presented at XVI COSPAR Plenary Meeting, Konstanz, Germany, 1973.

Gurnett, D. A., The earth as a radio source: terrestrial kilometric radiation, Rept. No. 74-11, Dept. of Physics and Astronomy, University of Iowa, Iowa City, Iowa, 1974.

Gurnett, D. A. and L. A. Frank, VLF hiss and related plasma observations in the polar magnetosphere, J. Geophys. Res., 77, 172, 1972.

Gurnett, D. A., S. R. Mosier, and R. R. Anderson, Color spectrograms of very-low-frequency Poynting flux data, J. Geophys. Res., 76, 3022, 1971.

Gurnett, D. A. and B. J. O'Brien, High-latitude geophysical studies with satellite INJUN 3. 5. Very-low-frequency electromagnetic radiation, J. Geophys. Res., 69, 65, 1964.

Guy, A. W., D. K. Reynolds, and H. M. Swarm, The characteristics of long antennas buried in polar ice, Tech. Rept. No. 101, Dept. of Electrical Engineering, University of Wash., Seattle, Wash., 1966.

Helliwell, R. A., Whistlers and Related Ionospheric Phenomena, Stanford University Press, Stanford, Calif., 1965.

Helliwell, R. A. and D. L. Carpenter, Whistlers excited by nuclear explosions, J. Geophys. Res., 68, 4409, 1963.

Helliwell, R. A. and T. L. Crystal, A feedback model of cyclotron interaction between whistler-mode waves and energetic electrons in the magnetosphere, J. Geophys. Res., 78, 7357, 1973.

Jørgensen, T. S., Interpretation of auroral hiss measured on OGO 2 and at Byrd Station in terms of incoherent Cerenkov radiation, J. Geophys. Res., 73, 1055, 1968.

Kimura, I., A survey on observations and theories of the VLF emissions, Planet. Space Sci., 15, 1427, 1967.

Kuhn, T. S., The Structure of Scientific Revolutions, University of Chicago Press, Chicago, Ill., (2nd ed.), 1970.

Lim, T. L. and T. Laaspere, An evaluation of the intensity of Cerenkov radiation from auroral electrons with energies down to 100 eV, J. Geophys. Res., 77, 4145, 1972.

Martin, L. H., R. A. Helliwell, and K. R. Marks, Association between aurorae and VLF hiss observed at Byrd Station, Antarctica, Nature, 187, 751, 1960.

Morozumi, H., Diurnal variation of aurora zone geophysical disturbances, Rept. Iono. & Space Res., Japan, 19, 1965.

Morozumi, H. M. and R. A. Helliwell, A correlation study of the diurnal variation of upper atmospheric phenomena in the southern auroral zone, Tech. Rept. No. 2, Stanford Electronics Labs., Stanford University, Stanford, Calif., 1966.

Rao, M., S. K. Dikshit and B. A. P. Tantry, Incoherent Cerenkov radiation in the magnetosphere and the ground observations of VLF-hiss, J. Geophys. Res., 78, 191, 1973.

Roederer, J. G., The earth's magnetosphere, Science, 183, 37, 1974.

Siren, J. C., Dispersive auroral hiss, Nature, Phys. Sci., 238, 118, 1972.

Smith, R. L., An explanation of subprotonospheric whistlers, J. Geophys. Res., 69, 5019, 1964.

Smith, R. L. and N. Brice, Propagation in multicomponent plasmas, J. Geophys. Res., 69, 23, 1964.

Smith, R. L., R. A. Helliwell, and I. W. Yabroff, A theory of trapping of whistlers in field-aligned columns of enhanced ionization, J. Geophys. Res., 65, 815, 1960.

Storey, L. R. O., An investigation of whistling atmospherics, Ph.D. Thesis, University of Cambridge, Cambridge, England, 1953a.

Storey, L. R. O., An investigation of whistling atmospherics, Phil. Trans. Roy. Soc. (London) A, 246, 113, 1953b.

Taylor, W. W. L., Generation and propagation of electromagnetic waves in the magnetosphere, Ph. D. Thesis, Dept. of Physics and Astronomy, University of Iowa, Iowa City, Iowa, 1973.

Taylor, W. W. L. and S. D. Shawhan, A test of incoherent Cerenkov radiation for VLF hiss and other magnetospheric emissions, J. Geophys. Res., 79, 105, 1974.